2011

Bioorthogonal Chemical Reporters Reveal Fatty-Acylation of Histone H3 Variants and Cholesterol Modification of Proteins and Trafficking in Cells

John P. Wilson

BIOORTHOGONAL CHEMICAL REPORTERS REVEAL FATTY-ACYLATION OF HISTONE H3 VARIANTS AND CHOLESTEROL MODIFICATION OF PROTEINS AND TRAFFICKING IN CELLS

A Thesis Presented to the Faculty of
The RockefellerUniversity
in Partial Fulfillment of the Requirements for
the degree of Doctor of Philosophy

by
John P. Wilson
June 2011

BIOORTHOGONAL CHEMICAL REPORTERS REVEAL FATTY-ACYLATION OF HISTONE H3 VARIANTS AND CHOLESTEROL MODIFICATION OF PROTEINS AND TRAFFICKING IN CELLS

John P. Wilson, Ph.D.
The Rockefeller University 2011

Lipids are essential components to all known life. They serve many functions from basic building blocks to covalent protein modification and are particularly involved in signaling. Many rare and widespread human health concerns involve lipids but despite their importance, their analysis either free or protein-bound has remained difficult for decades. Here, using bioorthogonal chemistry, we have developed a robust system to identify the proteins modified by lipids and advanced the ability to image cholesterol in cells and tissues.

The unbiased proteomic analysis of fatty-acylated proteins using chemical reporters undertaken here revealed a greater diversity of lipid-modified proteins in mammalian cells than had previously been appreciated. Proteins targeted by a series of fatty acid chemical reporters ranging from myristic to stearic acid showed their involvement in a vast range of cellular processes from all cellular compartments. Many nuclear proteins were found, in particular histone H3 variants. Histones H3.1, H3.2 and H3.3 were demonstrated to be modified with fatty acid chemical reporters on the conserved cysteine 110, a novel site of S-acylation on histone H3.2. This newly discovered modification of histone H3 variants could have implications for nuclear organization and chromatin regulation.

Cholesterol is an abundant sterol in the membranes of higher eukaryotes that is important in mammalian physiology and disease. This ancient lipid serves multiple essential functions in membranes and signaling, but the precise mechanisms of its trafficking and function as a protein PTM remain to be fully elucidated. The multiple techniques developed to visualize cholesterol often give conflicting results and can inaccurately depict cholesterol distribution due to structural perturbations of analogs or staining specificities. Here, using click chemistry, we developed the fluorescent visualization of cholesterol protein modification and cholesterol trafficking *in vivo* with 25-azidonorcholesterol (az-chol). Az-chol exhibits minimal structural perturbation, is covalently attached to proteins, incorporates into membranes like cholesterol, faithfully detects alterations in lipid trafficking and reveals an asymmetrical cholesterol distribution in the brain of the developing mouse embryo. The bioorthogonal chemical reporter az-chol provides a new, sensitive and versatile tool to investigate cholesterol distribution from individual proteins to whole organisms.

Lovingly dedicated to my family, generations after and generations before.

ACKNOWLEDGEMENTS

For continual support, understanding, technical prowess and beautiful collaboration, I first thank my wife and family for their understanding of "lab." I thank the Hang Lab members for their assistance and companionship, in particular Guillaume Charron, Yu-Ying Yang Anuradha S. Raghavan for their assistance with chemistry and reagents. I thank my mentors of the past, especially Dean Malencik and Sonia Anderson, who taught me "real biochemistry" and its tools, and Douglas Barofsky, who taught me mass spectrometry and its applications. For their insight, support and assistance, I thank my committee Brian Chait, Tom Muir and Nick Davis. I thank the core facilities of Rockefeller, particularly and Alison North of the microscopy core and Haiteng Deng, Joe Fernandez and Haiqiang "Bill" Yu of the proteomics core. Finally, I thank my advisor Howard Hang, who gave me the opportunity to research in an exciting field.

TABLE OF CONTENTS

LIST OF FIGURES

LIST OF TABLES

LIST OF ABBREVIATIONS

17-ODYA	17-octadecynoic acid
ABC	Ammonium bicarbonate
ABE	Acyl-biotin exchange
ACBP	Acyl-CoA binding protein
Alk-12	Alkyne myristic acid analog
Alk-14	Alkyne palmitic acid analog
Alk-16	Alkyne stearic acid analog
Alk-azo-biotin	Sodium dithionite cleavable alkynyl azobenzene biotin affinity tag
Alk-FAs	Alkynyl-fatty acids
Alk-Rhod	Alkynyl-rhodamine
Az-Rhod	Azido-rhodamine
ARFs	ADP-ribosylation factors
Az-12	Azido myristic acid analog
Az-15	Azido stearic acid analog
Az-azo-biotin	Sodium dithionite cleavable azido azobenzene biotin affinity tag
Az-chol	25-azidonorchoesterol
Az-FAs	Azido-fatty acids
az-Rhod	Azido-rhodamine
BAF	Barrier-to-autointegration factor
BCA	Bicinchoninic acid
Bet3	Trafficking protein particle complex subunit 3

BHK	Baby hamster kidney cells
BSA	Bovine serum albumin
C11orf59	RhoA activator C11orf59
CANX	Calnexin
CD-FBS	Charcoal-dextran treated fetal bovine serum
CHO	Chinese hamster ovary cells
COR1A	Corronin-1A
CuAAC	Cu^{I}-catalyzed [3+2] azide-alkyne cycloaddition
DHHC-PATs	Asp-His-His-Cys-containing protein acyltransferases
DMEM	Dulbecco's Modified Eagle's Medium
DMSO	Dimethyl sulfoxide
ECL	Enhanced chemiluminescence
EDTA	Ethylenediaminetetraacetic acid
EGF	Epidermal growth factor
EGFP	Enhanced green fluorescent protein
ELISA	Enzyme-linked immunosorbent assay
ER	Endoplasmic reticulum
ESI	Electrospray ionization
FA	Fatty acid
FBS	Fetal bovine serum
GAPDH	Glyceraldehyde-3-phosphate dehydrogenase
Gnax	Guanine nucleotide-binding protein x also known as G proteins
GO	Gene ontology

GRP94	Endoplasmin also known as 94 kDa glucose-regulated protein or heat shock protein 90 kDa beta member 1
H3	Histone H3 and variants
HEK	Human embryonic kidney cells
Hh	Hedgehog precursor protein
HILIC	Hydrophilic interaction liquid chromatography
Hint	Hedgehog/intein domain
hnRNP	Heterogeneous nuclear ribonucleoprotein complexes
HPLC	High performance liquid chromatography
HSA	Human serum albumin
HSP90	Heat shock protein 90
IHC	Immunohistochemistry, immunohistochemical
IP	Immunoprecipitation
IPI	International Protein Index
KIAA0152	Malectin
LAT	Linker-associated with T cell activation
LBR	Lamin B-receptor
Lck	Lymphocyte-specific protein tyrosine kinase
LC-MS	Liquid chromatography-mass spectrometry
MALDI	Matrix-assisted laser desorption/ionization
MARCKS	Myristoylated alanine-rich C-kinase substrate
MPP	Myelin proteolipid protein
MS	Mass spectrometry, mass spectrometric

MudPIT	Multidimensional protein identification technology
MβCD	Methyl-β-cyclodextrin
NMTs	N-myristoyltransferases
NPC	Niemann-Pick disease type C
P/S	Penicillin/streptomycin
p97	Transitional endoplasmic reticulum ATPase
PBS	Phosphate buffered saline (10 mM sodium phosphate, 150 mM NaCl, pH 7.4)
PBST	PBS with 0.1% tween-20
PMSF	Phenylmethylsulfonyl fluoride
PP1β	Serine/threonine-protein phosphatase PP1β catalytic subunit
PP1γ	Serine/threonine-protein phosphatase PP1γ catalytic subunit
PPM1G	Protein phosphatase 1G
PTM	Post-translational modification
PVDF	Polyvinylidene fluoride
Ras	Rat sarcoma small GTPase
RPMI	Roswell Park Memorial Institute
RT	Room temperature (~22 ºC)
SDS	Sodium dodecyl sulfate
SDS-PAGE	Sodium dodecyl sulfate polyacrylamide gel electrophoresis
Shh	Sonic hedgehog
Shh-293T	Stably transfected ecdysone inducible murine Shh secreting 293T cells
Ski	Skinny hedgehog

Snapx	Synaptosomal-associated protein x
TBTA	Tris[(1-benzyl-1H-1,2,3-triazol-4-yl)methyl]amine
TCEP	Tris(2-carboxyethyl)phosphine hydrochloride
TEA	Triethanolamine
TFA	Trifluoroacetic acid
TfR, Tfrc	Transferrin receptor
Txndc1	Thioredoxin-related transmembrane protein 1
VCP	Transitional endoplasmic reticulum ATPase

INTRODUCTION: LIPIDS AND THEIR STUDY

Lipids are essential components of all cells that are unique in their ability to self-assemble, organizing through membrane segregation. They are also unique in their heterogeneity: the lipidome of yeast exhibits several hundred species[1] and hundreds of thousands of variant exist within biology[1]. Matching their biological importance, lipid binding domains are among the most common modular domains of the eukaryotic proteome[2]. In health, alterations of lipid metabolism can lead to diseases as common as cardiovascular disease and obesity, as well as rarer disorders such as Niemann-Pick or Tay-Sachs Diseases. Despite this importance, lipid analysis remains challenging and progress in analytical techniques is greatly needed.

Lipid function

Free lipids

Lipids and their derivatives function in a vast array of cellular functions. In membranes, they are the primary building block, with different membranes exhibiting remarkable compositional variation. Localized membrane domains are important in signaling and other processes such as catabolism and photosynthesis. In metabolism, lipids serve not only as energy storage but also as essential vitamins for many organisms. Some, like the eicosanoids (leukotrienes and prostaglandins)[3] and diacylglycerols are signaling molecules, while others such as sterols serve multiple roles as signaling molecules, nutrient and membrane components. Lipids play a role in all cellular processes from the cell boundary to the catalytic center of some enzymes.

Covalently protein-bound lipids

Lipids are a covalent post-translational modification (PTM) on proteins where they serve to modulate protein localization, activity and signaling. This occurs for a variety of lipids (see Figure 1) including fatty acids (caprylic[4], myristic, palmitic and stearic acids and others) on their *N*-termini, cysteines, serines, threonines or lysines; isoprenoids (farnesol and geranylgeraniol and dolichol) on cysteines; and cholesterol and glycosylphosphatidylinositol on processed C-termini. These post-translational modifications (PTMs) play important roles in eukaryotic physiology and human disease[5]. Lipid modification of proteins typically increases their affinity to membranes and subsequent interaction with other proteins for cell signaling[5,6] (Figure 2). Biologically, known fatty-acylated proteins have wide-ranging roles in cellular proliferation (Ras), lymphocyte activation (Lck) and synaptic transmission (PSD-95)[5], among many others. *N*-myristoylation and *S*-palmitoylation in particular compromise two major mechanisms of protein lipidation by which eukaryotic cells control protein activity spatially and temporally[5]. Partially due to prior limitations in analytical techniques, much remains to be understood about the diversity of lipidated proteins and the mechanisms of their regulation[5]. This research is further complicated by the actions of other PTMs which simultaneous affect the activity of lipid modified proteins. For example, phosphorylation and fatty-acylation work in concert to regulate the activity of MARCKS[7], c-Abl kinase[8,9] and potassium channels[10].

Modification		Modifying group	Example(s)	Modifying enzymes
Fatty-acylation	***Chain(s)***			
N-Myristoylation	14:0	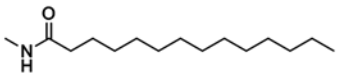	ARFs, MARCKS, S/T kinases, pathogen proteins	NMT1, NMT2
S-Palmitoylation	16:0, 18:0...	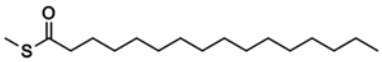	Rases, Wnt-3a, PSD95, Gαs, GAPDH, tubulin isoforms	DHHC-PATs (23), proteins themselves
N-Palmitoylation	16:0, 18:0...	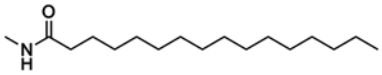	Shh, Spitz, $G\alpha_s$	Hhat (Rasp), protein itself
O-Acylation	14:1, 16:1	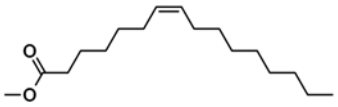	Wnt-3a	Porcupine
O-Capryloylation	8:0	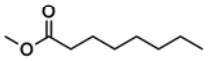	Ghrelin	Ghrelin O-Acyltransferase (GOAT)
O-Caproylation	10:0	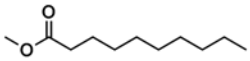	Ghrelin	Ghrelin O-Acyltransferase (GOAT)
Prenylation				
S-Farnesylation		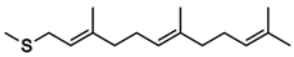	Rases, Rabs, Lamin B, GTP-binding protein Rheb, centromere-associated proteins E and F	FFTase
S-Geranylgeranylation		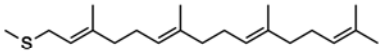	Rases, Rabs	GGTase-I and -II
S-Dolichylation		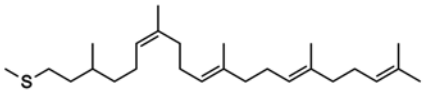	Unknown	Unknown
Other lipidation types				
C-Cholesterylation		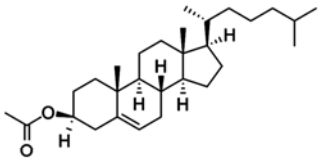	Shh, Hedgehog family	Shh, Hedgehog family
C-Glycosylphosphatidyl-inositolation (glypiation, GPI-anchoring)		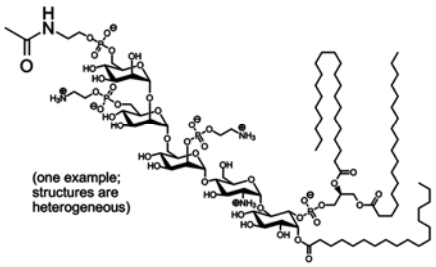	Neural cell adhesion molecule 120 (NCAM-120), prion protein (PrP), erythrocyte acetylcholinesterase, ciliary neurotrophic factor receptor (CNTFR) α subunit	GPI-anchor transamidase complex (five subunits)

Figure 1 Covalent lipid modifications and their structure.

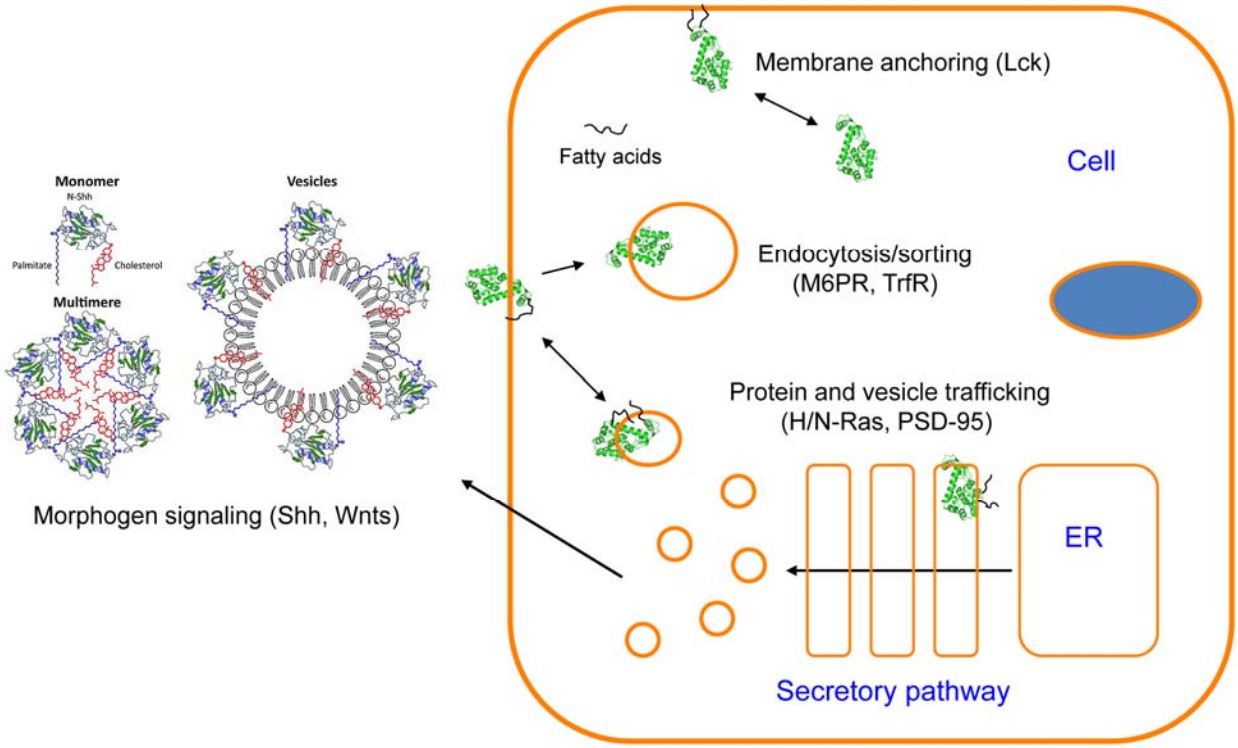

Figure 2 Cellular pathways involving lipid PTMs.

N-Myristoylation is a constitutive cotranslational modification in which myristic acid (14:0) is attached to *N*-terminal glycine residues through the action of *N*-myristoyltransferases (NMTs)[11]. It can also occur post-translationally after proteolytic events which expose new NMT recognition sites. For example, during programmed cell death, the apoptosis effector tBid is *N*-myristoylated after cleavage by caspase-3, resulting in mitochondrial membranes localization during apoptosis[12,13]. Alternative splicing of mRNA transcripts may also yield substrates for *N*-myristoylation, as with the p35 isoform of OCA-B, a transcription factor required for late-stage B cell development[14,15].

Palmitoylation denotes the addition of palmitic (16:0) and other fatty acids onto proteins, most commonly onto a cysteine thiol side chain (*S*-acylation) although other residues including the N-terminus can be modified[16,17]. The terms "palmitoylation" and S-acylation are commonly used interchangeably to indicate modification not exclusive to palmitic acid. The modification is biased to palmitic acid but includes a heterogeneous mix of fatty acids both longer and shorter which can also vary in degree of saturation and oxidation. Stearate (18:0), oleate (18:1), arachidonate (20:4), and eicosapentaenoate (20:5) have all been shown to be incorporated onto palmitoylated proteins[18,19]. The thioester bond of *S*-acylation can be cleaved by hydroxyl amine; this sensitivity is often used to distinguish fatty acylation of cysteine from N-terminal modification. Palmitoylation can occur enzymatically, through a conserved family of Asp-His-His-Cys-containing protein acyltransferases (DHHC-PATs)[20], or by autocatalytic mechanisms intrinsic to a protein. Palmitoylation is unique in its reversibility with two thioesterases known to depalmitoylate. Dissecting the regulatory mechanisms of palmitoylation presents a significant challenge as the 23 DHHC-PATs of humans or mouse exhibit overlapping substrate specificities and have no known consensus sequence[21]. Predictive algorithms based on known sites do exist, but with unknown sensitivity and specificity outside of their training set[22].

Isoprenoid modification, in particular farnesylation and geranylgeranylation, is an irreversible post translational event which occurs at cysteines in the C-terminal region. One farnesyltransferase (FTase) and two geranylgeranyltransferases (GGTase-I and GGTase-II) can transfer one or more isoprenoid moieties to C-terminal cysteines yielding thioether bonds[23-25]. FTase and GGTase-I recognize the consensus sequence CaaX in which *a* is aliphatic the residue *X* determines modification by FTase (A, C, M, Q or S) or GGTase-I (L or F). GGTase-II has no known

consensus sequence[23-25]. Like other lipidation events, isoprenylation causes membrane targeting and mediates protein-protein interactions[23-25].

Protein cholesterylation is currently only known in the hedgehog family of secreted signaling molecules. Its function is known on Sonic hedgehog (Shh), where it restricts the spatial diffusion to generate the morphogen gradients controlling vertebrate development[26,27]. Cholesterol is installed by an autocatalytic processing event of the 45 kDa Shh precursor in which an internal G-C bond in an absolutely conserved GCF tripeptide first undergoes an autocatalytic N to S shift within the so called **H**edgehog/**int**ein (Hint) domain[28], a motif so named due to sequence, mechanistic and three-dimensional structure similarities between inteins and hedgehog protein autoprocessing domain (see Figure 3). The thiol side-chain of cysteine of the GCF tripeptide nucleophilically attacks the carbonyl carbon of G, forming an activated thioester intermediate. Subsequently, the intermediate undergoes a nucleophilic attack by cholesterol and the covalently cholesterylated 19 kDa N-terminal portion of Hh

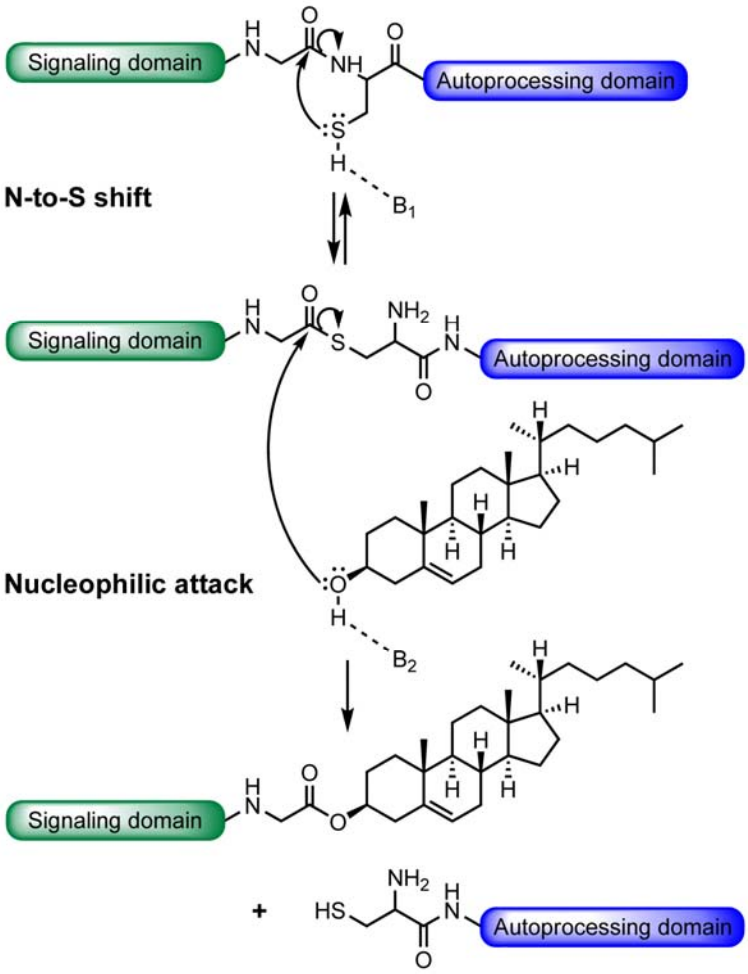

Figure 3 Mechanism of cholesterylation in Shh.

is released. All biological activity is associated with this N-terminal fragment. Cholesterylation null mutants show gross mispatterning and embryonic lethality in *Drosophila* embryos and mutations in humans result in holoprosencephaly[27].

Glycosylphosphatidylinositylation has the most complex structure of lipid PTMs consisting of a phosphoethanolamine linker to the protein, a glycan core, and a phospholipid tail[29]. GPI-anchor modification results in localization to the outer leaflet of the plasma membrane and occurs within a wide variety of biological processes[29]. The exact structure is heterogeneous and species dependent but like cholesterylation, GPI anchors are installed during a proteolytic event. A GPI-transamidase complex recognizes a C-terminal GPI anchor attachment signal with no known consensus sequence and cleaves the signal at the so named omega (ω) site[30]. A preassembled GPI core structure is subsequently attached covalently to the nascent C-terminus[30]. Animals defective in glycosylphosphatidylinositol modification die as embryos[29].

Lipid analysis

Despite their significance, lipids analysis on or off proteins has for decades remained difficult. Progress in chromatography over the last five decades – in particular thin layer chromatography (TLC) and gas-chromatography (GC) – opened the doors to lipid separation and identification[1]. This trend has been built upon by advances in mass spectrometry, in particular matrix assisted laser desorption ionization (MALDI)[31] and electrospray ionization (ESI)[32]. While powerful, these advances are typically applicable only after lipid extraction and often hydrolysis. Deciphering biological function requires identifying what lipids are where within cells, when, and their interactors. A host of techniques have thus been developed for lipid analysis. Strategies for indirect

detection include hydrophobic and fluorogenic membrane dyes (e.g. DiI[33], filipin or 1,6-diphenyl-1,3,5-hexatriene, DPH); lipid-binding proteins either internally expressed or externally applied (lipid binding domains fused to fluorescent proteins[34] or chemically conjugated proteins; a few antibodies also exist); linked enzymatic assays (e.g. cholesterol oxidase) and chemical tools to manipulate lipid levels such as cyclodextrins. Caution must be used with indirect techniques as they have varying degrees of sensitivity to external factors such as membrane composition or lipid accessibility. In addition, indirect techniques may suffer issues of selectivity, commonly interacting with more than one lipid. Alternatively, lipids may be directly detected directly with three different varieties of analogs (Figure 4).

Analysis with radioactivity

The oldest technique for lipid analysis involves radioactive molecules and autoradiography. Fatty acids[35], cholesterol[36] or isoprenoids, or lipid precursors[37], in particular acetate, pyruvate and mevalonate, can be incorporated both *in vivo* or *in vitro*. This approach can reveal lipid localization in tissue slices[38], image lipidated proteins within SDS-PAGE gels[39] or be used to track lipidated proteins through chromatographic separations. For ultra-high resolution imaging, autoradiographic visualization can also be combined with electron microscopy (EM)[40]. Due to their identical chemical nature, radiolabeled reporters most faithfully recapitulate true biological behavior. However, the approach cannot be easily combined with other common analyses such as immunohistochemistry (IHC). It also suffers from long exposure times (often weeks to months, precluding live autoradiography) and the disadvantages of radioactivity. Detection times can be substantially reduced with the use of ^{125}I iodinated lipids[41], but at the cost of changes in structure, additional health exposure and regulatory overhead.

Analysis with analogs

The second and third variations of direct imaging involve chemically modified lipid analogs. Fluorophore-conjugated lipids[42-45] allow immediate imaging of lipids from proteins to organisms. Many fluors have been employed including BODIPY[46,47], NBD[48-50], dansyl[51-53], rhodamine[54], anthracene[55,56], pyrene[57-61], DPH[62], naphthyl[63] as well as others. Likewise, lipid analogss bearing photochemical crosslinking groups[64] can be employed to assay lipid interactions. To enable detection, crosslinking analogs typically contain an additional mark such as radioactivity, an affinity handle or fluorophore. While useful tools, both analog variations are intrinsically limited by the alteration of relatively small lipids[44]. Added fluorophores are often larger than the molecules to which they are fused and can greatly alter essential properties such as hydrophobicity and charge. These changes can result in altered biological behavior[44,65] such as lipid sorting by differential partitioning[66,67] or endogenous lipid recognition. For example, NBD-cholesterol has been shown to orient itself "up-side-down" with the 3β-hydroxyl pointing into the membrane[68] and with other BODIPY-[69] and NBD-labeled[50] lipids, fluors exist "looped back," preferring the surface rather than the membrane interior, apparently in reflection of additional polarity. Such interference has led to fluorescently labeled lipids being termed "ill-suited" to the study of lipid microdomains[67].

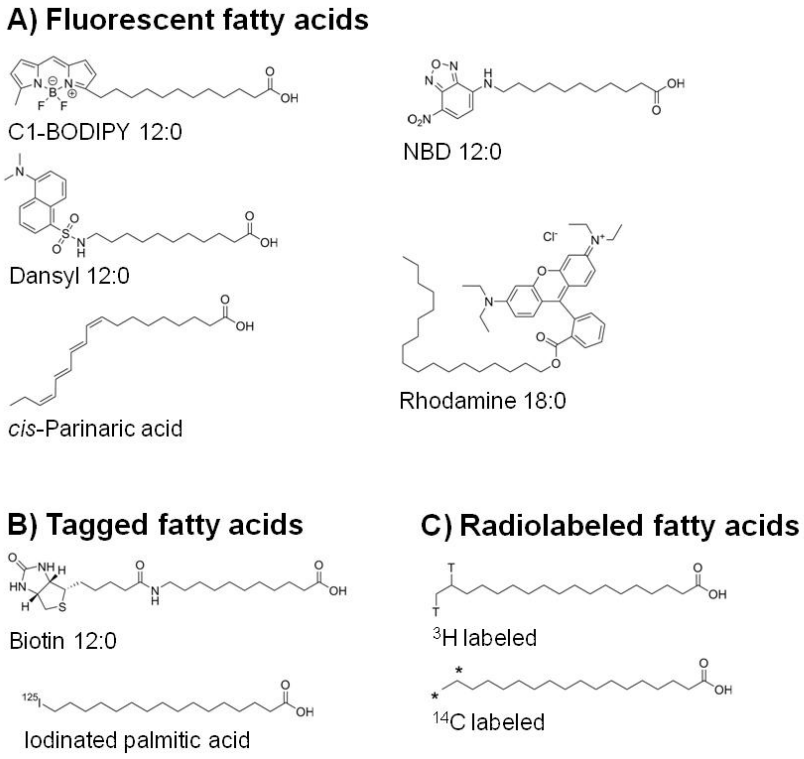

Figure 4 Classes of marked or modified lipids. Fluorescent (A) or tagging (B) modifications can cause large perturbations in biological or chemical behavior. Radiolabeling (C) suffers from long exposure times, but are the most faithful analogs.

Analysis with intrinsically fluorescent analogs

Intrinsically fluorescent lipids such as the dehydroergosterol (DHE)[70-73] or polyenes like the naturally occurring *cis*-parinaric acid[74], pentaene-carboxlic acids[75,76] or didehydrogeranylgerany[77] provide more faithful fluorescent reporters. However, DHE and parinaric acid suffer from low quantum yield, rapid bleaching and ultra-violet (UV) excitation and emission, thus necessitating specialized, UV-transparent imaging equipment[78]. Conjugated pentaene analogs are sufficiently red-shifted to allow imaging with standard optics, but still suffer from rapid photobleaching and require two-photon excitation to minimize fluorophore damage[75]. These non-ideal photochemical

properties often compel cellular loading with reporter concentrations sufficiently high that atypical pathways may be preferred[79]. In addition, while autoflorescent analogs maintain more structural similarity than analogs fused to fluorophores, even subtle alterations such as the presence or absence of a methyl group[80,81] or *cis* versus *trans* stereochemistry[82,83] can significantly alter biological function. Indeed, the additional rigidity imposed by conjugated desaturation has been observed to modify both membrane structure and biological behavior: DHE disturbs membrane lipid packing density at concentrations of >1 mol%[68] and is esterified >7-fold more rapidly than [^{3}H]cholesterol[84]; parinaric acid remains essentially unesterified in fibroblasts[83] and can be cytotoxic[85]; and didehydrogeranylgeranyl is incorporated 60% as effectively as geranylgeranyl[77].

BIOORTHOGONAL CHEMICAL TECHNIQUES

The disadvantages of indirect labeling (dependence on multiple factors and accessibility) and direct labeling (alteration of properties) can be circumvented by directly marking the molecule of interest with a small, specifically reactable chemical handle which causes minimal alteration in cellular behavior. In this bioorthogonal strategy, the third strategy using analogs, reporter molecules are first metabolically incorporated, allowing proper metabolism and localization. Subsequently, the chemical handle is interrogated to covalently add tags for visualization or affinity retrieval. These are typically fluorophores, some of which are fluorogenic, or common affinity tags such as biotin, which can be probed with Western blots or used in affinity retrieval. Especially for lipids, it must be noted that the advantage of similar biochemical behavior is likely abrogated after addition of visualization tags. The application of bioorthogonal chemistry to live lipid analysis[86] thus necessitates great attention to behavior before and after analog modification. Table 1 contrasts bioorthogonal approaches with intrinsically labeled molecules.

Bioorthogonal techniques require unique constraints within chemical reaction space and have only recently been introduced. The reaction must occur in cellular environments (i.e. at physiological temperature and pH within aqueous solutions containing salts, nucleophiles and oxygen); it must be highly specific, not reacting with the functional groups present in cells; it must proceed efficiently at very low concentrations; the reaction must occur in a biologically relevant time frame (seconds to hours); it must be irreversible; and the chemical handle must be biologically inert (bioorthogonal): it must not be metabolized by the cell, not present within the cell, nor alter cellular recognition or metabolism. These very specific bioorthogonal needs have been best met

by two general chemistries: the Staudinger reaction and Huisgen azide-alkyne cycloadditions (Figure 5).

Table 1 Contrasting properties of bioorthogonal probes and tagged analogs.

Attribute		**Tagged molecules**
Size	Small change	Usually much larger (excepted by intrinsically fluorescent analogs)
Hydrophobicity	Very little difference	Similar to very different
Charge	No change	Same to reversed charge
Overall chemical similarity	Generally similar to native molecules (but substantially altered after click reaction)	Generally different
Live imaging	Limited; usually stepwise or cell exterior	Usually possible (tag dependent)
Biocompatibility	Tolerated as part of an organic molecule	Tag dependent
Orthogonality	Absent (N_3) and infrequent (–≡)	Usually absent (although autofluorescence or pigments can interfere)
Reaction specificity	Specific with low background	No reaction after incorporation
Modularity	Highly modular	Limited
Synthetic accessibility	Relatively accessible	Tag dependent

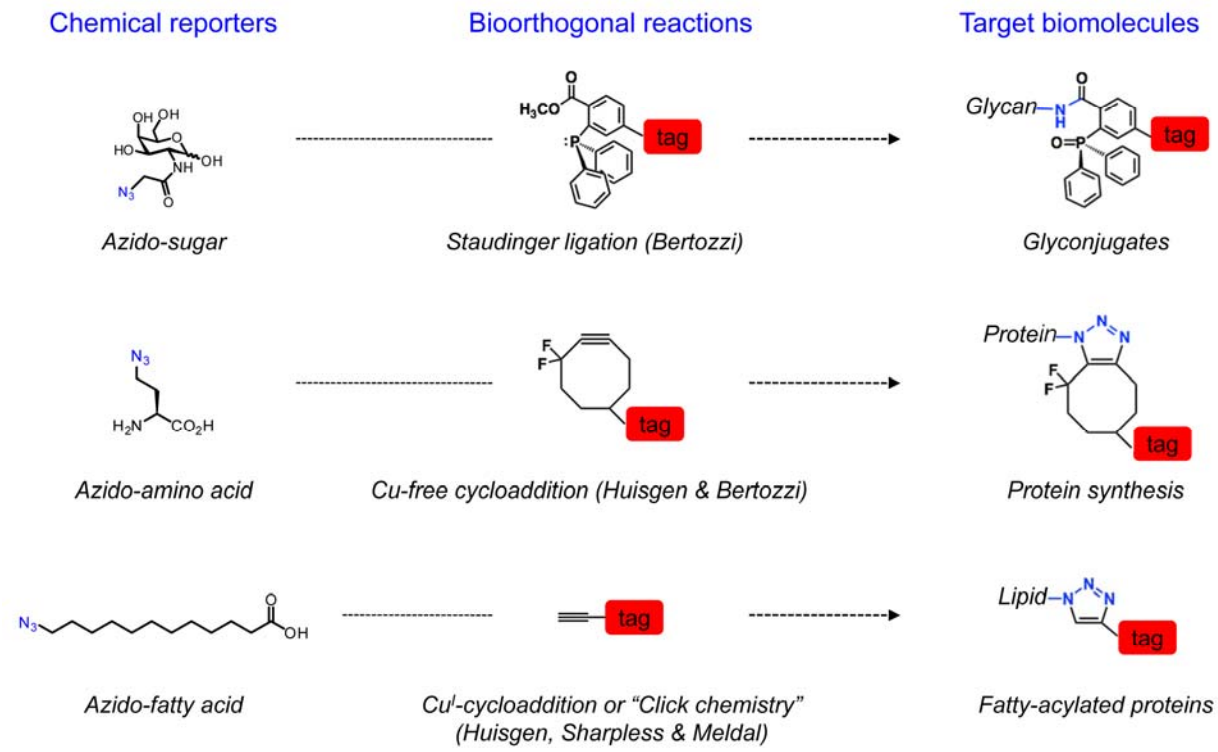

Figure 5 Bioorthogonal chemistries in various applications.

The Staudinger reaction

Bioorthogonal chemistry was pioneered by the Staudinger reaction in 2000 by Bertozzi and coworkers, who employed the selective reaction between a modified phosphine and an azide in biological conditions[87]. Through rearrangement of an aza-ylide intermediate, a stable amide bond results between the oxidized phosphine reagent and the azide bearing analog (Figure 5). Due to the phenylated phosphine size and hydrophobicity, analogs employed for bioorthogonal chemistry using the Staudinger reaction carry an azide. In the original application, metabolic incorporation of N-azidoacetylmannosamine (ManNAz) in HeLa and Jurkat cells labeled surface glycans, which were then reacted with a biotin derivatized phosphine and visualized with fluorescent avidin. The reaction has been further expanded by the development of a "traceless" version, in

which amide bonds are formed with exit of the phosphine[88]. Multiple phosphine reagents have been developed including fluorogenic dyes which remain quenched until reacting including a coumarin derivative[89] and a fluorescein compound[90] initially silenced by a fluorescence resonance energy transfer (FRET). The phosphines have a distinctive smell but are not particularly toxic and have been applied to live cells[90,91] and in mice[92]. Within lipids, the Staudinger reaction has since been applied to fatty acids[93-99], isoprenylation[100-105], targets damaged by lipid peroxidation[106], gangliosides[107] and ceramide synthesis[108]. Despite the large body of work, the reaction suffers from relatively slow reaction kinetics and sensitivity of the phosphine to air oxidation[109]. Unfortunately, success in improving phosphine reactivity also increased rates of oxidation[109] and other bioorthogonal chemistries have been consequently sought.

Click chemistry and Cu^{I}-catalyzed [3+ 2] azide-alkyne cycloadditions (CuAAC)

Shortly after the biological application of the Staudinger reaction, in 2002 Meldal and coworkers[110] as well as Sharpless and coworkers[111] discovered that copper(I) can catalyze Huisgen azide-alkyne cycloadditions to give 1,4-disubstituted 1,2,3-triazoles (Figure 5). The reaction proceeds in aqueous conditions at room temperature rapidly with high yield and was illustrated on proteins, nucleic acids and sugars. The field of Cu^{I}-catalyzed [3+ 2] azide-alkyne cycloadditions (CuAAC) has since exploded[112-114] with applications of terminal alkyne and azide analogs applied to all classes of biological building block. While it is only one of a family of reactions exhibiting the modular philosophy and properties of "click chemistries,"[115] the ease and widespread applicability of Huisgen azide-alkyne cycloaddition have lead it to it commonly being known by the "click chemistry" moniker. The cycloaddition was advanced by the development of copper ligands that increase reaction kinetics catalyst stability[116,117] and CuAAC has been applied to fat-

ty acids[94,96-98,118-123], isoprenoids, cholesterol[124], choline[125], phospholipids[86] and azido diacylglycerol (DAG)[126]. Despite its utility, the metal-catalyzed cycloaddition remained limited by the requirement of cytotoxic copper which prevented live imaging that remained possible using the Staudinger reaction.

Strain promoted alkyne-azide cycloadditions (SPAAC)

Consequently, in 2004 Bertozzi and coworkers developed a copper-free version of azide-alkyne cycloaddition catalyzed by the strain of a cyclooctyne[127] (Figure 5), the smallest stable cycloalkyne, and illustrated its use again on glycans[128]. Strain-promoted alkyne-azide cycloaddition (SPAAC) generates the same triazole ring and has been further developed with more stable and more reactive cyclooctyne derivatives[129-131]. The lack of copper lends it particularly well to *in vivo* imaging and the strategy has been applied to live visualization of a phosphatidic acid analog[132] and to surface proteins bearing azido caprylic acid (Az-8)[133].

Considerations in choice of bioorthogonal chemistries and reaction pairs

Owing to its fast kinetics, CuAAC has been found to be more rapid and sensitive in the detection of bioorthogonal probes[129] and in particular with lipid analogs[94,97]. Both the Staudinger reaction and SPAAC can both be used in live imaging to circumvent copper toxicity, although the stability of reagents in click chemistry reactions increases its appeal. In click chemistry, reacting alkyne analogs with azido probes produced a lower background than the respective reaction with azido analogs and alkyne probes[94,134,135] but the side products remain unknown. Many SPAAC reagents are exceedingly hydrophobic and we have found them poorly suited to work on cell interiors or permeabilized cells: they tend to function as dyes rather than reagents which can be

washed away. Fluorogenic reagents, in particular coumarin derivatives, are appealing possible alternatives to reduce such background[86,89,118].

The biology and chemical properties of bioorthogonal handles

Both click chemistry and the Staudinger reaction employ azides and many analogs modified either with an azide or alkynes have been synthesized and employed (Table 1 and sections below). As for all modified molecules, consideration must be given to their possible biological presence, their potential biological activity and the possibility for change in alterations in chemical behavior.

The azide in biology

The azido group is unique within organic chemistry for its ease of introduction and reactivity. Azides are typically added with well-established nucleophilic substitution or azo transfer reactions and can be substituted for a methyl. As an anion, the azide displays toxicity similar to cyanide and, perhaps consequently, is virtually non-existent within biology[136]: exactly one azido containing product from a dinoflagellate[137] is listed in the *Natural Products Dictionary* and 2-amino-3-azidopropanoic acid can be produced by *Salmonella* in the presence of azides[138]. In contrast, synthetic organic azides have for decades functioned as photolabile probes[64] and appear to be biologically well tolerated: 12-Az-12 causes no cellular toxicity in CEM cells[139] and multiple azido-derivatized fatty acids support the growth of *E. coli*[140,141], *pseudomonad*[142] and *S. cerevisiae*[143] fatty acid auxotrophs. In our own work, we have not observed toxicity of azido fatty acids up to 100 μM in Jurkat, HeLa, RAW and DC2.4 cells. However, caution must always be used as toxicity of azido derivatized sugars has been observed[144], 12-Az-12 was found to be an inhibitor of HIV replication[139] and it inhibits mitochondrial phosphate uptake at 100 μM[145]. Likewise, organic azides are part of four bioactive, FDA approved drugs (3′-azidothymidine, an anti-HIV; Azidocillin and Azidamfenicol, antibiotics; and zidometacin, an anti-inflammatory). Metabolism

of aryl azides has been observed in yeast[143] and the reduction of aryl azides to amines was seen after *ex vivo* exposure to mouse liver microsomes[146].

The alkyne in biology

Contrasting the biological absence of azides, alkynes are found in a large diversity of natural products from fungi, moss and lichens, plants, marine algae, tunicates, sponges, insects, frogs and in traces quantities, even in mammals[147]. Plants, mosses and fungi in particular can accumulate high concentrations of alkynyl lipids, and, of the >2000 polyacetylenes known, more than 1100 are found in the plant family *Asteraceae* (the aster or sunflower family)[147]. Acetylenic groups are found both internally and at molecule terminals[148,149]. Both natural and synthetic alkyne lipids have been shown to have anticancer[148], antibacterial, antifungal, anti-HIV and pesticidal activities[150]. Several alkyne-containing compounds, including ethynylic steroids, are approved drugs and various acetylenic compounds are known to inhibit monoamine oxidases A and B, aromatase, cytochrome P450 isozyme families including 1A, 3A and 22A, and thymidylate synthetase[151]. Others serve as cholinergic and muscarinic agents[151]. Terminal alkyne compounds, in particular 17-octadecynoic acid (ODYA) or alk-16, are known irreversible mechanism-based inhibitors of plant[152] and mammalian[153-155] fatty acid ω-hydroxylases, as well as P450 hydroxylases[156,157]. Alk-16 is unable to support growth of unsaturated fatty acid auxotrophs of *E. coli* or *S. cerevisiae* although the fatty acid was found in membranes and could be esterified[158]. The equivalent experiment with saturated fatty acid auxotrophs was not performed, however the myristic acid analog alk-12 is a better substrate for *S. cerevisiae* N-myristoyl transferase than myristic acid[159]. In our hands, with Jurkat, HeLa, RAW and DC2.4 cells, alkyne fatty acids up to 100 μM show the same overt lack of toxicity as azido fatty acids but we did not examine possi-

bly inhibited enzymes. Synthetic acetylenic analogs can be made through synthesis of an analog desaturated at a terminal secondary-primary carbon pair, or by the addition of an ethynyl to an accessible atom. Alkyne synthetic schemes can be more complicated than their equivalent azides due to the requisite alteration in carbon-carbon bonds, although not necessarily, as an ethynyl might also be added to a heteroatom.

Chemical properties of azides and alkynes

Like the cyano (–C≡N), the atoms of acetylene (–C≡CH) and azido (–$N=N^+=N^-$) groups exist within a π electron rich cylinder. An acetylene group attached to a carbon forms a linear array of four atoms which emanate at the angle of the originating carbon hybridization; azides in contrast are bent slightly off axis with a C-N^1 angle of around 120°. Due to the linear alignment, the distance from a terminally ethynylated carbon to the final hydrogen of the acetylene (3.72 Å) is actually longer than the corresponding maximum distance of an ethylated carbon to one of its terminal hydrogens (3.06 Å) despite the shorter carbon-carbon bond (1.21 Å vs. 1.54 Å). For lipids, this linear "kink" and its position can have significant implications for enzyme recognition[159] and membrane function: only three of 16 isomers, 7-, 8- and 10-octadecynoic fatty acids, can support growth of an *S. cerevisiae* unsaturated fatty acid auxotroph[158]. Unlike ethynyl groups, azides are mostly – but not perfectly – linear, and must be terminal, while alkynes can exist within a hydrocarbon chain. In length, azides are shorter than an ethynyl group yet still slightly longer than an ethyl group (3.29 Å from the azido bearing carbon to the last nitrogen). Both functions are relatively nonpolar: the dipole moment for phenylazide (C_6H_5-N_3) is 1.44 D and for phenylacetylene (C_6H_5–C≡CH) 0.66 D[160]; these values contrasts to benzonitrile (C_6H_5–C≡N) at 4.05 D. Both groups have a similar effect on water solubility: at 25 C, phenylazide is soluble to 4.2 mM[161] and

phenylacetylene to 4.46 mM[162] (these values contrast with benzene at 22.1 mM[163]). The molecular volume of both functional groups is small: the conformational preference ($-\Delta G°$) for the equatorial position of cyclohexane is 1.70 kcal/mol for a methyl ($-CH_3$); 1.75 kcal/mole for an ethyl ($-CH_2-CH_3$); 0.48 ± 0.07 kcal/mol for an azido[164]; and 0.41 ± 0.05 kcal/mol for an acetylene group[165].

Thus, azides and acetylenes are around the length of an ethyl group (and are both linearly longer) but occupy less volume and are rigid. They are more polar, but not drastically so, and more reactive, though stable under typical physiological temperatures and solvent conditions (aqueous solutions around neutral pH containing many dissolved salts and other substances). Neither adds charge and they are usually biologically stable. However, both stability and unexpected biological effects should be studied; the careful controls required to exclude side-effects remains unexamined for many published analogs. Alkynes and azides thus offer a good opportunity to faithfully recapitulate cellular localization, metabolism and enzyme recognition, while offering chemical reactivity.

Bioorthogonal lipid probes

A wide variety of alkyne and azide probes have been described for many lipid classes. In particular, owing to their synthetic accessibility and utility in photocrosslinking, a wide variety of azido (especially aryl-azide) lipid analogs have been published. For decades, they have been employed to identify lipid-binding proteins or membrane domains. Reported azide and alkyne lipid analogs include saturated and unsaturated fatty acids, isoprenoids, glycosides, 4-hydroxynonenal (HNE, a byproduct of unsaturated lipid peroxidation) sterols and sterol derivatives, sphingosines, ceramides and diacylglycerol. However, only a few have been subsequently utilized in bioorthogonal chemical investigations. In those cases, frequently a corresponding alkyne has been synthesized due to background labeling issues. The pair also serves as an internal control, similar to N- and C-terminal tagging with fluorescent proteins.

Probes for fatty acids

Azido and alkyne fatty acid probes from 10 to 18 carbons in length have been described and employed using both the Satudinger reaction and CuAAC with fluorescent and Western blot detection (see Table 2). The relative activity of az-12 and alk-12 was previously studied in depth for *S. cerevisiae* NMT (~140% and ~100%-120% relative to myristic acid, respectively[139,159]) and subsequent studies have employed well studied, known fatty-acylated proteins such as Lck[93,94,119,120], various forms or fusions of Ras[94,118,119], LAT[94,119] GAPDH[118,119] to validate proper incorporation. Direct comparison of alkyne and azido analogs of myristic acid (alk-12 and az-12) as well as stearic acid (az-15 and alk-16), revealed very similar incorporation profiles indicating that the orientation has little influence on cellular recognition of fatty acids[94]. In contrast, work to isolate palmitoylated mitochondrial proteins revealed a large discrepancy between iodopalmitoyl

CoA and az-14[95], indicating that the large halogen alters cellular processing. As described below, these probes have been applied to visualizing fatty acids in membranes and on proteins, as well in discovering the identity of fatty-acylated proteins.

Probes for isoprenoids

Geranyl[103,105,166], farnesyl[101,105,167] and geranylgeranyl[102,168] analogs have been described in both azido and alkyne varieties (see Table 3). FTase and GGTases can show both substrate tolerance[100] and specificity, allowing some degree of control over the prenyl analog incorporation[104]. In contrast to fatty acid probes, several analogs incorporate hetero atom changes in their backbone; despite the change in hydrophobicity, this alteration seems to be well tolerated such as for alk-FFP and Alk-GPP1[166,167], though not always, as in the case of GPP2, which was ineffective at displacing the natural substrate[100].

Probes for other lipids

A propargyl analog of choline[125] and analogs of phosphatidic acid[132] have also been described (See Table 4). Metabolic labeling with propargylcholine resulted in biosynthetic incorporation into phospholipids which were incorporated into expected classes of lipids in CHO cells with similar efficiency to choline[125]. The three phosphatidic acid analogs include a cyclooctyne derivative which allowed live visualization of membranes in cell culture using a fluorogenic coumarin azide[132] but no comparison of analog with native phosphatidic acid. The phosphate of all analogs was capped with a S-acetylthioethyl group (SATE) which is rapidly cleaved in living cells by esterase to release the free phosphate[132].

Table 2 Bioorthogonal probes of fatty acids and their applications

Structure	Probe	Rxn.		Incorp.			Prot.		Detection				Application	Ref.
		Staudinger	CuAAC	*In vivo*	*Ex vivo*	*In vitro*	Population	IP	On blot (Western)	In gel fluorescence	Histochemical	Mass spectrometric		
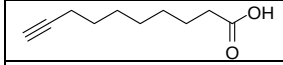	Alk-8		x	x					x				Visualization of protein short chain acylation in PC3 cells	121
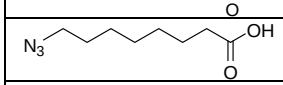	Az-8		SPAAC										Surface labeling of proteins engineered to be labeled with microbial lipoic acid ligase (LplA)	133
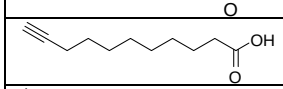	Alk-9		x	X					x				Visualization of protein short chain acylation in PC3 cells	121
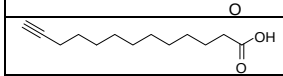	Alk-11		x	x					x				Visualization of protein short chain acylation in PC3 cells	121
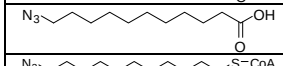	Az-11	x	x	x				x	x				NMT-mediated tagging of overexpressed proteins in *E. coli*	97,98
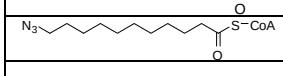	Az-11-CoA	x	x			x		x	x				NMT-mediated tagging recombinant peptide	97,98
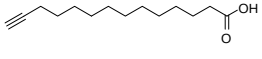	Alk-12		x	x			x	x	x	x	x		Visualization of protein myristoylation in multiple cell lines and myristic acid in HeLa cell membranes	94
			x	x			x		x		x		Visualization of protein myristoylation in PC3 cells	121
			x	x				x	x				NMT-mediated tagging of overexpressed proteins in *E. coli*	97
			x	x			x	x	x				Visualization of protein myristoylation in Jurkat cells with and without apoptosis and COS-7 cells overexpressing EGFP fusions	118
			x	x			x	x	x	x		x	Large scale ID of myristoylated proteins and their validation in fully solubilized Jurkat cells	119
			x	x			x	x		x			Determination of palmitoylation turnover in Jurkat cells	120
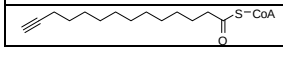	Alk-12-CoA		x			x							NMT-mediated tagging recombinant peptide	97

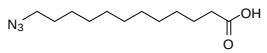	Az-12	x		x			x	x					Visualization of protein myristoylation in RAW264.7 cells	93
		x	x	x			x	x	x	x	x		Visualization of protein myristoylation in multiple cell lines	94
		x		x			x	x	x				Visualization of myristoylation on proteins predicted to be post-translationally modified during apoptosis	96
			x	x			x	x	x	x		x	Large scale ID of myristoylated proteins and their validation in fully solubilized Jurkat cells	119
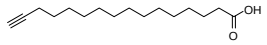	Alk-14		x	x			x		x	x			Visualization of protein myristoylation/palmitoylation in multiple cell lines	94
			x	x					x		x		Visualization of protein myristoylation/palmitoylation in PC3 cells	121
			x	x			x	x	x	x		x	Large scale ID of myristoylated/palmitoylated proteins in fully solubilized Jurkat cells their validation	119
			x	x			x	x	x				Visualization of protein myristoylation/palmitoylation in Jurkat cells, COS-7 cells overexpressing EGFP-Ras fusions and RAS IPed from mice	118
													Visualization and identification of bacterial lipoproteins from *E. coli*	169
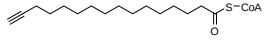	Alk-14-CoA		x			x							NMT-mediated tagging of peptide	97
			x			x			x	x			Visualization of protein palmitoylation on autocatalytic HMGCS and GAPDH	118
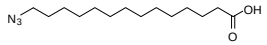	Az-14	x		x			x		x				Visualization of protein myristoylation/palmitoylation in RAW264.7 cells	93
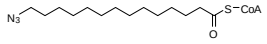	Az-14-CoA	x			x	x			x				Identification of mitochondria protein palmitoylation through chromatographic separation followed by protein ID	95
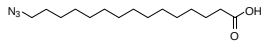	Az-15	x		x			x	x					Visualization of protein palmitoylation in RAW264.7 cells	93
		x	x	x			x	x	x	x	x		Visualization of protein palmitoylation in multiple cell lines and stearic acid in HeLa cell membranes	94
			x	x			x	x	x	x		x	Large scale ID of palmitoylated proteins and their validation in fully solubilized Jurkat cells identifying	119

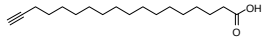	Alk-16		x	x			x	x	x	x	x		Visualization of protein palmitoylation in multiple cell lines and stearic acid in HeLa cell membranes	94
			x	x			x		x		x		Visualization of protein palmitoylation in PC3 cells	121
			x	x			x			x		x	Large scale ID of palmitoylated proteins from Jurkat cell membranes and their validation by overexpression	122
			x	x			x	x	x	x		x	Large scale ID of palmitoylated proteins and their validation in fully solubilized Jurkat cells	119
			x	x			x	x		x		x	Large scale ID from DC2.4 dendritic cells	123
			x	x			x	x		x			Determination of palmitoylation turnover in Jurkat cells	120
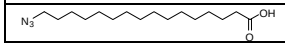	Az-16	x		x			x		x				Visualization of protein palmitoylation in RAW264.7 cells	93

Table 3 Probes for isoprenyl lipids.

Probe	Staudinger	CuAAC	*In vivo*	*In vitro*	Population	Purified prot. or IP	Peptide	On blot (Western)	Fluorescence	Mass spectrometric	Application	Ref.
Az-FPP1	x		x		x	x		x		x	Visualization of farnesylation in COS-1 cells and identification of 18 modified proteins	101
	x			x			x				N-terminal geranylation of peptide by FTase	105
Az-F-OH	x		x					x		x	Visualization of farnesylation in COS-1 cells and identification of 18 modified proteins	101
Az-GPP	x			x			x				N-terminal geranylation of peptide by FTase	103,105
Az-GPP1 (APO-GPP)	x			x		x	x			x	Geranylation of peptides and proteins by FTase.	100
Az-GPP2 (AAA-GPP)	x			x		x	x			x	Geranylation of peptides and proteins by FTase.	100
Az-GG-OH		x	x		x				x		Identification of geranylgeranylated proteins through 2D gel separation and identification	102
		x	x		x				x		Visualization of geranylgeranylated proteins	168
Az-GGPP		x		x					x		Visualization of geranylgeranylated proteins in HEK293A and mouse tissue cells	104
Alk-GPP		x				x					Geranylation of eGFP for FRET between added fluorophore	166
Alk-FPP1		x		x					x		C-terminal farnesylation for subsequent covalent attachment	167
Az-FPP2	x	x		x					x		C-terminal farnesylation for subsequent covalent attachment	167

Table 4 Probes for other lipids.

Probe	In vivo	CuAAC	SPAAC	Application	Ref.
Alk-Cho	X	X		Imaging choline phospholipids in CHO cells and mice.	[125]
Alk-PA1	X	X		Imaging lipid distribution in cells.	[132]
Alk-PA2	X	X			[132]
Calk-PA	X		X		[132]

Applications of lipid bioorthogonal chemical reporters

Visualization of lipids in membranes

The application of bioorthogonal chemistry to the study of lipids in cells and their membranes is one of the most promising advances in lipid imaging. The Staudinger reaction and click chemistry allow work with stable, nonradioactive lipid analogs with high sensitivity which do not suffer the disadvantages of bulky fluorophores and which are relatively unperturbed. Likewise, the need for specialized UV transparent microscopes is negated and analysis is made both accessible and rapid. This approach has been applied to myristic and stearic acids, imaged with rhodamine addition by CuAAC in HeLa cells revealing strong, detergent (0.1% triton X-100) and methanol sensitive membrane labeling[94].

Propargyl choline was imaged in CHO cells and in mice[125]. In both cases, membrane structures such as the plasma membrane were clearly labeled[125]. The use of regents of different cell permeability (fluorescently tagged streptavidin and Alexa Fluor 568) also allowed distinction between surface and internal analog[125]. As for fatty acids, choline analog did not colocalize with any one subcellular markers in CHO cells[125], likely a reflection of the complex composition of cellular membranes and their fast diffusibility. Supporting techniques used to analyze lipid rafts, different detergents had marked effects on labeled lipid: tween-20 does not alter the signal of fatty acid analogs[94], but triton X-100 is sufficient to remove membrane signal completely for fatty acids or choline containing lipids[94,125].

Phosphatidic acid imaging by the three different reporters yielded similar images in RAW cells whether by CuAAC after fixing or by live imaging SPAAC with the cyclooctyne. The reporters remains membrane bound after reaction in live cells, however no further study was done to determine the effect of reaction[132] and the subcellular localization of any analog has not yet been examined.

Visualization of lipid PTMs on isolated proteins

Bioorthogonal chemistry provides a convenient and nonradioactive alterative to determine if a particular protein of interest is lipidated both *in vivo* and *in vitro*. Purified proteins can be modified in reconstituted enzymatic reactions or proteins can be immunoprecipitated (IPed) following metabolic incorporation and reacted while held on the solid phase. Such analyses have been performed for multiple fatty acylated proteins including Ras, LAT, Fyn, PAK2, Lck and others from cells[93,94,96,118-120,123] or animals[118], as well as for prenylation: isolated proteins have been examined for farnesylation (Ras and Hdj-2[101]), geranylation[100,166] and geranylgeranylation (progerin in the study on Hutchinson-Gilford progeria syndrome[168]). Immunoprecipitation and in-gel fluorescence combined with mutational analysis is helpful to establish the exact residues of modification. In the case of IFITM3, a HA-tagged overexpression was studied to establish the role of palmitoylation in membrane clustering necessary for activity[123]. As an alternative to antibodies, a His tag can also be employed, as was done to verify a tagged, overexpressed bacterial lipoprotein[169]. Visualization has been achieved by the Staudinger reaction[93,94,96-98,100,101] or CuAAC[94,97,98,118-120,123,166,168,169]. SPAAC has also been employed to visualize a specific engineered protein in the unisolated environment of a cell surface[133]. Validation of protein lipidation status may alternatively be achieved by transient overexpression, reaction and examination of signal, as

was done by in-gel fluorescence for the validation of many candidate palmitoylated proteins identified by mass spectrometry[122] or on blot in the overexpression of EGFP-Ras fusions in COS-7 cells[118]. Finally, an expected site of lipidation can be fused to proteins such as GFP for subsequent IP, reaction and detection, or for live fluorescence microscopy. This technique was taken to validate 15 proteins predicted to undergo post translational myristoylation during apoptosis[96] and benefits from the use of general IP reagents as well as the ability to examine *in vivo* membrane localization. Visualization of fatty-acylation on isolated proteins has allowed radioactivity-free study of the turnover of palmitoylation[120].

Visualization of lipid PTMs in proteomes

Visualization of lipid PTMs during cell state and comparison of preferences have been globally surveyed. Fatty-acylation machinery preference for various fatty acid chain lengths from myristic to stearic acids has been surveyed on blot with the Staudinger reaction in RAW[93] and Jurkat cells[94]. The profile of palmitoylated mitochondrial proteins has also been profiled on blot after *ex vivo* az-14-CoA incorporation[95]. Alkyne analogs from myristic to stearic acids (alk-12, alk-1 and alk-16) were directly compared to their azido counterparts (az-12 and az-15) using CuAAC with in-gel fluorescence[94]. Many cell lines were profiled, each showing uniqueness as well as commonalities suggesting both common pathways and distinctive regulation of fatty-acylation[94]. Both on-blot and in-gel, it was shown that the signal of NMT labeled proteins, which are preferentially labeled with shorter length fatty acid chains, remains after treatment with hydroxylamine, which cleaves the thioester bonds of proteins palmitoylated with longer fatty acids[93,94,121]. A later study extended the range of short chain fatty acids downward to include alk-8, alk-9, and alk-11[121]. In PC3 cells and it was discovered that signal from shorter chain lengths are hydroxyl-

amine sensitivity[121], consistent with proteins such as acyl carrier proteins that are covalently attached to shorter length fatty acids attached via thioester bonds[170]. Bacterial chain length preference was also surveyed, showing that the palmitic acid analog alk-14 was best incorporated onto proteins in *E. coli*[169]. Using the Staudinger reaction, post-translational myristoylation in Jurkat cells has been examined during apoptosis[96,118], leading to validation of proteins with newly exposed NMT sites[96]. Jurkat cell geranylgeranylation has been profiled with CuAAC, one and two-dimensional electrophoresis and in-gel fluorescence[102] as well as in mouse embryo fibroblasts[168], and farnesylation was visualized by the Staudinger reaction and blotting in COS-1 cells[101].

To image the localization of fatty acylated proteins in cells, two studies have employed CuAAC in histochemical examination in HeLa cells[94], PC3, RAW264.7 and mouse fibroblast L-cells[121] using clickable analogs from myristic to stearic acid. Methanol or triton X-100 have been employed to remove membrane lipids, leaving behind fixed proteins which were then visualized. While no particular colocalization with any subcellular marker was observed[94,121], both studies found that fatty-acylated proteins are distributed in vesicle and membrane like structures, consistent with membrane targeting of this class of PTM. Interestingly, in PC3 cells, the cleavage furrow formed during cytokinesis is rich in palmitoylated proteins[121], indicating a function for fatty-acylation in the segregation events of membranes and other cellular materials during cell division. Also notably, during interphase, distinctive colocalization of tubulin and palmitoylation was occasionally pronounced[121], perhaps providing insight into the function and timing of tubulin palmitoylation[171].

Identification of lipid-modified proteins

The ability of bioorthogonal chemistry to attach an affinity handle after incorporation offers an obvious advantage to more traditional biochemical isolations such as analog-biotin fusions. Bioorthogonal techniques have been used to study fatty-acylation[122], farnesylation[101] and modification by 4-hydroxynonenal (HNE)[106,172] (a reactive unsaturated α,β aldehyde generated during reactive oxygen species (ROS) damage by peroxidation of polyunsaturated fatty acids (PUFA) which attacks cellular nucleophiles). In such analyses, metabolically lipidated proteins are labeled with a biotin secondary reagent and captured on streptavidin. Due to the very high affinity of the streptavidin biotin interaction, proteins can be identified by on-bead digestion with trypsin[101,106,122] and subsequent mass spectrometric identification. An alternative has been developed in the form of a photocleavable linker, but this requires the use of glass beads and induced noticeable UV degradation of UV-eluted proteins[172].

In fatty acid analysis, alk-16 (ODYA-17) and CuAAC were applied to identify palmitoylated proteins from Jurkat cell membranes by on-bead digestion and MudPIT proteomics[173]. 125 proteins were identified with high confidence including known GTPases, G-protein-subunits and receptors[173]. Of the many new candidate fatty-acylated proteins, a previously unknown family of uncharacterized serine hydrolases termed FAM108 was discovered; for this family, palmitoylation determines plasma membrane localization[173]. Although alk-16, a stearic acid analog, was used, many N-myristoylated proteins were also selectively retrieved[173], consistent with metabolic processing and fatty-acylation heterogeneity. Azido-farnesyl fed to COS-1 cells and subsequent application of the Staudinger reaction resulted in the identification of 18 putatively farnesylated proteins[101]. Likewise, alkyne[106,172] and azide[106] HNE identified multiple proteins tar-

geted by HNE. These included proteins involved in stress response[106] like heat shock proteins (HSP), as well as plasma proteins such as human serum albumin (HAS) and apolipoproteins[172]. Sites of modification were identified in the latter case showing modification to take place mostly on histidine, followed by lysine and then cysteine[172].

Lipid modified proteins can also be identified using bioorthogonal chemistry without the use of affinity handles. In this case, detection tags such as fluorophores are installed and proteins are separated using traditional chromatographic or electrophoretic[102] techniques. The isolated proteins are then identified by mass spectrometry. This was applied to identify 10 geranylgeranylated proteins of the Rab and Ras families from MCF-7 cells[102] and 21 putatively palmitoylated proteins from mitochondria[95].

Other applications

Bioorthogonal lipid analogs have found use in a variety of other contexts. To enable latter chemical modification, bioorthogonal chemistry can be combined with enzyme-mediated protein tagging to install a derivatizable lipid *in vivo* or *in vitro*. This has been achieved by geranylation[100], farnesylation[167] and in *E. coli* simultaneously overexpressing *Candida albicans* NMT a recombinant protein with an N-terminal NMT recognition sequence[97,98], offering a strategy suited to large scale production. Likewise, surface proteins engineered to be substrates for azido caprylic acid (Az-8) transferred by a microbial lipoic acid ligase can be easily visualized by SPAAC fluorophores[133]. Derivatizable liposomes allow modular installation of multiple targeting reagents, such as antibodies or peptide ligands, and imaging agents. Liposomes with terminal acetylenic lipids have been applied to imaging the uptake by UMR-106 cells when derivatized with a

FITC dye and an integrin receptor uptake peptide GRGD[174]. Likewise, azide phospholipids allowed derivatization with an N-terminally labeled fluorescent peptide, GPGGCGG, which was taken up by HeLa cells[175]. Finally, lipid modification of DNA constructs accelerated the uptake of oligonucleotides and did not inhibit biological activity[176].

Scope of this work

Building on this foundation, this work set out with two goals. First at the level of proteins, to develop a robust platform for affinity enrichment and identification of chemical reporter modified proteins. This system must have low background, must keep all proteins in solution, and must allow quantitative release of captured proteins. Second, this work sought to apply bioorthogonal techniques to one of nature's most conserved and important lipids: cholesterol.

MATERIALS AND METHODS

Proteomic analysis

HPLC-MS analysis of biotinylated detection tags

Biotinylated detection tags were diluted to 100 μM in 50 mM triethanolamine (TEA), 150 mM NaCl and treated for 1 hr with the different reductants listed in Figure 8. The reactions were terminated by reverse phase extraction on a C18 column, washed, eluted and vacuum concentrated. Samples were analyzed on a Waters Acquity HPLC and separated on a C18 column. The gradient of solvent A (water with 0.1% TFA) and solvent B (CH_3CN with 0.1% TFA) was increased from 1% B to 40% B over 9 min, 60% B for 1 min and 100% B for 2 min. Mass to charge ratios were determined on a Thermo Scientific TSQ Vantage triple stage quadrupole.

Cell culture and metabolic labeling

Jurkat T cells (human T lymphoma) were cultured in RPMI medium 1640 supplemented with 10% fetal bovine serum (FBS), 100 U/mL penicillin and 100 mg/mL streptomycin (P/S). Cells were maintained in a humidified 37 °C incubator with 5% CO_2. Trypan blue exclusion was used to determine cell viability. Cells were labeled at 5 x 10^6 cells/mL for 8 hours in 25 μM myristic acid analogs (alk-12 and az-12) or 50 μM palmitic (alk-14) and stearic acid analogs (az-15 and alk-16) in RPMI 1640 containing 2% charcoal dextran-treated FBS (CD-FBS) and P/S. Cells were spun down, washed once with PBS, snap frozen in liquid N_2 and stored at -80 °C.

Preparation of total cell lysates

Cells were lysed first in a hypotonic buffer (5 mM TEA, pH 7.4, 5 mM $MgCl_2$, 10 mM PMSF, Roche Complete EDTA-free protease inhibitors) to which benzonase at 1000 U/mL had been added. Cells were intermittently vortexed and sonicated for 30 min at 4 ºC after which an equal volume of 8% SDS, 300 mM NaCl, 100 mM TEA pH 7.4 was added. Cells were again sonicated and incubated for 10 min at RT room temperature (RT); at this point the solution was clear. The supernatant was centrifuged at 10,000 g, 0 ºC for 30 min and the supernatant removed and stored at -80 ºC until future use. Protein concentration of cell lysates was determined by a BCA assay using BSA as a standard and equal amounts of protein from 2-20 mg were precipitated overnight with 8 volumes of methanol at -80 ºC. The precipitated proteins were resolubilized to 5-15 mg/mL in 4% SDS, 150 mM NaCl and 50 mM TEA pH 7.4 containing 0.5 mM PMSF and 1x Roche Complete protease inhibitors with sonication.

CuAAC labeling of cell lysates and in-gel fluorescence scanning

Cell lysates were labeled in 4% SDS, 150 mM NaCl and 50 mM TEA with protease inhibitors at 1 mg/mL. Protein was reacted for 2 hr at RT with 100 µM azido- or alkynyl-Rho or biotinylated detection tags from a 10 mM DMSO stock solution, 1 mM tris(2-carboxyethyl)phosphine hydrochloride (TCEP) from a 50 mM freshly prepared aqueous stock solution, 100 µM tris[(1-benzyl-1*H*-1,2,3-triazol-4-yl)methyl]amine (TBTA) from a 25 mM DMSO stock and 1 mM $CuSO_4$ from a 50 mM freshly prepared aqueous stock solution. The reactions were terminated by the addition of 8 volumes of -20 °C methanol and placed at -20 °C overnight. Precipitated proteins were pelleted by centrifugation (18,000 g, 10 min, at 0 °C) and the supernatant discarded. Protein pellets were air dried for 10 min, resuspended in 35 µL of resuspension buffer (4% SDS, 50 mM trieth-

anolamine pH 7.4, 150 mM NaCl), diluted with 12.5 µL 4X reducing SDS-loading buffer (40% glycerol, 200 mM Tris-HCl pH 6.8, 8% SDS, 0.4% bromophenol blue) and 2.5 µL 2-mercaptoethanol, heated for 5 min at 95 ºC and ~20 µg of protein was loaded per gel lane for separation by SDS-PAGE (10% or 4-20% Bio-Rad Criterion Tris-HCl gel). Protein gels were then visualized by in-gel fluorescence scanning with an Amersham Biosciences Typhoon 9400 variable mode imager (excitation 532 nm, 580 nm filter, 30 nm band-pass).

Immunoprecipitations and CuAAC labeling/in-gel fluorescence scanning

Jurkat cells were labeled and lysed as described above with the exception that 8% SDS was replaced with 2% Brij-97 for a final lysate in 1% Brij-97, 50 mM TEA pH 7.4 and 150 mM NaCl. 500 µg of Brij cell lysate was mixed with 10 µL protein G beads and 2 µg anti-HSP90 and incubated for 1 hr with agitation at RT. Beads were washed 3x with Brij-97 buffer and resuspended in 14 µL of 4% SDS buffer containing all CuAAC reagents. Histone IPs were performed as described before[177]. Beads were reacted for 1 hr at RT after which 5 µL of 4X LDS sample buffer, 1 µL BME was added and 20 µL of supernatant taken and analyzed by SDS-PAGE. Gels were scanned as described above.

Transfection and metabolic labeling of constructs bearing exogenous tags

293T cells were grown to 95% confluency in DMEM supplemented with 10% and 100 U/mL penicillin and 100 mg/mL streptomycin. Cells were transfected with various plasmids using lipofectamine-2000 according to the manufacturer's instructions. After 10 hr, media was supplemented either with 100 µM palmitic acid or 100 µM alk-14. 8 hr later cells were harvested using a cell scraper, washed with PBS and frozen at -80 ºC until use. Protein pellets were handled

identically as for Jurkat cells. Plasmids were as follows: PP1γ C-terminally tagged with EGFP pEGFP-C1 (Lei Tan and Tarun Kapoor), HSP90α N-terminally His- and C-terminally 3×FLAG tagged in pcDNA3.1+ (Laura Donlin and Alexander Tarakhovsky) and H3 variants C-terminally Myc-His tagged in pcDNA4 (Aaron Goldberg and David Allis[178]).

Western blot analysis

Proteins separated by SDS-PAGE were transferred (50 mM Tris, 40 mM glycine, 0.0375% SDS, 20% MeOH in deionized water, Bio-Rad Trans-Blot Semi-Dry Cell, 20 V, 1 hr) onto a PVDF membrane. PVDF membrane was incubated with PBST (0.1% Tween-20 in PBS) or PBST with 25 mM $Na_2S_2O_4$ for 1 hr, and then with PBST containing blocking buffer (5% non-fat dried milk, 1% BSA and 0.1% Tween-20 in PBS) for 1 hr at 25 °C. The membrane was washed thrice with PBST, incubated with primary antibodies (manufacture's recommendations) and horseradish peroxidase-conjugated secondary-antibodies (~1:20,000 in PBST, Jackson ImmunoResearch, West Grove, PA) and subsequently developed with ECL Western blotting detection reagents (Amersham).

Streptavidin enrichment of azide/alkyne-modified proteins

Total cell lysates were reacted with azido- or alkynyl-biotinylated detection tags as described above and protein pellets washed with -80 °C methanol thrice. The protein pellet was resuspended in 4% SDS buffer to which 10 mM EDTA was added to solubilized protein-chelated copper. The labeled cell lysate was diluted to ~0.5% SDS with 1% Brij 97 in 150 mM NaCl, 50 mM TEA at pH 7.4 and incubated with streptavidin agarose (0.2 mL slurry/1 mg of protein) for 1 hr at RT. The streptavidin beads were washed in batch format with 6 times with of 20 column vol-

umes of 2% SDS in PBS, 8 M urea in 250 mM ammonium bicarbonate (ABC), 2.5 M NaCl in PBS, 0.5 M ABC, 0.25 M ABC and finally 0.05 M ABC. Proteins were eluted from the streptavidin beads with 150 µL of 25 mM sodium dithionite in 0.25% SDS twice and subsequently with 150 µL 25 mM sodium dithionite in 8 M urea twice for 15 min each at RT. The sodium dithionite eluent were combined, exchanged to 50 mM ABC and concentrated to 14 µL on a 10 kDa MW Centricon. The recovered protein were then diluted with reducing SDS-loading buffer, heated for 5 min at 95 ºC, separated by SDS-PAGE on 4-20% Tris-glycine gels and stained with Coomassie blue. Each lane from the gel were cut into 10-24 pieces and digested by previously described protocols [179]. Samples were analyzed on an LTQ-Orbitrap and data analyzed as described below. A total of 18 runs were analyzed, composed of 6 negative controls (DMSO), 5 myristic acid analog (az-12/alk-12), 3 palmitic acid analog (alk-14) and 4 stearic acid analog (az-15/alk-16).

Liquid chromatography – mass spectrometry (LC-MS) analysis

LC-MS analysis was performed with a Dionex 3000 nano-HPLC coupled to an LTQ-Orbitrap ion trap mass spectrometer (Thermo Fisher). Peptides were pressure loaded onto a homemade 75 µm diameter, 15 cm C_{18} reverse phase column and separated with a gradient running from 95% buffer A (HPLC water with 0.1% formic acid) and 5% buffer B (HPLC grade CH_3CN with 0.1% formic acid) to 55% B over 30 min, next ramping to 95% B over 10 min and holding 95% B for 10 min. One full MS scan (300-2000 MW) was followed by 3 data-dependent scans of the n^{th} most intense ions with dynamic exclusion enabled. The spray voltage was set to 1.94 kV and the flow rate through the column was set to 0.25 µL/min.

Analysis of protein hits from mass spectrometry data

Peptides were identified using SEQUEST version 28 (revision 13) and X!Tandem searched against the human IPI database version 3.50 (74,016 entries); searches were also run against the same database containing a randomized version of all sequences (148,032 entries). Mass tolerances were set at 10 ppm precursor mass and 1 Da fragment mass. Cysteines were considered constantly modified by carboxyamidomethylation. Allowable variable modifications in SEQUEST included oxidation on methionine and tryptophan, deamidation of asparagine and glutamine, and acetylation on the N-terminus and lysine; lysine acetylation was rarely observed except for histones. Allowable variable modifications in X!Tandem were the same with the addition of amino acid cyclization with an N-terminal glutamine or iodoacetamide-capped cysteine (-NH3), or glutamic acid (-OH) resulting in N-terminal pyrrolidone carboxylic acids.

SEQUEST and X!Tandem search results were imported into Scaffold for PeptideProphet filtering. To generate a large space for PeptideProphet to model possible incorrect identifications, peptides were initially searched against a database generated with KRNLH trypsin specificity allowing 5 missed cleavages. Only peptides judged by PeptideProphet to have a ≥95% likelihood of correct assignment were accepted. PeptideProphet probabilities are a combined function of both Xcorr and Δcn and, in particular with high mass accuracy data, some spurious peptide identifications received a high probability due to a very high Δcn despite a low Xcorr (i.e. < 1). These spurious hits represent, for example, environmental contaminants which match very well in mass to one possible peptide, but which exhibit minimal fragmentation. Thus, in addition to the primary PeptideProphet probability filter, all peptide identifications with an Xcorr ≤1, Δcn ≤ 0.02 or E

≤ 1 were deemed unacceptable. With these filter criteria, SEQUEST Xcorr averaged ~3.1 and X!Tandem E ~2.9.

After this peptide-level filter, proteins were deemed identified if they matched two or more tryptic peptides with a maximum of three missed cleavages. After this, high probability semi- and non-tryptic peptides from the initial broad search were accepted as additional sequence coverage. Only proteins identified in more than two runs are listed. This analysis was also performed with a randomized database appended to the real sequences. No randomized proteins were present after these filter criteria. Proteins were allowed to share homologous peptides and redundant proteins were identified similar to the procedure described by Kearney et al. [180]. Protein accession numbers matching a subset of peptides were determined and are indicated but not counted in the number of identified proteins. For example, if protein P1 is matched by peptides A, B and C and protein P2 is matched by A and B, P2 is listed as a subhit and not counted. Likewise, in the case that two accession numbers match exactly the same peptides, the first (lowest numerical) IPI accession number is reported and the others are listed and not counted. Note that all accession numbers matching a distinct set of peptides are listed. For example, if protein P3 is matched by peptides D, E and F; protein P4 is matched by peptides D, E and G, and protein P5 is matched by peptides D, F and G, then P3, P4 and P5 will all be listed. In these cases, accession numbers are highlighted with an asterisk. Appendix Table 7 lists the peptides associated with each IPI accession number with shared peptides underlined and Appendix Table 8 lists all IPI numbers which match to a particular peptide.

Independent MS runs were normalized by determining the analog with the most accepted and identified peptides ("counts") in each run and normalizing those maximum counts to a constant value. This normalization constant was then applied to the counts for all proteins of all other analogs; averaged normalized counts were calculated for each protein across all runs. The first two myristic acid analog experiments were handled slightly differently because these experiments lacked other analogs. In this case, the average of the normalized myristic acid signal from all experiments except the first two was first calculated and a constant was calculated to bring the total maximum signal of myristic analog counts to this normalized average. To allow presentation across different abundances, these averaged, normalized spectral counts were presented as percentage of maximum, with full red representing 100% of maximal signal strength and full white representing 0%. Figure 10 also shows the total positive abundance and total abundance normalized for protein molecular weight. For the normalized abundance, spectral counts were scaled such that: 1) the total number of counts remains the same; and 2) counts are linearly scaled by the molecular weight of the proteins. Thus, if two proteins, P1 at 50 kDa and P2 at 100 kDa, were both observed to have 10 spectral counts, the adjusted abundance of P1 would be 13.3 and P2 would be 6.7 (total = 20 and P1 abundance twice that of P2).

Bioinformatic analysis of protein identifications

For prediction of N-myristoylation and S-palmitoylation, MYRbase and CSS-Palm were used respectively. In the case of N-myristoylation, three levels of confidence in order of decreasing certainty were respectively given the numerical value (red shading) of 100%, 67% and 33%. Confidence levels of 100% and 67% correspond respectively to the "RELIABLE" and "TWILIGHT ZONE" predictions of MYRbase. The lowest confidence level reflects no prediction of myristoy-

lation by MYRbase, but the presence of an N-terminal glycine or methionine-glycine. Likewise, protein sequences predicted to be palmitoylated by the CSS-Palm set at the "high," "medium," and "low" cutoffs were assigned S-palmitoylation prediction confidence values of 100%, 67% and 33% respectively. For comparison of our data with published data sets, three separate approaches were required for each published set. For comparative analysis of Martin and Cravatt data, both IPI numbers and gene symbols were compared. High confidence proteins were assigned 100% confidence and medium confidence proteins 50% coloration. In all comparisons, caution must be exercised as each IPI number may have more than one gene symbol and likewise one gene symbol may exist for multiple IPI numbers. Due to the difference in species, all comparisons involving the Davis data were performed solely at the level of gene symbol (protein homology). Gene symbols for all accession numbers from both datasets were taken from current database entries; in the cases where gene symbols had not yet been entered, they were determined by BLAST. Gene symbols were compared and the confidence for Davis data calculated as follows: for both the cultured neuron and rat synaptosomal fractions, confidences of 50%, 33% and 16.7% were assigned to high, medium and low confidence protein identifications as classified by Davis and coworkers. The confidences for the cultured neuron and rat synaptosomal fractions were then summed, so that a protein found in both and characterized at a high confidence received a total of 100% confidence, while a protein found once in a high confidence and once in a medium confidence would receive 83% red shading. For Zacharias data, all reported peptides were searched against the human IPI database; these IPI numbers were compared to the data here. Those peptides observed more than once were assigned 100% confidence, while those observed once were assigned 50% confidence. Freeman data was treated like Cravatt with high

confidence proteins assigned 100% coloration and medium confidence identifications assigned 50%.

Cholesterol imaging

Az-chol[181], az-15[94], TBTA and alkyne-rhodamine[94] were prepared as previously described. M-12 cells were kindly provided by Dr. Daniel Ory (Washington University in St. Louis, Saint Louis, MO). 293T-Shh cells were obtained from American Type Culture Collection (cat. no. CRL-2782, Manassas, VA). Cell-culture grade cholesterol (C3045) and palmitic acid (P5585), filipin (F4767), cyanogen bromide activated Sepharose 4B fast flow beads (C9142), FITC-conjugated cholera toxin B (C1655) muristerone A (M7888), paraformaldehyde (158127), glutaraldehyde (G5882), cell culture grade DMSO (D2438), ultrapure benzonase (E8263) and methyl-β-cyclodextran (C4555) and all buffer reagents were purchased from Sigma (St. Louis, MO). SYTO 11 (S7573), DAPI (D3571), Zeocin (R250), ProLong Gold and Gibco cell culture media were purchased from Invitrogen (Carlsbad, CA). Sera were obtained from Omega Scientific (Tarzana, CA). 20% and 4 – 20% Tris-HCl Criterion gels were from Biorad (Hercules, CA). Antibodies against calreticulin (1:500, ab2907, Abcam, Cambridge, MA), LAMP-1 (1:500, ab24170, Abcam), EEA1 (1:100, 2411, Cell Signaling Technology, Danvers, MA), and golgin-97 (1:100, ab33701, Abcam) were used. Anti-N-Shh clone 5E1[182] was obtained from the Developmental Studies Hybridoma Bank (University of Iowa, Iowa City, IA). Polyclonal goat anti-mouse Shh (AF464) was purchased from R&D Systems (Minneapolis, MN). HRP conjugated anti-goat secondary (705-035-147) was obtained from Jackson ImmunoResearch Laboratories (West Grove, PA).

Cell culture, metabolic labeling and Shh induction

293T and 293T-Shh cells were cultured in high glucose DMEM with glutamine containing 10% fetal bovine serum (FBS), 100 U/mL penicillin and 100 μg/mL streptomycin. Both cell lines were grown to 30 to 40% confluency at which time medium was changed, replacing FBS with 10% delipidated charcoal-dextran filtered fetal bovine serum (CDFBS). 293T-Shh cells were selected by the inclusion of Zeocin (360 μg/ml), and G418 (400 μg/ml). CHO and M12 cells were cultured in F-12 with 10% delipidated CDFBS, 100 U/mL penicillin and 100 μg/mL streptomycin. Cells were maintained in a humidified 37 ºC incubator with 5% CO_2. For microscopy, cells were cultured on glass coverslips in 24-well tissue culture plates.

Stock solutions of 50 mM cholesterol and az-chol were prepared in absolute ethanol. 50 mM stocks of palmitic acid and az-15 were kept in cell culture grade DMSO. All stocks were stored at –20 C. For all experiments, lipids were added into warm culture media containing 10% CDFBS and placed in a sonication bath for 30 min – 1 hr. The temperature of the culture media and bath water was continually monitored; sonication was paused above 40 ºC to allow for cooling. Metabolic labeling of CHO and M12 cells for visualization was done at 50 μM cholesterol or az-chol for ~16 hrs (overnight). 293T and 293T-Shh cells labeled identically except at 100 μM; palmitic acid or az-15 was applied at 12.5 μM for 8 hr. 293T-Shh cells were grown to ~90% confluency and induced with 1 μM muristerone A from a 10 mM stock in absolute ethanol for 8 hrs prior to addition of medium containing cholesterol or az-chol; Zeocin and G418 were eliminated from induction media. 8 hrs later, palmitic acid or az-15 was added. 293T and 293T-Shh cells were harvested 8 hr later after three PBS washes and prepared as described below.

Cell lysate preparation, CuAAC labeling and in-gel fluorescence imaging

For analysis by SDS-PAGE, 293T and 293T-Shh cells were lysed in hypotonic buffer (5 mM TEA, pH 7.4, 5 mM $MgCl_2$, 10 mM PMSF, Roche Complete EDTA-free protease inhibitors at 20x) to which benzonase at 1000 U/mL had been added. Cells were intermittently vortexed and sonicated for 30 min at 4 ºC after which an equal volume of 8% SDS, 300 mM NaCl, 100 mM TEA pH 7.4 was added. Cells were again sonicated and incubated for 10 min at RT; at this point the solution was clear. The supernatant was centrifuged at 10,000 g, 0 ºC for 30 min and the supernatant removed and stored at -80 ºC until future use. Cell lysis for immunoprecipitation was identical with the exception that 8% SDS was replaced with 2% Brij-97 for a final lysate in 1% Brij-97, ~50 mM TEA and ~150 mM NaCl; a pellet was present with Brij lysis. Protein concentration of cell lysates was determined by a BCA assay using 2 mg/mL BSA as a standard.

Cell lysates were labeled in 4% SDS, 150 mM NaCl and 50 mM TEA with protease inhibitors at 1 mg/mL. Protein was reacted for 2 hr at RT with 100 μM alk-Rho from a 10 mM DMSO stock solution, 1 mM tris(2-carboxyethyl)phosphine hydrochloride (TCEP) from a 50 mM freshly prepared aqueous stock solution, 100 μM tris[(1-benzyl-1H-1,2,3-triazol-4-yl)methyl]amine (TBTA) from a 25 mM DMSO stock and 1 mM $CuSO_4$ from a 50 mM freshly prepared aqueous stock solution. The reactions were terminated by the addition of 8 volumes of -20 °C methanol and placed at -20 °C overnight. Precipitated proteins were pelleted the next day by centrifugation (18,000 g, 10 min, at 0 °C and the supernatant discarded. Protein pellets were air dried for 10 min, resuspended in 35 μL of resuspension buffer (4% SDS, 50 mM triethanolamine pH 7.4, 150 mM NaCl), diluted with 12.5 μL 4X reducing SDS-loading buffer (40% glycerol, 200 mM Tris-HCl pH 6.8, 8% SDS, 0.4% bromophenol blue) and 2.5 μL 2-mercaptoethanol, heated for 5 min

at 95 ºC and ~20 μg of protein was loaded per gel lane for separation by SDS-PAGE (10% or 4-20% Bio-Rad Criterion Tris-HCl gel). Protein gels were then visualized by in-gel fluorescence scanning with an Amersham Biosciences Typhoon 9400 variable mode imager (excitation 532 nm, 580 nm filter, 30 nm band-pass).

Immunoprecipitation and Western blotting

Ascites fluid containing anti-N-Shh monoclonal antibody 5E1 was buffer exchanged against water with a Pierce Zeba column and coupled as per manufacturer's instructions to CNBr-activated Sepharose 4B. 750 μg of induced 293T-Shh Brij lysate was mixed with 15 μL 5E1 beads and incubated for 1 hr with agitation at RT. Beads were washed 3x with Brij-97 buffer and resuspended in 28 μL of 4% SDS buffer containing all CuAAC reagents. Beads were reacted for 1 hr at RT after which 10 μL of 4X LDS sample buffer and 2 μL 2-mercaptoethanol were added. The reaction was sonicated, supernatant removed and analyzed by SDS-PAGE. 19 μL was applied to a 4 – 20% tris-HCl gel for fluorescence scanning as described above; 19 μL was applied to a 20% tris-HCl gel for Western blotting. Blots were transferred (50 mM Tris, 40 mM glycine, 0.0375% SDS, 20% MeOH in deionized water, Bio-Rad Trans-Blot Semi-Dry Cell, 20 V, 40 min) onto a PVDF membrane and the membrane was blocked in 0.1% Tween-20 in PBS (PBST) with 5% non-fat dried milk and 1% BSA for 1 hr at 25 °C. After a short rinse, the blot was incubated with goat anti-N-Shh at 1:500 in 5% casein, 1% BSA in PBST, washed three times and incubated with horseradish peroxidase-conjugated secondary-antibodies (~1:15,000 in PBST). Blot was subsequently developed with ECL Western blotting detection reagents (Amersham).

Cellular az-chol labeling and filipin staining

Cells grown on coverslips were washed three times with PBS prior to fixation. Cells to which only chemical techniques were applied were fixed in 1% glutaraldehyde and 4% PFA in PBS for 1 hr; fixation for antibody staining was with 4% PFA for 15 min at RT. Both fixations were followed by 3 x 5 min PBS washes. Cells were subsequently blocked for 1 hr in 20% CDFBS at RT followed by 3 x 5 min PBS washes. Samples intended for antibody analysis were permeabilized with 1% tween-20 in PBS for 10 min at RT. Alternatively, cholesterol was depleted by the addition of -20 ºC HPLC grade methanol (JT Baker) for 10 min or 10 mM MβCD in PBS for 10 min. In both cases, samples were again washed 3 x 5 min PBS. Primary antibodies were applied in PBST for 1 hr followed by 3 x 5 min PBST washes. Fluorescent conjugated secondary antibodies diluted 1:750 in PBST were applied for 45 min followed by the same washing. For all samples, filipin was prepared at 25 μg/mL in PBS; reagents for CuAAC were added to this solution at the same concentrations as with labeling of cell lysates and samples were labeled for 1 hr. Samples were then washed 3 x 5 min in PBST containing 5 mM EDTA, followed by 5 min incubation in 1:40,000 SYTO 11 and 2 x 5 min PBS washes. Cells were mounted in Prolong Gold and imaged as described below. All negative controls were handled identically and in parallel with az-chol labeled samples.

In vivo az-chol labeling and tissue sectioning

Mice work was performed according to approved Memorial Sloan-Kettering animal protocols. Swiss-Webster mice pregnant with E12.5 embryos were anesthetized with isoflurane. In the supine position, a 4 cm vertical incision was made from below the ribcage to middle of the intestines. The uterine horns were carefully laid on a sterile field and 1 – 2 μL of 50 mM az-chol

stock mixed with 1 – 1.5 µL cell culture grade DMSO was injected directly into the lateral ventricle of a single embryo using a pulled glass capillary needle. Upon completion, the uterus was returned to the abdominal cavity, the skin and muscle were sutured closed and the closure was reinforced with veterinary staples. The analgesic buprenorphine (Buprenex™) was administered at a dose of 0.1 mg/kg and the mouse was removed from the anesthetic and placed on a warming pad for recuperation. Once awoken, the mouse was returned to its cage for 6 hours for analog incorporation. After incorporation, the embryos were collected and decapitated. The heads were immediately fixed in 4% paraformaldehyde-PBS for 20 minutes, cryoprotected in 30% sucrose in PBS and embedded in OCT for cryo-sectioning. 14 µm sections were cut on a Leica3050 S cryostat; mounted sections were stored at -20 ºC until use. Tissues were mounted and fixed sections were hydrated with 3 x 5 min PBS, blocked as described above and washed again with PBST. CuAAC labeling was performed as described above with the exception that filipin was not included. After washing excess CuAAC reagents, samples were incubated with DAPI (5 mg/mL solution diluted 1:40,000 in PBS) for 15 min followed by identical rinsing and mounting. All negative controls were handled identically and in parallel with az-chol labeled samples.

Fluorescence microscopy

All cell culture samples and high magnification brain images were obtained on a DeltaVision Applied Precision Image Restoration Inverted Olympus IX-70 microscope using a 60x oil objective. Images were deconvolved in SoftWoRx (Applied Precision / DeltaVision); identical image display settings were applied to positive and negative samples. Low magnification (10x) fluorescent images were collected on a Zeiss Axio Observer.Z1 microscope equipped with Axiovision

software. Pearson's coefficients were determined in ImageJ with the JACoP (Just Another Colocalization Plugin) plugin (Fabrice P. Cordelieres, Institut Curie, Orsay, France).

PROTEIN ACYLATION IN MAMMALIAN CELLS

Introduction

The diversity of fatty-acylated proteins and their mechanisms of regulations are not completely understood[5]. Prediction algorithms such as Myrbase[183] and CSS-Palm[22] provide useful bioinformatic tools for the analysis of candidate fatty-acylated proteins based on previously observed modification motifs, but require experimental validation and offer no insight into the post-transcriptional mechanisms of fatty-acylation. For example, alternative splicing of mRNA transcripts may yield substrates for N-myristoylation as in the case of the p35 isoform of OCA-B, a transcription factor required for late-stage B cell development[14,15]. Alternatively, protein fatty-acylation may be altered during cellular regulation. During programmed cell death, the apoptosis effector tBid is post-translationally N-myristoylated after proteolytic cleavage by the cysteine protease caspase-3, which targets tBid to mitochondrial membranes during apoptosis [12,13]. Dissecting the regulatory mechanisms of S-palmitoylation in mammals also presents a significant challenge as ~23 DHHC-PATs have been identified in human and mouse genomes with overlapping substrate specificities[21]. Moreover, the functions of fatty-acylated proteins can be regulated by other post-translational modifications (PTMs) such as phosphorylation, as exemplified by studies on MARCKS[7], c-Abl kinase[8,9] and potassium channels[10]. Robust experimental methods are therefore needed to fully appreciate the diversity and functional roles of protein fatty-acylation.

Figure 6 Protein fatty-acylation and its analysis with bioorthogonal chemical reporters. A) Chemical modification of fatty-acylated proteins. Palmitoylation is heterogeneous in length and saturation; only palmitic acid is shown. B) Schematic for proteomic analysis of fatty-acylated proteins with chemical reporters using cleavable affinity tags. Jurkat T cells were metabolically labeled with DMSO control (-) or alk-FAs (20 μM myristic analogs, 100 μM all other analogs; 6-8 hr). Total cell lysates were then subjected to click chemistry reaction with az-azo-biotin (100 μM), small molecule removal, affinity-enrichment with streptavidin-beads, selective elution from beads with sodium dithionite ($Na_2S_2O_4$, 25 mM, 1 hr) and separation by SDS-PAGE. Selectively recovered proteins were analyzed by immunoblot using specific antibodies or stained with Coomassie blue and processed for mass spectrometry-based protein identification. X = NH (N-myristoylation) or S (S-palmitoylation). C) Profile of alkynyl-fatty acid-labeled proteins in total cell lysates visualized by click chemistry reaction with az-Rho/in-gel fluorescence scanning (left panel) or with az-azo-biotin, streptavidin enrichment, $Na_2S_2O_4$ elution and Coomassie blue staining (right panel). Coomassie staining of total cell lysates from each sample (-, alk-12, alk-14, alk-16) demonstrates comparable amounts of protein loading for both fluorescence imaging and affinity enrichment of labeled proteins (middle panel). Similarities such as the ~20kDa band marked with an asterisks are apparent between fluorescence and Coomassie detection.

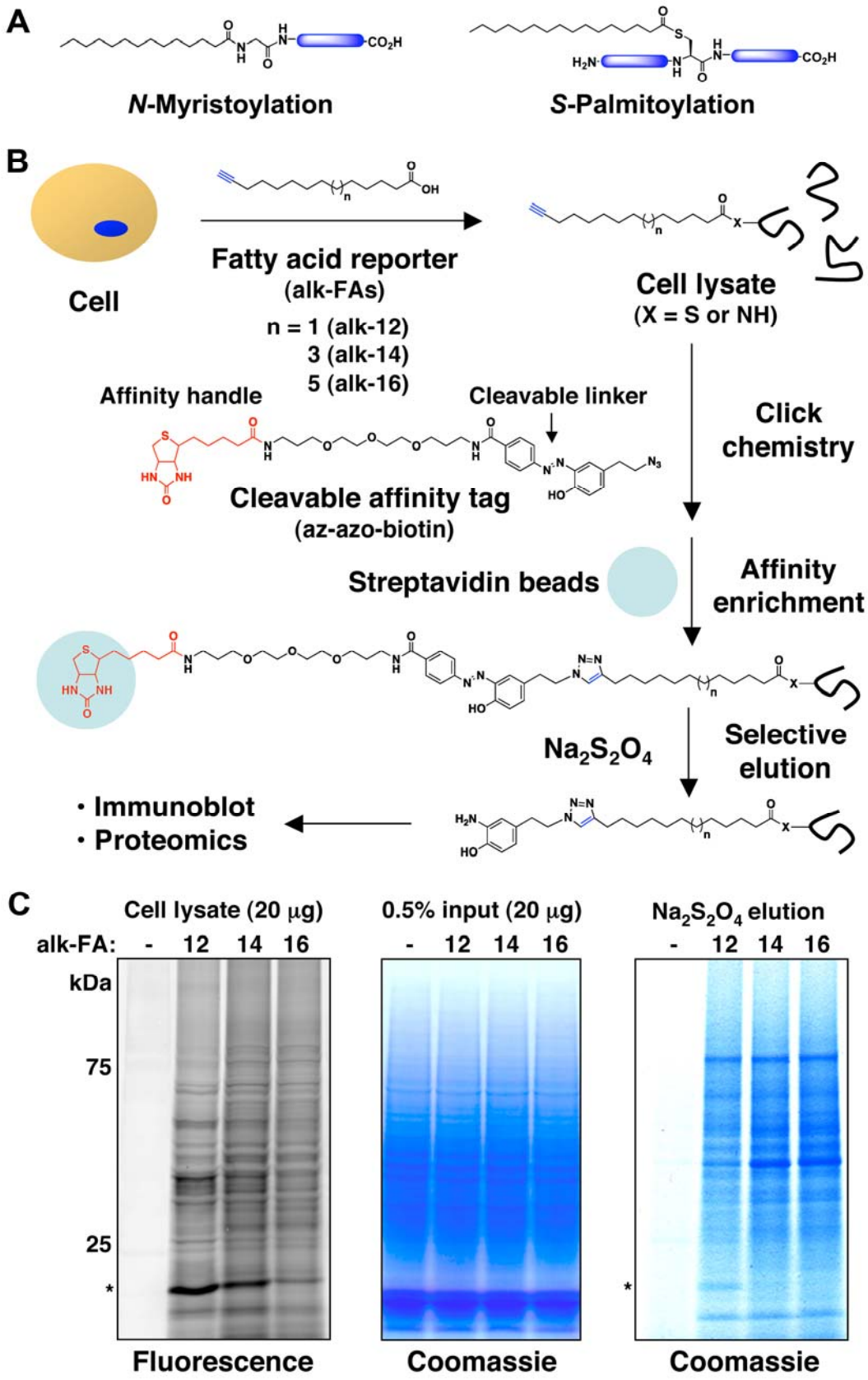
A
N-Myristoylation
S-Palmitoylation
B
Cell
Fatty acid reporter
(alk-FAs)
n = 1 (alk-12)
3 (alk-14)
5 (alk-16)
Cell lysate
(X = S or NH)
Affinity handle
Cleavable linker
Cleavable affinity tag
(az-azo-biotin)
Click chemistry
Streptavidin beads
Affinity enrichment
Na2S2O4
Selective elution
• Immunoblot
• Proteomics
C
Cell lysate (20 μg)
0.5% input (20 μg)
Na2S2O4 elution
alk-FA: - 12 14 16
kDa
75
25
*
Fluorescence
Coomassie
Coomassie

Two chemical methods have been developed to overcome the limitations of radiolabeled fatty acids for the detection and identification of fatty-acylated proteins[184]. The acyl-biotin exchange (ABE) protocol developed by Drisdel and Green exploits the differential sensitivity of thioesters to hydroxylamine (NH_2OH) for selective biotinylation of S-acylated proteins and non-radioactive visualization by streptavidin blot[185] as well as enrichment of S-acylated peptides or proteins for proteomic analysis by mass spectrometry[186-189]. The global profiling of S-palmitoylation in budding yeast with ABE identified several new S-palmitoylated proteins and highlighted the differential and overlapping substrate specificities of the DHHC-PATs[186,187]. The application of ABE to neurons revealed isoform-specific S-palmitoylation of the GTPase Cdc42 in the brain as well as many new candidate S-palmitoylated proteins[188]. Enrichment of S-acylated peptides from mammalian cells by ABE has also expanded the list of S-palmitoylated proteins and sites of S-acylation[189,190]. Alternatively, we[93,99,191] and others[95-98,121,122,192] have developed fatty acid chemical reporters of protein fatty-acylation that enable rapid non-radioactive detection of fatty-acylated proteins from mammalian cells using bioorthogonal ligation methods[109] such as the Staudinger ligation or Cu^{I}-catalyzed [3+2] azide-alkyne cycloaddition (CuAAC)[184,193] (Figure 6). Metabolic labeling of mammalian cells with azido/alkynyl-fatty acid (az/alk-FA) chemical reporters followed by reaction of azide/alkyne-modified proteins with biotinylated or fluorescent detection tags allows the visualization of fatty-acylated proteins by streptavidin blot[93,95-99,121] or in-gel fluorescence[122,191,192,194], respectively. The direct comparison of various detection modes has demonstrated that metabolic labeling of cells with alkynyl-fatty acids (alk-FAs) in combination with CuAAC and in-gel fluorescence scanning affords the optimal method for the visualization of protein fatty-acylation[191]. Indeed, the analysis of various mammalian cell lines with fatty acid chemical reporters and CuAAC/in-gel fluorescence scanning revealed unique and diverse

profiles of fatty-acylated proteins[191]. Large-scale profiling of S-acylated proteins in Jurkat T cell membrane fractions with an alkynyl-palmitate reporter (17-octadecynoic acid abbreviated 17-ODYA or alk-16) by Martin and Cravatt using CuAAC labeling/enrichment methods, on-bead proteolysis and multidimensional protein identification technology (MudPIT) recovered many new candidate S-palmitoylated proteins and identified a family of serine hydrolases that is targeted to membranes by palmitoylation[122]. Herein, we describe the proteomic analysis of fatty-acylated proteins in mammalian cells in which we employ a series of fatty acid chemical reporters representing myristic to stearic acids (Figure 6). This survey is unbiased in that all cellular proteins were solubilized and analyzed; no fractionation such as membrane preparations was used. Our studies of total cell lysates from Jurkat T cells have revealed known and novel candidate fatty-acylated proteins, including nuclear components such as *S*-acylated histone H3 variants.

Results

Characterization of cleavable affinity reagents for CuAAC-based proteomics

To facilitate the identification of azide- and alkyne-modified proteins targeted by bioorthogonal chemical reporters, we utilized clickable and cleavable affinity reagents for CuAAC, streptavidin enrichment and selective elution of recovered polypeptides for proteomic analysis (Figure 6). While the biotin-avidin interaction provides an excellent system for selective detection and retrieval of biomolecules, the high affinity binding (~K_D 10^{-15} M) of this interaction makes quantitative elution of biotinylated proteins from streptavidin beads challenging. Indeed, selective elution strategies using protease-[135,195,196], pH-[197-199], redox-[200-202] or photo-cleavable[203-205] linkers have been described to recover peptides or proteins following streptavidin enrichment. We employed the azobenzene linker as this functional group can be efficiently cleaved by mild reduction with sodium dithionite[200-202] ($Na_2S_2O_4$, see

Figure 7) and stable to click chemistry conditions[177,206]. Exposure of azido-azo-biotin previously generated by our laboratory[177] to various reducing agents demonstrated the azobenzene linkage was stable to reducing agents such as TCEP (tris(2-carboxyethyl)phosphine), but readily cleaved with 25 mM $Na_2S_2O_4$ (Figure 8) These experiments demonstrated that the cleavable affinity tags, alk-azo-biotin and az-azo-biotin, are compatible with click chemistry (1 mM TCEP) and reductive alkylation (10 mM TCEP) reaction conditions used for proteomic studies. We have previously utilized az-azo-biotin for CuAAC-based proteomic analysis of acetylated proteins in mammalian cells[177] and lipoproteins in bacteria[207]. For this study, alk-azo-biotin was also synthe-

sized to explore CuAAC, enrichment and identification of proteins targeted by azido-fatty acids (Figure 9).

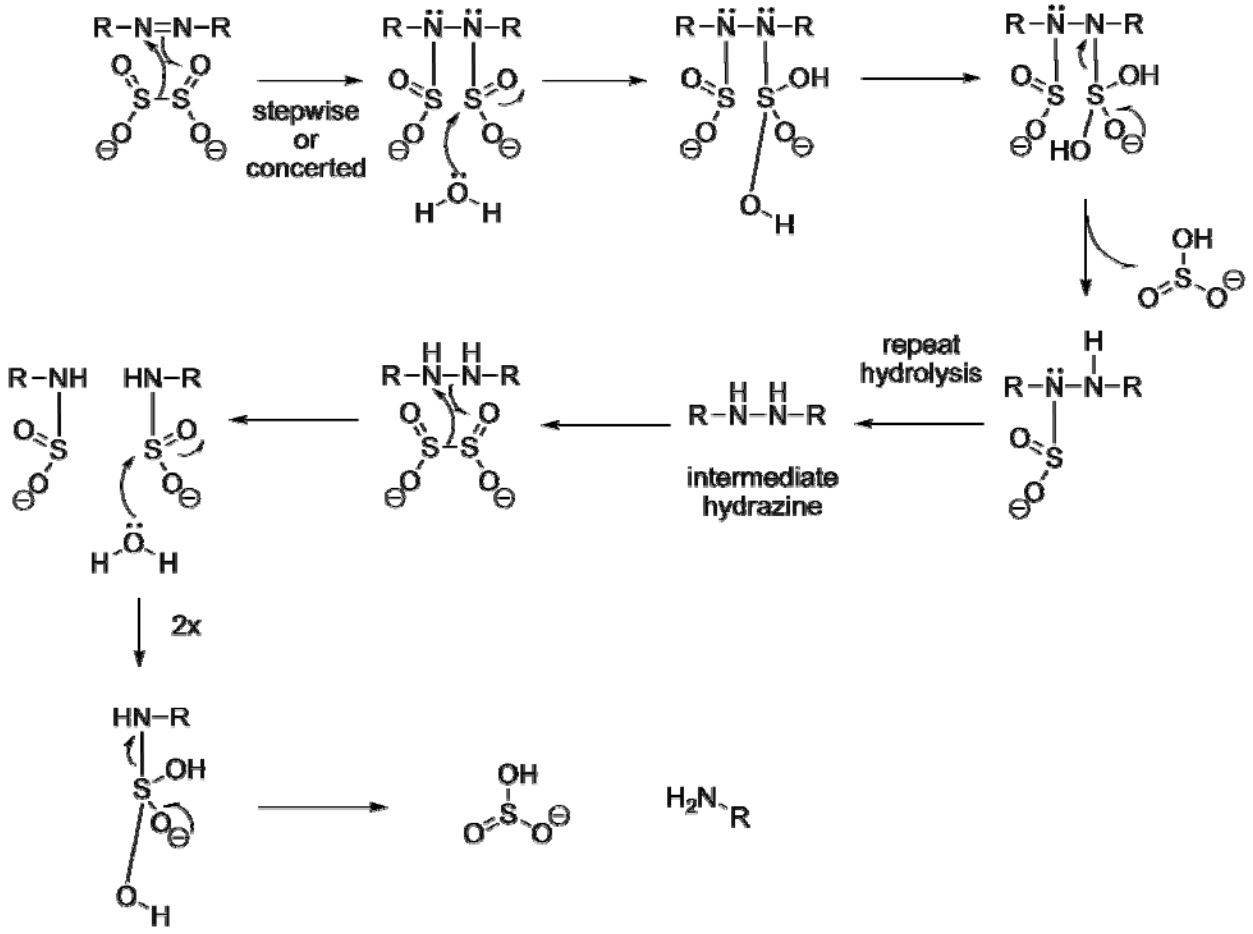

Figure 7 Mechanism of azo cleavage by sodium dithionite. The first step can proceed in either a stepwise or concerted fashion.

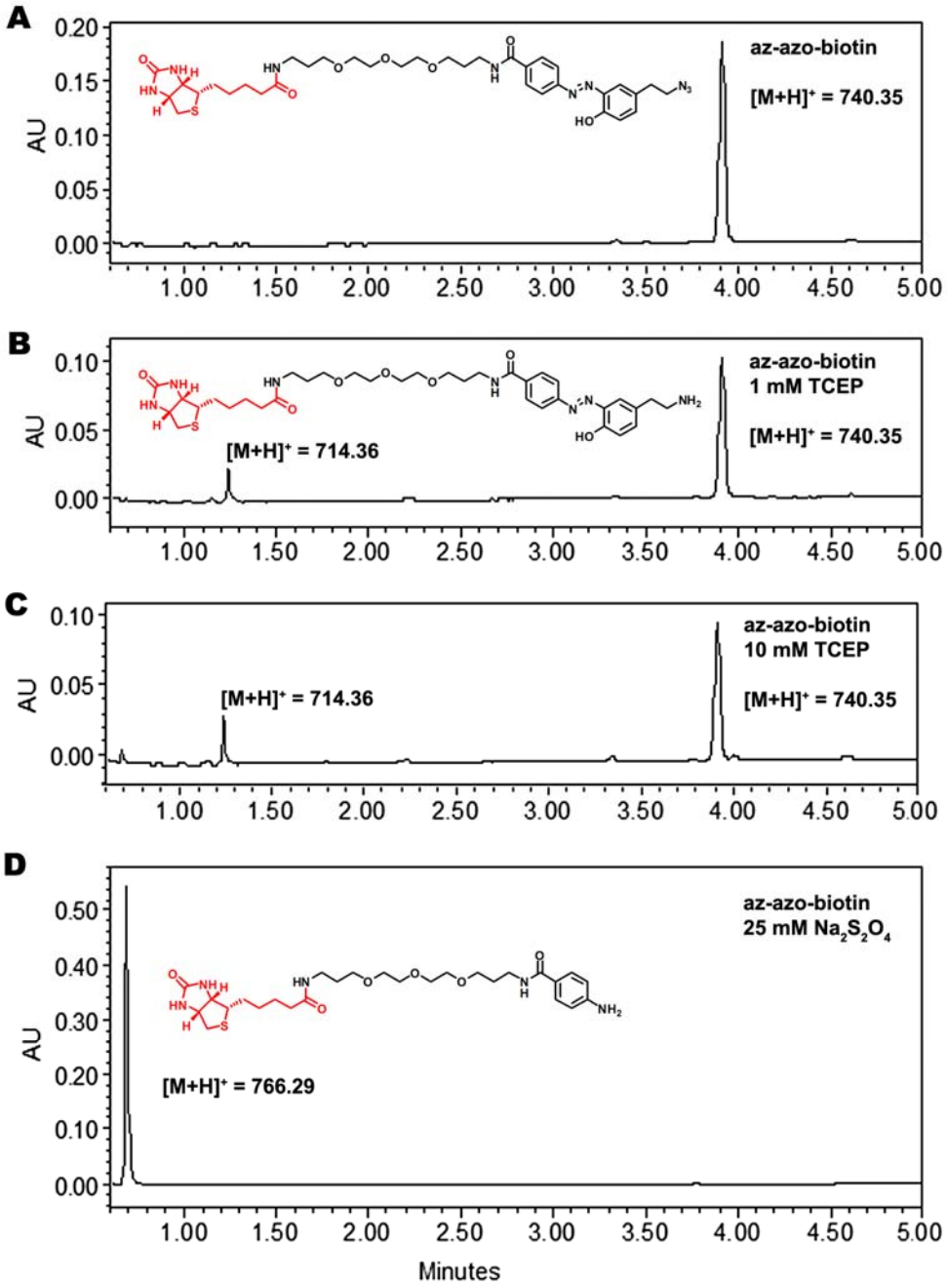

Figure 8 Analysis of azido-biotinylated cleavable linker (az-azo-biotin) under reductive conditions. A) Structures of reduced cleavable linkers and their mass to charge ratios. B) Linker at 100 µM was exposed to the different reducing conditions of panel B in 50 mM TEA, 150 mM NaCl at pH 7.4. After reduction for 1 hr, reactions were stopped by reverse-phase solid phase extraction, washed, concentrated and analyzed by HPLC. Only 25 mM $Na_2S_2O_4$ was able to cleave the azo-benzene bond. Note the reduction of the terminal azide to an amine (NH_2-azo-biotin) cannot happen after the click reaction.

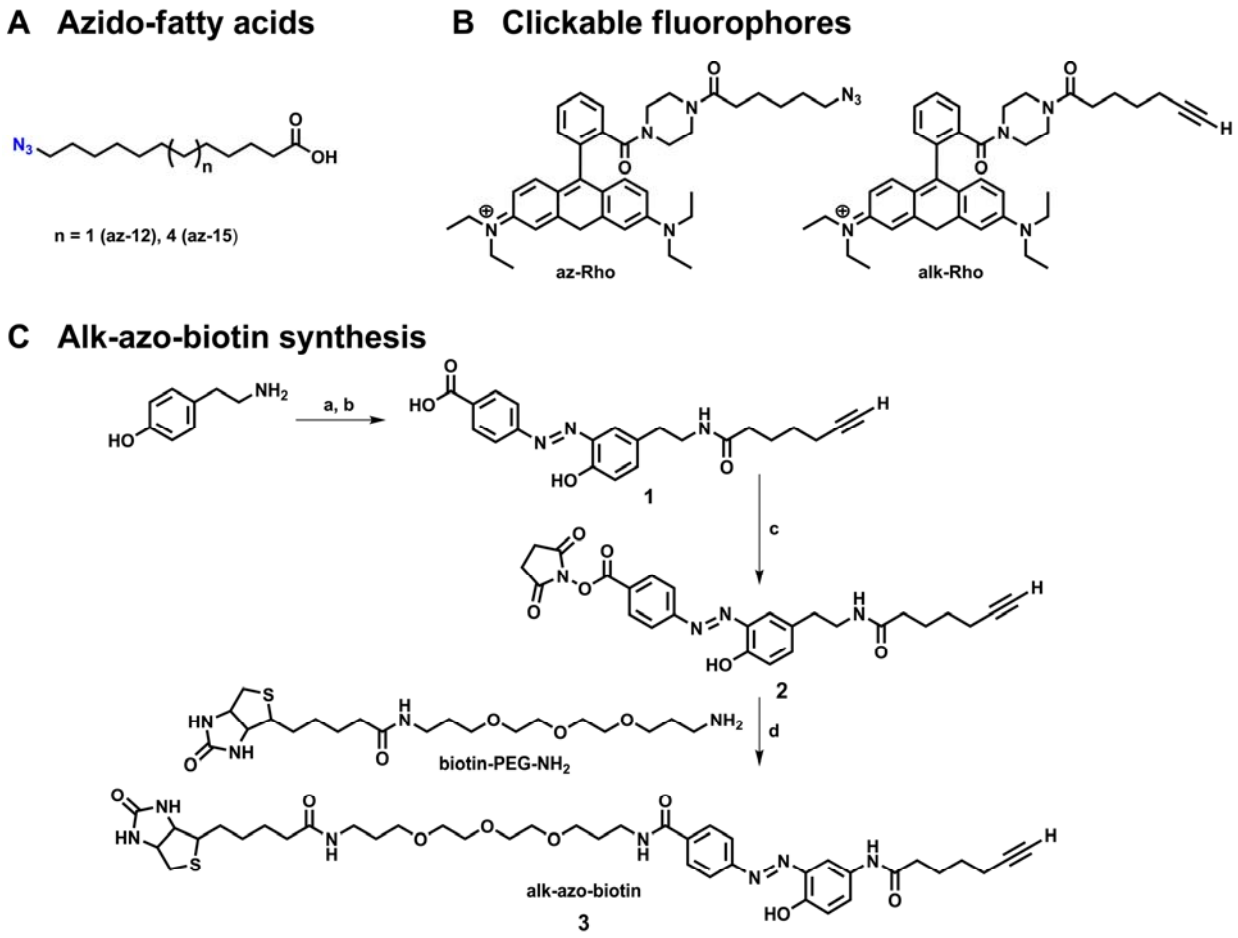

Figure 9 A) Azido-fatty acids. B) Clickable rhodamine dyes. C) Synthesis of alk-azo-biotin: (a) NaNO2, 6M HCl, 4-aminobenzoic acid. (b) 6-heptynoic-NHS ester, Et3N, THF, 30% yield over two steps. (c) DCC, N-hydroxysuccinimide (NHS), THF, 70%. (d) biotin-PEG-NH2, DMF, 24% yield.

Proteomic analysis of fatty-acylated proteins in mammalian cells

To identify proteins targeted by fatty acid reporters, az-FA- and alk-FA-labeled Jurkat T cell lysates were reacted with the alk-azo-biotin and az-azo-biotin, respectively, incubated with streptavidin beads and extensively washed with denaturing buffers to remove non-specifically bound proteins (Figure 6B). Proteins that remained bound to streptavidin beads were selective eluted with 25 mM $Na_2S_2O_4$, separated by SDS-PAGE and analyzed by Coomassie blue staining or immunoblotted for specific proteins (Figure 6B). Coomassie blue staining of the polypeptides selectively eluted from streptavidin beads revealed significantly greater amounts of proteins recovered from alk-FA and az-FA-labeled cell lysates compared to control (-) (Figure 6C, Figure 10B, D and E). A fraction of the cell lysates analyzed in parallel demonstrated equal levels of input material (Figure 6C). The profile of selectively recovered polypeptides roughly mirrors the fatty-acylated proteins visualized by CuAAC/in-gel fluorescence scanning although the modes of protein detection are different (Figure 6C). For example, the ~20 kDa polypeptide that is preferentially labeled in az-12/alk-12 cell lysates by in-gel fluorescence is also apparent by the Coomassie blue-stained gel of selectively recovered proteins from streptavidin enrichment and $Na_2S_2O_4$ elution (Figure 6C, Figure 10C). Western blot analysis of az-FA-labeled samples for known fatty-acylated proteins in Jurkat T cells such as Lck[93] and Tfr[208,209] demonstrated the specificity of the CuAAC, streptavidin enrichment and $Na_2S_2O_4$ elution protocol (Figure 10C).

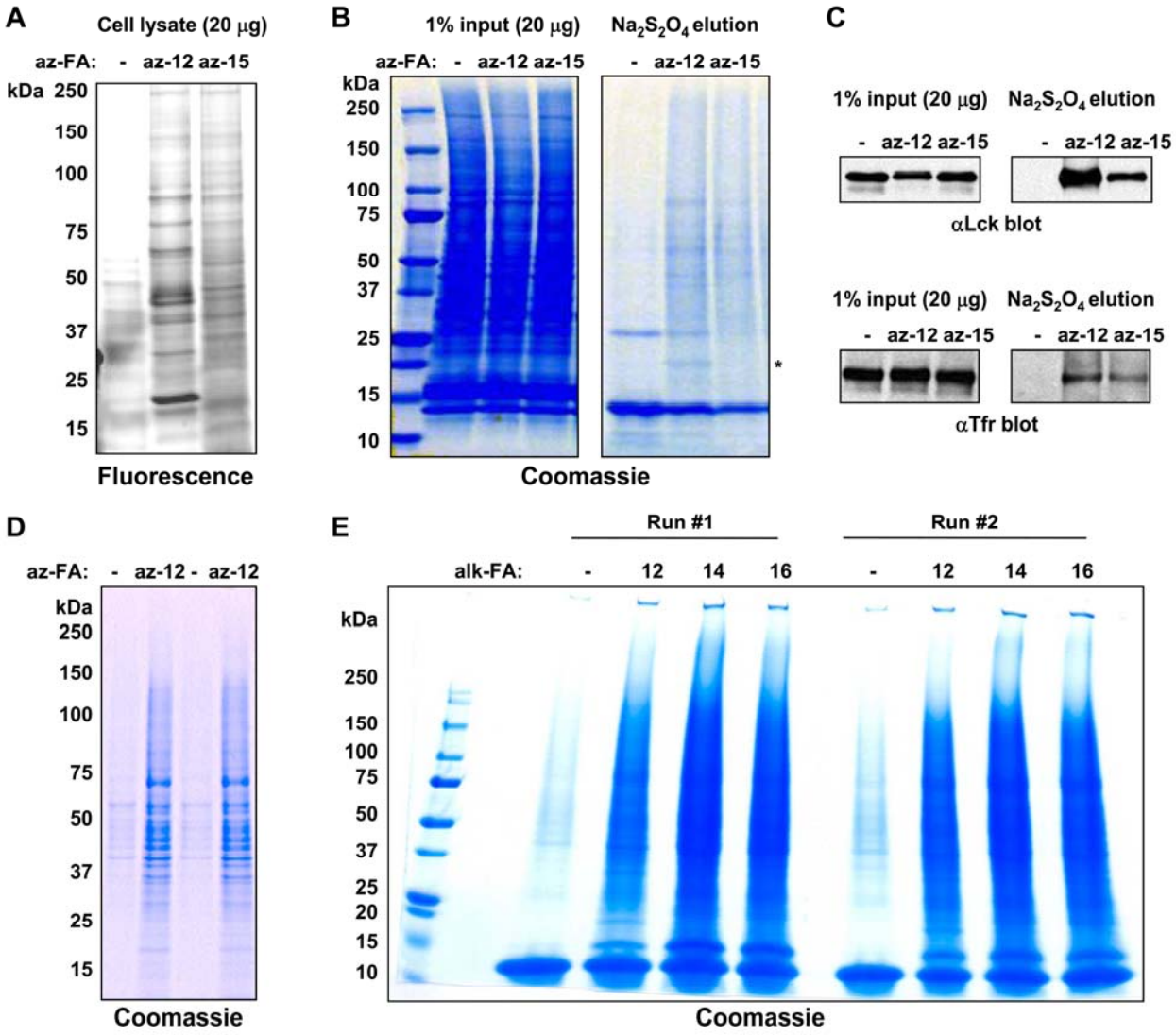

Figure 10 Enrichment of azide/alkyne-modified proteins targeted by fatty acid chemical reporters. A) In-gel fluorescence profile of azido-fatty acid labeled proteins from Jurkat T cells after CuAAC reaction with alk-Rho. B) Coomassie staining of azido-fatty acid labeled proteins following CuAAC reaction with alk-azo-biotin, streptavidin enrichment, sodium dithionite elution and SDS-PAGE. C) Validation of azido-fatty acid recovered proteins by western blot. D) Preliminary runs of az-12 labeled proteins following CuAAC reaction with alk-azo-biotin, streptavidin enrichment, sodium dithionite elution and SDS-PAGE. E) Enrichment of alk-FA-modified proteins after CuAAC labeling with az-azo-biotin, streptavidin enrichment, sodium dithionite elution and SDS-PAGE.

Figure 11 Proteins identified from Jurkat T cells metabolically labeled with click-chemistry compatible fatty acids of different chain lengths (myristic acid = az- and alk-12), (palmitic = alk-14), (stearic = az-15 and alk-16) or DMSO carrier control (-); high confidence only (≥ 5 identifications with 5-fold enrichment over DMSO control). Proteins with the same gene symbol but different IPI numbers are marked with an asterisks (*). Under experimental, intensity of heat map coloration represents normalized peptide counts for each protein hit averaged over 6 independent proteomic experiments. Proteins are clustered by their propensity to be modified from short to long chain fatty acids and assigned to seven groups: I: modified mainly by myristic acid; II: modified mainly by myristic and palmitic acids; III: myristic and stearic acids; IV: palmitic acid; V: palmitic and stearic acids; VI: palmitic acid; VII: myristic, palmitic and stearic acids. Group VIII are proteins enriched in the negative control (marked with a dagger (†); counts are negatives in excess of positive). Proteins labeled by all fatty acids are sorted by the correlation between their averaged normalized signal strengths and the physical length of the fatty acid chains. Intensity of red in prediction and in comparative analysis to other reported experimental datasets represents confidence of prediction or identification, respectively, given criteria set by each study. N-terminal myristoylation was predicted by MYRbase. S-palmitoylated was predicted by CSS-Palm. In comparative analysis, a black box means a protein was identifiable by our data which matched an accession number published in other data sets, but which differs from the reported accession number of this figure due to additional sequence coverage or uncertainty in peptide-level identification. A grey box represents the same situation, except that 1) both an unlisted, interpretable accession number and the exact accession number listed match published reports; and 2) the confidence of the unlisted number is higher than the accession number listed here. In that case, the higher confidence of the unlisted accession number is shown. The total number of peptide counts in excess of any negative (log scale) and the number of times the protein was identified. Nearly four orders of magnitude are spanned (11 – 8075 raw counts)

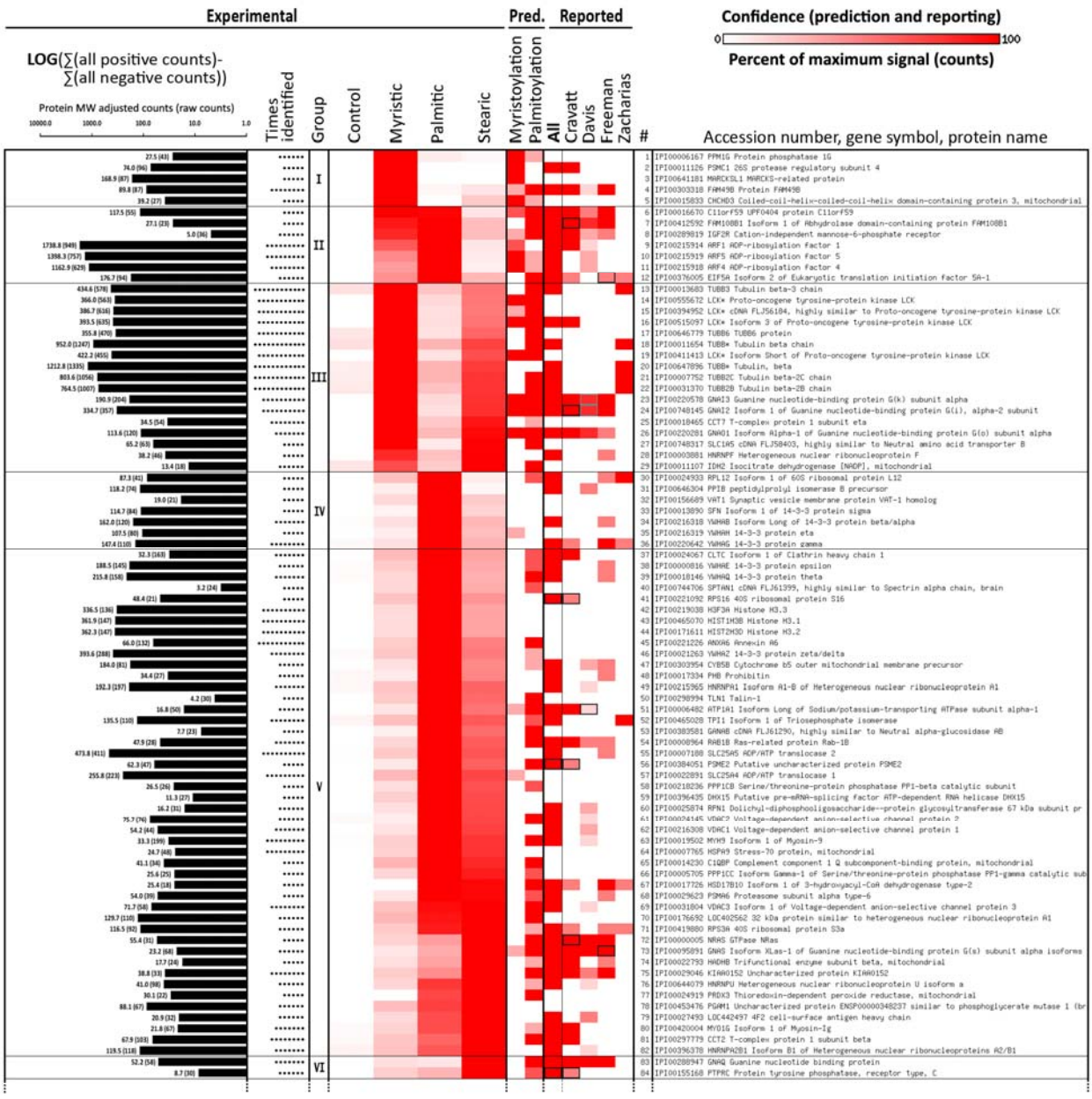
Experimental
Pred.
Reported
Confidence (prediction and reporting)
0
100
Percent of maximum signal (counts)
LOG(∑(all positive counts)-∑(all negative counts))
Protein MW adjusted counts (raw counts)
10000.0
1000.0
100.0
10.0
1.0
Times identified
Group
Control
Myristic
Palmitic
Stearic
Myristoylation
Palmitoylation
All
Cravatt
Davis
Freeman
Zacharias
#
Accession number, gene symbol, protein name
I
II
III
IV
V
VI

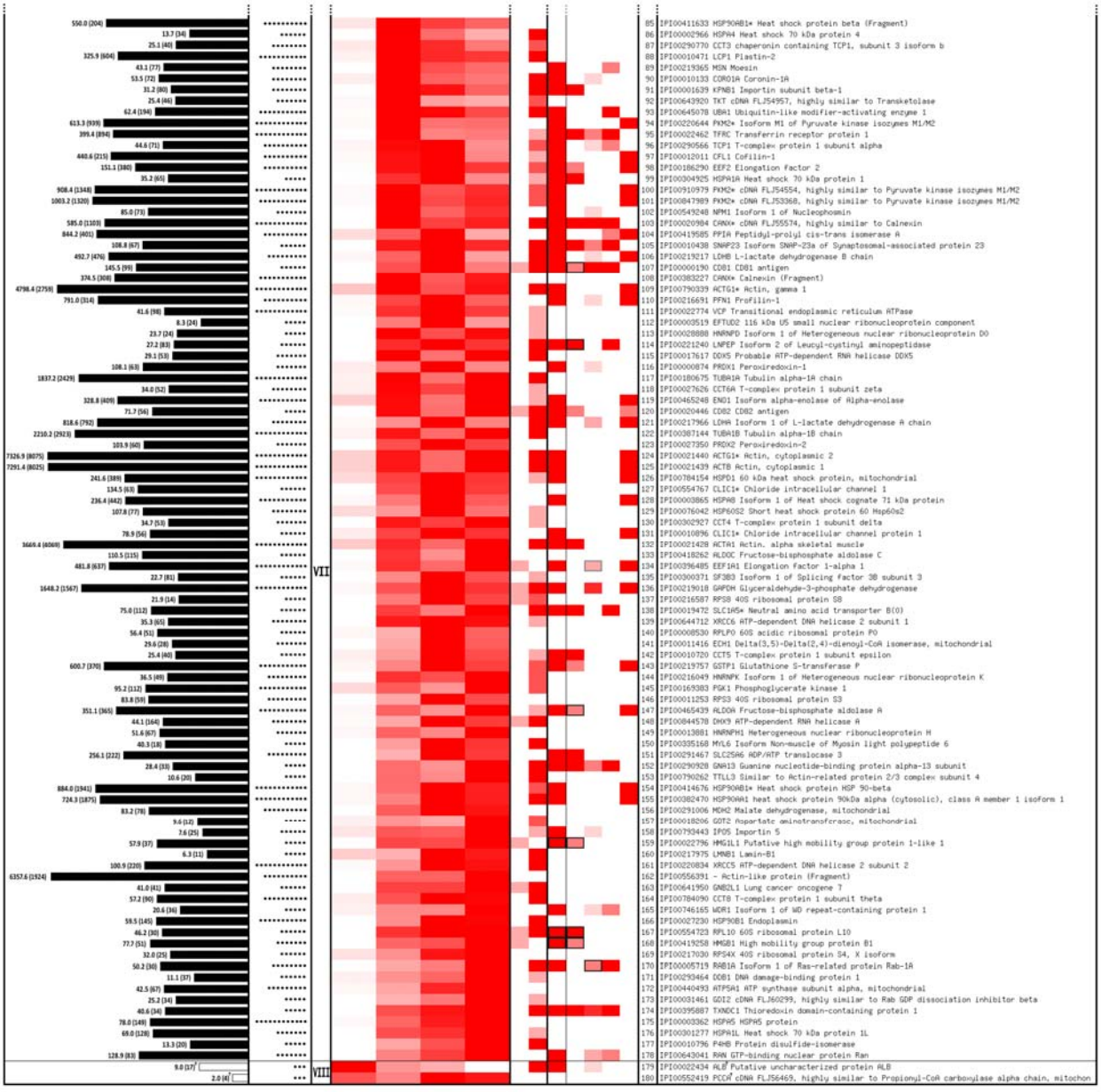

Figure 11 cont.

Having confirmed the specificity and low background of CuAAC and affinity enrichment methods, we proceeded with the large-scale identification of proteins targeted by the az/alk-FAs in Jurkat T cells. Az/alk-FA-labeled and control total cell lysates were reacted with clickable and cleavable affinity reagents (alk-azo-biotin, az-azo-biotin, respectively), purified by streptavidin enrichment and sodium dithionite elution protocol described above (Figure 6B). The Coomassie blue-stained gels of the recovered proteins were then processed using standard protocols for gel-based proteomics and analyzed by nano-reverse-phase liquid chromatography and tandem mass spectrometry for protein identification using the LTQ-Orbitrap. Two initial proteomic runs were performed with az-12-labeled cell lysates, followed by four additional experiments using az/alk-FAs of different chain length (Figure 6C). Tandem MS/MS analysis of tryptic peptides followed by database searches using Sequest and X!Tandem with standard peptide hit filter criteria and two-unique peptide cut-off for protein identification revealed many known fatty-acylated proteins and new candidate fatty-acylated proteins not present in or significantly enriched compared to negative controls (Appendix Tables 1 and 2). Preliminary analysis of proteins selectively recovered from az-12 and alk-12-labeled cell lysates yielded a similar composition of protein hits (Appendix Tables 1, 2 and 6), which is consistent with our previous experiments that demonstrated az-FA and alk-FA both function as efficient chemical reporters of protein fatty-acylation on known proteins such as Lck, LAT and Ras[191]. Proteomic data based on peptide spectral counts from negative control lanes (-, n = 6), myristic (az-12, n = 3 and alk-12, n = 3), palmitic (alk-14, n = 3) and stearic (az-15, n = 1, alk-16, n = 3) acid analogs were therefore combined and collated to evaluate proteins that were selectively labeled with fatty acid chemical reporters and separated into high and medium confidence groups (Appendix Tables 1 and 2). The normalized peptide spectral counts from the protein hits were represented in a heat map for

comparative analysis (Figure 11). A total of 178 proteins were identified $\geq$ 5 times in az/alk-FA labeled cells with at least $\geq$ 5-fold enrichment of normalized peptide counts compared to negative controls were sorted into the high confidence group; only two proteins were inversely enriched in the negative controls (Figure 11). Another 183 proteins in the medium confidence list were selectively identified at least twice in az/alk-FA labeled cells and yielded at least 3-fold enrichment of normalized peptide counts compared to negative control (Appendix Table 2). Direct comparison of selectively identified protein hits from two proteomic runs of alk-16 performed in parallel suggested that the high confidence protein hits are reproducibly recovered from independent experiments. Many known candidate fatty-acylated proteins were recovered from our proteomic studies. For example, N-myristoylated proteins such as ADP-ribosylation factors (ARF1, ARF4 and ARF5), Src-family kinase Lck, protein phosphatase 1G (PPM1G), G-protein subunits (G_i, G_k and G_o) and myristoylated, alanine-rich protein kinase C substrate (MARCKS), as well as S-palmitoylated proteins including the transferrin receptor (TfR), calnexin (CANX), N-Ras, and tetraspanins (CD81 and CD82) were identified from az/alk-FA labeled Jurkat T cells in the high confidence group (Figure 11).

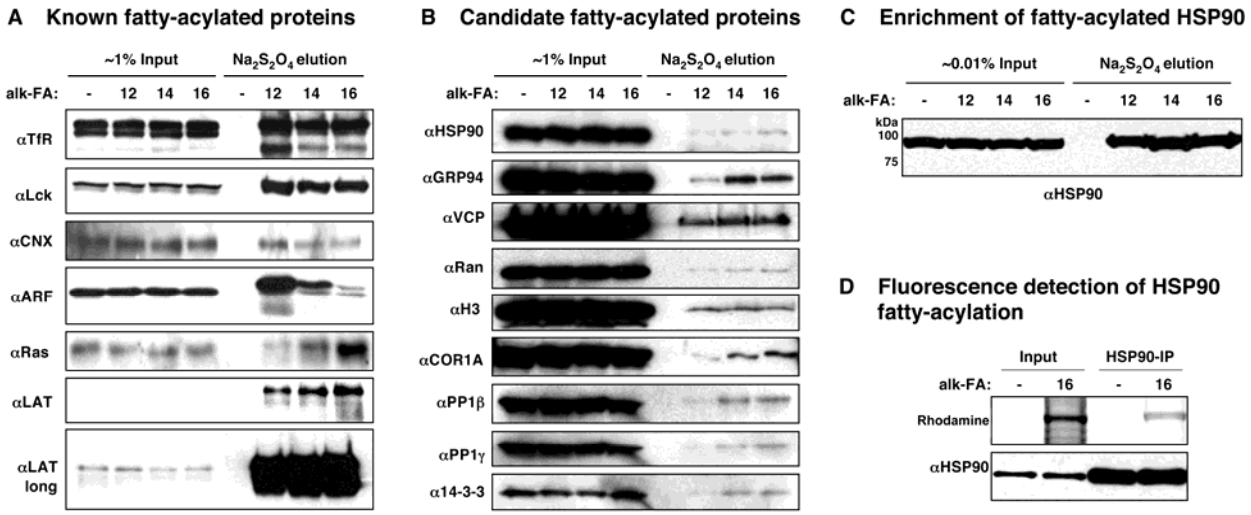

Figure 12 Immunoblot analysis of selectively recovered proteins. A) Known fatty-acylated proteins. B) New candidate proteins. C) Robust enrichment of endogenously fatty-acylated HSP90. D) In-gel fluorescence detection of immunoprecipitated HSP90 metabolically labeled with alkynyl-fatty acid after CuAAC reaction with az-Rho.

To evaluate the specific recovery of protein hits from az/alk-FA-labeled cell lysates in our proteomic dataset, total cell lysates and $Na_2S_2O_4$ eluents were analyzed by Western blot. Immunoblot analysis for known fatty-acylated proteins such as transferrin receptor (TfR), Lck, calnexin (CANX), linker-associated with T cell activation (LAT), N-Ras, and ADF-ribosylation factors (ARFs) confirmed mass spectrometric identification and specific retrieval from az/alk-FA-labeled cell lysates (Figure 12A). We also evaluated other proteins from our proteomic dataset that have not been previously confirmed to be fatty-acylated. For example, Western blot analysis for heat shock proteins (HSP90, GRP94), phosphatase subunits (PP1β, PP1γ) and other proteins (Ran, histone (H3), coronin-1A (COR1A), 14-3-3, transitional endoplasmic reticulum ATPase (p97/VCP) confirmed their selective retrieval and identification by mass spectrometry (Figure 12B). The analysis of fatty-acylated protein levels in total cell lysates compared to the amount of protein recovered from affinity enrichment affords a qualitative measure of how much

protein is metabolically labeled with fatty acid reporters. N-myristoylated proteins such as Lck and ARFs appeared to be recovered in significant amounts compared to total cell lysates (Figure 12A). Interestingly, the S-palmitoylated protein LAT was robustly enriched in $Na_2S_2O_4$ elutions compared to cell lysates (Figure 12A). In contrast, relatively low amounts of HSP90, GRP94, PP1β, PP1γ and Ran are recovered from fatty acid reporter labeling and affinity enrichment compared to cell lysates (Figure 12B), indicating a large dynamic range of fatty-acylation stoichiometry; the robust signal for known fatty-acylated proteins is likely a factor in their previous discovery. As expected, increasing the amount of alk-FA/CuAAC enriched proteins relative to total cell lysate demonstrated more robust relative signal intensity of alk-FA labeled endogenous HSP90 (Figure 12C). Fatty-acylation of endogenous HSP90 was also confirmed following alk-16 labeling of Jurkat cells, immunoprecipitation, CuAAC reaction with az-Rho and in-gel fluorescence scanning (Figure 12D).

To further validate mass spectrometric and antibody detection of low level fatty-acylation of proteins and clarify highly homologous histone H3 variants, we analyzed the fatty acid reporter labeling and enrichment of overexpressed constructs bearing epitope-tags (Figure 13). These experiments employed alk-14, as this analog yielded the broadest labeling amongst the candidate proteins analyzed. The results for HSP90, PP1γ and the histone H3 variants recapitulated the data obtained for endogenously expressed proteins and revealed similar labeling and enrichment of histones H3.1, H3.2 and H3.3. Because all histone H3 variants share a single conserved cysteine at position 110, we analyzed alk-14 labeling and enrichment of epitope-tagged H3.2 and C110A mutant as well as endogenous calnexin in parallel as a positive control (Figure 13B). Although calnexin signal was similar for both alk-14 labeled samples, H3.2 labeling was completely

abrogated in C110A construct, indicating that Cys110 is the site of H3.2 fatty-acylation. These results highlight the utility of bioorthogonal chemical reporters for large-scale profiling of fatty-acylated and identification of novel fatty-acylated proteins from fully solubilized cell lysates.

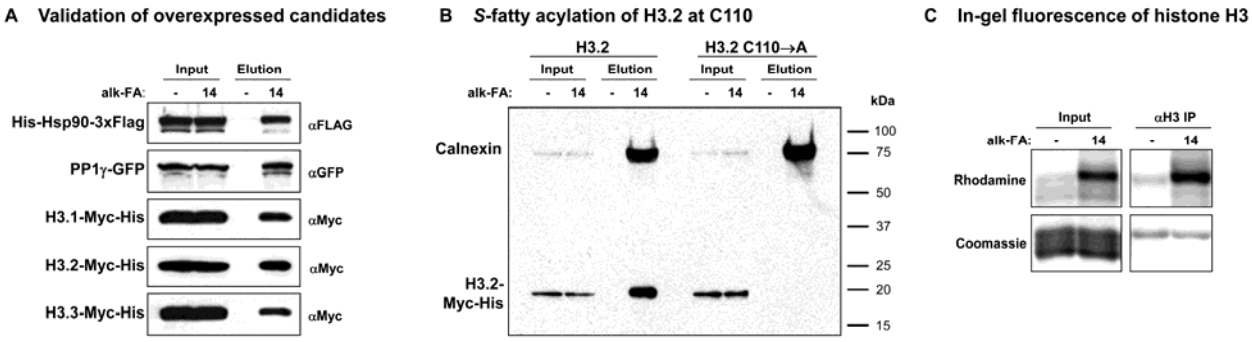

Figure 13 Further validation of candidate proteins. A) Validation of Hsp90, PP1γ and histone H3 variants by transfection with tagged constructs. B) Identification of Cys110 in histone H3.2 as the site of S-palmitoylation. While endogenous calnexin is similarly enriched and detected, all recovery of H3.2 is lost with a C110A mutation. C) Isolation of histone H3 by immunoprecipitation and in-gel fluorescence detects fatty-acylation directly.

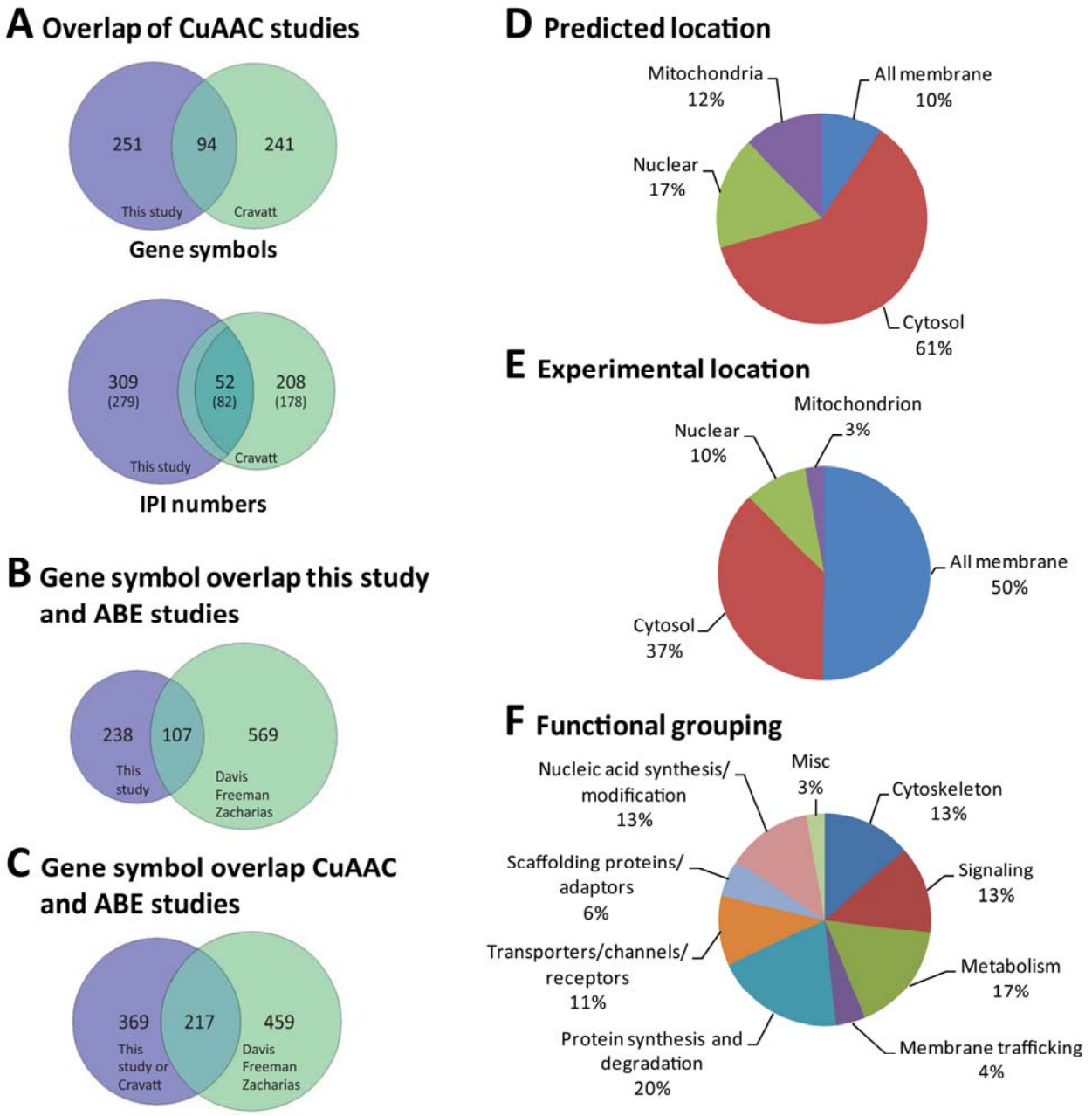

Figure 14 Overlap of fatty-acylated protein studies and analysis of selectively recovered proteins from this study. A) Comparative analysis of high and medium confidence protein hits recovered CuAAC studies by gene symbol and IPI numbers. For IPI numbers, parentheses represent values including possible interpretations of peptide identification not reported in Figure 2 or Supplementary Figure 4. B) Overlap of this study with acyl-biotin exchange studies. C) Overlap of all CuAAC studies and ABE studies by gene symbol. D) Subcellular distribution of high confidence protein hits based upon WoLF PSORT prediction algorithm. E) Subcellular distribution of high confidence protein hits based upon biochemical fraction studies of Jurkat T cells. F) Biological pathway analysis of high confidence protein hits.

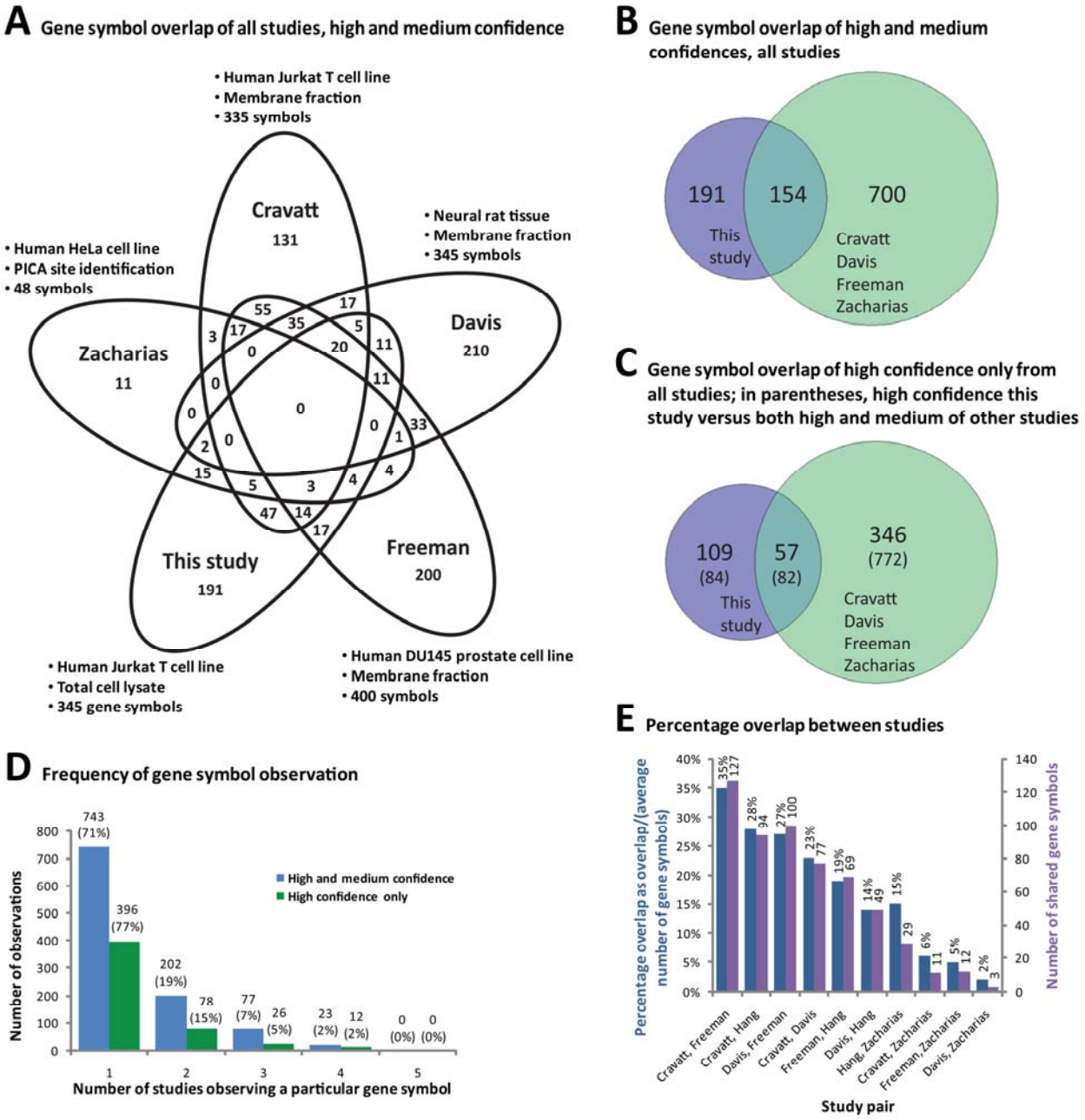

Figure 15 A) Gene symbol overlap of all studies, high and medium confidence. B) Full overlap of high and medium confidences, all studies. C) Gene symbol overlap of high confidence only from all studies; in parentheses, high confidence of this study versus both high and medium confidence of other studies. D) Frequency of gene symbol observation from all studies of fatty-acylated proteins. E) Percentage of overlap between study pairs. Right axis: number of shared gene symbols. Left axis: percentage of overlap calculated as (the number of shared gene symbols)/(the average number of gene symbols reported).

Comparative analysis of fatty-acylation proteomic studies

A comparative analysis of our proteomics dataset with other recently described large-scale studies of fatty-acylated proteins[122,188-190] yields a significant degree of overlap with reported fatty-acylated proteins as well as new candidate fatty-acylated proteins (Figure 14, Figure 15). The proteomic analysis of alk-16 (17-octadecynoic acid 17-ODYA) labeled Jurkat T cells by Martin and Cravatt using CuAAC ligation with biotin-azide, streptavidin enrichment and on-bead digestion followed by multidimensional protein identification technology (MudPIT)-based protein identification yielded ~125 high confidence fatty-acylated protein hits and another ~200 proteins with medium confidence[122]. Of the total list of fatty-acylated proteins identified by Martin and Cravatt, 52 IPI numbers (or 82 considering possible alternate identifications) and 94 gene symbols were shared with our dataset, representing a 17% – 26% overlap (Figure 14A). Even the lowest possible interpretation, this overlap is statistically significant for any reasonable assumption of active genes. As determined by hypergeometric distribution,[i] the chance of 52 proteins being randomly choosen for these survey sizes from the full 74,016 enteries of the IPI database is 1.08 E -67. At a reasonable number of expressible human genes, 24,500, the liklihood has grown to 1.74 E -43 and, assuming the 5381 proteins of Jurkat T cells identified by proteomics[210] represent the full repitoir of expressed proteins, the chance increases to a still unlikely 1.60 E -13. The number of expressed proteins must fall below 2294 for the chances of

[i] The hypergeometric distribution calculates the chances of a given number of marked samples being taken from a finite population of marked and unmarked entities without replacement. In the classical example, if *x* marbles are taken from an urn with *y* white and *z* black marbles, it calculates the liklihood of choosing *n* black marbles. In this case, the urn would contain e.g. 74,016 marbles of which 361 (the number of proteins identified in this work) would be black. If 260 are chosen at random (the number of proteins identified in the Cravatt study), the chance of those 260 containing 52 black marbles is 1.08 E -67.

random overlap to exceed 0.01, indicating that the overlap in protein identification is not random.

In addition to the variability intrinsic to MS identification studies, two key features likely account for differences among our Jurkat T cell datasets. Our studies were performed with total cell lysates that included nuclear and cytosolic proteins, compared to enriched membrane fractions from the Martin and Cravatt studies[122]. Moreover, the clickable and cleavable reagents (alk-azo-biotin and az-azo-biotin) enabled the use of gel-based proteomics strategies, whereas Martin and Cravatt utilized on-bead protease digestion and MudPIT-based protein identification methods[122]. Our analysis also employed multiple fatty acid reporters, especially myristic acid analogs, and recovered N-myristoylated proteins (e.g. PPM1G, MARCKS, ARF4 and ARF5) not present in the Martin and Cravatt dataset (Figure 11), although alk-16 (17-ODYA) was also reported to target some N-myristoylated proteins[122]. While many known and new candidate fatty-acylated proteins from total cell lysates were identified in our high and medium confidence datasets (Figure 11), selective recovery and enrichment of some known S-palmitoylated proteins such as LAT not reaching those confidence levels could be clearly observed by Western blot analysis of sodium dithionite elutions (Figure 12). Time of incubation with fatty acid analogs, differential recovery of peptides by gel-based versus MudPIT proteomic strategies and subtle differences in MS analysis can all play a role for the differences in fatty-acylated protein profiling between this study and that of Martin and Cravatt.

ABE yields complementary datasets in comparison to CuAAC-based systems, as metabolic incorporation of analogs is not required. The ABE analysis of membrane fractions from rat

neural sources by the Davis laboratory yielded ~113 high confidence and ~318 medium confidence S-acylated proteins[211], 49 of these protein hits were also identified in our proteomic dataset when compared by gene symbol (Appendix Tables 1, 2 and 3). ABE can also be performed with isotopically-encoded thiol-alkylating reagents (iCAT) for comparative analysis of S-acylated peptides, which identified ~46 S-palmitoylated proteins as well as their potential sites of modification from HeLa cells[189]. Our study shares 29 gene symbols with this data and if peptides are searched against our dataset, 61 IPI numbers are common (Appendix Tables 1, 2 and 3). These degrees of overlap are statistically significant (Table 5). ABE enrichment of S-acylated peptides from lipid-raft and non-lipid raft associated proteins from a human prostate cancer cell line has also yielded ~67 known and ~331 candidate S-acylated proteins as well as many potential sites of Cys modification[190]; of these, 69 were also identified by our study by gene symbol or 68 by IPI number (Appendix Tables 1, 2 and 3). While the ABE and fatty acid reporter proteomic studies were performed in different cell types and protein samples, the proteomic studies using fatty acid chemical reporters in combination with CuAAC suggests that bioorthogonal ligation methods can have higher signal-to-noise (Figure 12)[122]. For example, ~1/4 of proteins recovered from alk-FA labeling were also found in negative controls, whereas ~2/3 of proteins recovered from ABE experiments were recovered from samples not treated with hydroxylamine. With respect to the chemical linkage of fatty acid protein modification, fatty chemical reporters enable the analysis of N-myristoylated proteins and other potential sites of amino acid modification[122] (Appendix Tables 1 and 2), whereas ABE selectively targets S-acylated proteins[186,188-190] and has enabled identification of site modifications[189,190]. Although the total number of proteins identified by ABE studies from three different protein sources was higher, the overlap with this study was not substantially greater (107 gene symbols versus 94

gene symbols;, see Figure 14 and Figure 15). Overall, both methods provide important insight into the diversity and biochemical properties of fatty-acylated proteins.

Within all five studies, ~70% – 80% of proteins were observed in only one study (Figure 15 and Appendix Table 3), ~15% – 20% were observed in two studies, ~5% – 7% were observed in three and only 2% were observed in four studies. With the exception of some comparisons to Zacharias data, the overlaps of all studies were statistically significant for reasonable assumptions of the number of expressed proteins (Table 5). No proteins were observed in all studies, reflective of the different methods of analysis, sample preparation and protein sources. Of the high confidence lists only, C11orf59, Canx, FAM108B1, Gna13, Gnai2, Gnai3, Gnaq, Gnas, KIAA0152, Snap23, Tfrc and Txndc1 were shared among four studies; expanding this to include medium confidence hits, Cd81, Dnajc5, GNAO1, Igf2r, Rab1b, Rap2b, RPL12, Rpl5, RPS3A, Scamp3, SLC25A5 are also observed. The greatest overlap between studies both in number of shared gene symbols and percentage overlap was observed between the Cravatt and Freeman studies (35%, 127 symbols), followed by Cravatt and this study (28%, 94 symbols) and Davis and Freeman (27%, 100 symbols). The high degree of overlap between this study and Cravatt's is likely due the same cell type (Jurkat T cells) and use of fatty acid chemical reporters. The Cravatt, Davis and Freeman datasets all analyzed membrane fractions of mammalian cells, which likely favored identification of similar protein compositions.

Table 5 Statistical significance of overlap between studies for Figure 15 using a hypergeometric distribution with various assumptions of the number of active genes (expressed proteins). 5381 proteins were identified by proteomics in the global survey of Jurkat T cells[210]. All pairs but the last are statistically significant even assuming 5381 (an underestimate) represents all proteins expressed in cells.

Pair	% overlap	Gene symbol overlap	*p*-value for assumed expression of				
			24,000 genes	12,000 genes	6,000 genes	5381 genes	3000 genes
Cravatt, Freeman	35%	127	1.61E-142	3.31E-105	6.45E-69	2.23E-63	4.91E-35
Cravatt, Hang	28%	94	5.48E-96	9.39E-69	1.10E-42	8.93E-39	2.58E-19
Davis, Freeman	27%	100	3.57E-97	2.32E-68	5.63E-41	6.71E-37	6.23E-17
Cravatt, Davis	23%	77	1.19E-70	1.00E-48	3.60E-28	3.71E-25	8.94E-11
Freeman, Hang	19%	69	2.74E-54	3.42E-35	6.09E-18	1.60E-15	5.37E-05
Davis, Hang	14%	49	3.93E-34	5.13E-21	1.09E-09	3.43E-08	0.0175887
Hang, Zacharias	15%	29	1.01E-41	4.27E-33	1.40E-24	2.94E-23	2.66E-16
Cravatt, Zacharias	6%	11	4.54E-11	5.59E-08	4.03E-05	0.0001044	0.0091529
Freeman, Zacharias	5%	12	1.38E-11	3.14E-08	3.81E-05	0.0001055	0.0117337
Davis, Zacharias	2%	3	0.026684	0.110640	0.229857	0.2321302	0.1071548

Functional analysis of fatty-acylated proteins targeted by chemical reporters

The large-scale analysis of proteins labeled with az/alk-FA chemical reporters of different chain lengths provides the opportunity to evaluate the specificity and diversity of protein fatty-acylation in mammalian cells. To determine the specificity of protein labeling with az/alk-FA reporters, the protein hits identified from our proteomics experiments were sorted into groups based on the frequency of their recovery with different chain length of az/alk-FA reporters using normalized peptide spectral counts. A survey of the protein hits revealed many proteins were la-

beled with multiple fatty acid chemical reporters (group VII) (Figure 11). In contrast, some proteins were labeled in a chain length-dependent fashion (group I and III) (Figure 11). For example, 44 proteins were only labeled by myristic analogs (az-12, alk-12) (group I) and 56 proteins were uniquely labeled by stearic acid analogs (az-15, alk-16) (group III). Many proteins labeled by alk-14 were targeted by shorter and longer fatty acid reporters (Figure 11), consistent with our previous observations that this fatty acid analog labels both *N*-myristoylated and *S*-palmitoylated proteins[191]. The fatty acid chain length labeling preferences were also evident by Western blot analysis of selectively recovered proteins (Figure 12A and B). *N*-myristoylated proteins such as ARFs were preferentially labeled by alk-12, whereas *S*-palmitoylated Ras was most efficiently recovered with alk-16 (Figure 12A). Alternatively, *N*-myristoylated and *S*-palmitoylated proteins such as Lck were recovered with multiple fatty acid reporters (Figure 12A). Other known *S*-palmitoylated proteins such as the transferrin receptor did not reveal a significant preference for length of fatty acid reporters (Figure 12B). Differences in relative signal intensity of isoforms of the same protein between input and elution, such as with the transferrin receptor, likely represent preferential fatty-acylation of particular isoforms.

Bioinformatic prediction of fatty-acylation of recovered proteins

Analyzing our proteomic dataset with the *N*-myristoylation prediction program Myrbase[183] showed that high and medium confidence predictions were limited exclusively to proteins of groups I, II and III labeled by short-chain analogs (az/alk-12/alk-14) (Figure 11). At 0.49 ± 0.47, the average confidence of predicted myristoylation for these groups is statistically different from the average confidence for groups IV-VII (average = 0.03 ± 0.10; $p = 1.16\text{E-}05$, two-tailed heteroscedastic T-test). (Note that these averages represent a combination of confidence and frequen-

cy of prediction, as the absence of predicted myristoylation is included and given a confidence of 0. Thus, at ~0.5, all "average" proteins within groups I-III are predicted to be fully myristoylated with half maximum confidence, or alternatively, half are predicted to be myristoylated with maximum confidence and half are predicted to bear no myristoylation.) In contrast, the CSS-Palm prediction program based on previously reported *S*-palmitoylated proteins[22] predicted fatty-acylation of proteins throughout the dataset (Figure 11). Predicted palmitoylation showed little correlation with chain length of fatty acid analog and less statistical difference (confidence of predicted palmitoylation for groups I-III, 0.71 ± 0.42; confidence in groups IV-VII, 0.51 ± 0.51; $p = 0.03$, two-tailed heteroscedastic T-test). The less significant difference between groups I-III and IV-VII is likely not reflective of biological correlation but rather the bias of prediction from known motifs: only 45% of proteins in groups IV-VII have been reported by any study, whereas 63% have been reported for groups I-III. Assuming that the average predicted confidence of palmitoylation based on known motifs scales linearly with the number of previously identified palmitoylated proteins, if 63% of proteins had been previously identified in groups IV-VII as they were for groups I-III, the average confidence of palmitoylation would increase to 0.70 and the statistical significance by the same test would increase to $p = 0.90$. Thus, palmitoylation prediction was distributed more or less uniformly and did not correlate to any particular analog chain length. These results are consistent with the reported specificity of protein fatty-acylation, which found that NMTs preferentially utilize myristoyl-CoA through a relatively defined enzyme active site for *N*-myristoylation of proteins[212], whereas *S*-acylated proteins typically contain a heterogeneous composition of fatty acids of different chain lengths and unsaturation[18,19,213,214].

Annotation of subcellular location of identified proteins

We evaluated the subcellular localization associated with proteins recovered from fatty acid chemical reporter labeling. It should be noted that protein samples from our studies represent an unbiased total cell lysates from lysis and solubilization using strong detergent (4% SDS) after nuclease treatment (benzonase), which eliminated the presence of any insoluble pellet. Our lysate thus includes nuclear, cytoplasmic, organelle and membrane proteins. Predicting protein localization for our dataset with the WoLF PSORT subcellular prediction algorithm[215] revealed that the majority of recovered fatty-acylated proteins are expected to be cytosolic (61%), with the remainder distributed to nuclei (17%), mitochondria (12%) and membranes (10%) (Figure 14D, Appendix Table 4A). Similar results were obtained from a corrected Bonferroni test for enrichment of GO cellular component annotations of recovered proteins (p-value < 0.01). Cytosolic and cytoplasmic annotations were the most enriched (18% and 32% respectively) followed by mitochondrial (11%), nuclear (6%) and ribosomal annotations (2% – 6%) (Figure 16, Table 6). Annotated and predicted localizations contrast in particular for membrane and cytosol with recent experimental data of Jurkat T cells generated by biochemical subcellular fractionation and proteomic analysis[210]. Based on that data, az/alk-FA-labeled proteins partition primarily in membranes (50%), followed by cytosol (37%), nucleus (10%) and mitochondria (3%) (Figure 14E). The difference between the predicted and experimental subcellular localization suggested that many proteins predicted or annotated to be cytosolic may be membrane associated through fatty-acylation. Interestingly, proteins recovered from total cell lysate were also significantly enriched in nuclear proteins (APEX1, HNRNPF, HNRNPH1, HNRNPL, DDB1, MCM2, MCM3, MCM6, NCL, PARP1, PCNA, PHB, PPP1CB, RANP1, RPS2, SUPT16H, UBC, XPO1, XRCC5,

XRCC6), suggesting that protein fatty-acylation could contribute to dynamic membrane targeting within the nucleus as well.

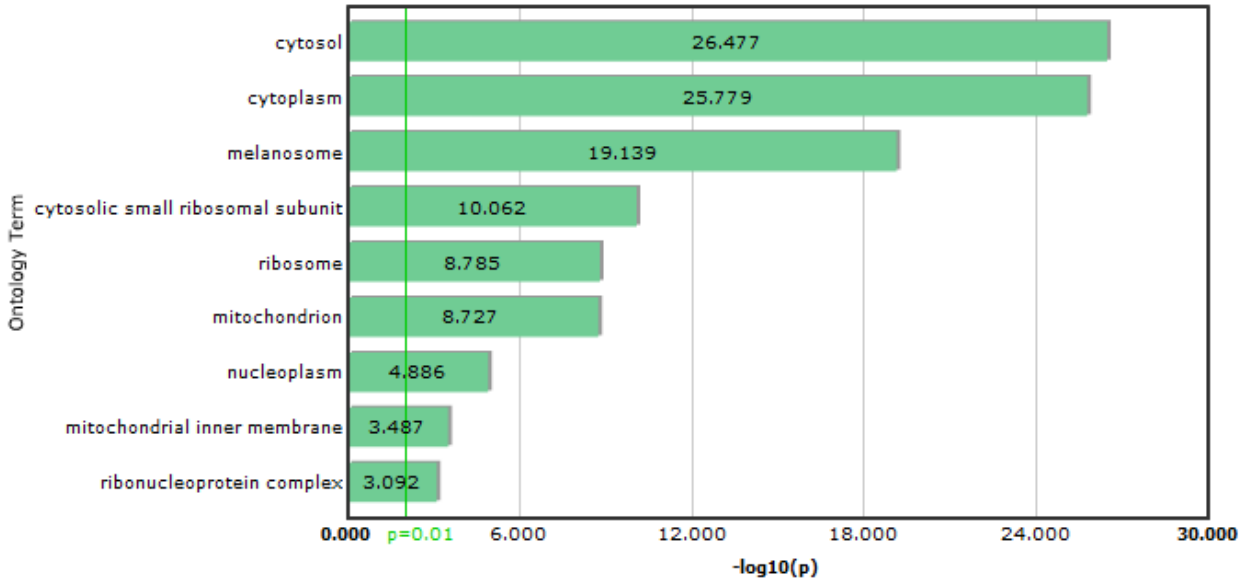

Figure 16 Enriched GO annotations of cellular component, sorted by corrected *p*-value. 204 proteins from high and medium confidences bore cellular component annotations and were tested with a Bonferroni and corrected Bonferroni test. At $p < 0.01$, recovered proteins were most enriched in cytosolic and cytoplasmic, ribosomal, nuclear, mitochondrial and ribonuclear proteins.

Term	*Identified of Total Existing*	*% of total in list*	*p-value*	*Corr. p-value*
cytosol	63 of 735 annotated in Human	18.05	4.69e-32	3.34e-27
cytoplasm	112 of 2445 annotated in Human	32.09	2.34e-31	1.66e-26
melanosome	20 of 57 annotated in Human	5.73	1.02e-24	7.27e-20
cytosolic small ribosomal subunit	12 of 36 annotated in Human	3.44	1.22e-15	8.66e-11
ribosome	20 of 165 annotated in Human	5.73	2.31e-14	1.64e-09
mitochondrion	39 of 680 annotated in Human	11.17	2.64e-14	1.88e-09
nucleoplasm	20 of 262 annotated in Human	5.73	1.83e-10	1.30e-05
mitochondrial inner membrane	15 of 176 annotated in Human	4.30	4.58e-09	3.26e-04
ribonucleoprotein complex	8 of 45 annotated in Human	2.29	1.14e-08	8.09e-04

Table 6 Enriched GO annotations of cellular component. Tabular data to Figure 16. Sorted by corrected Bonferroni *p*-value.

Function, biological processes and pathways of identified proteins

The biological processes of proteins labeled with fatty acid chemical reporters were first examined manually (Figure 14F, Appendix Table 5), revealing that fatty-acylated proteins take part in wide range of cellular processes from signal transduction to protein synthesis and degradation. Statistical analysis of GO annotations using the Bonferroni correction (p-value < 0.01) revealed multiple enriched annotations within identified fatty-acylated proteins. Within molecular function, identifications were enriched in proteins that bind nucleotides, unfolded proteins and other proteins; proteins with GTPase activity and those binding GTP or ATP; proteins of the ribosome; and proteins which bind RNA (Figure 17 and Table 7). These molecular functions correlate well to enriched GO biological process annotations: most enriched were proteins involved with transitional elongation (ribosomal proteins); protein folding, refolding and polymerization (processes requiring nucleotide, ATP or GTP binding); cellular component movement (ATP and GTP binding); several ubiquitin-dependent proteasome processes; and telomere maintenance (Figure 18, Table 8; appendix I). Finally, networks of functional association and protein-protein interactions within identified proteins were analyzed and visualized using STRING[216], a database and data mining tool which distills a wide variety of information to confidences of protein interactions that are then clustered (Figure 19). A high confidence level of interaction (0.876), this analysis strikingly revealed tight associations within the large protein complexes of the ribosome (circled in blue), heterogeneous nuclear ribonucleoprotein complexes (hnRNPs, yellow), and the proteasome (green). In addition to these highly pronounced associations, seven other major networks were also apparent involving: interrelated cytoskeleton components including 1) the tubulins in particular and their regulatory molecules (highlighted in red); 2) actins and their regulatory molecules (periwinkle), and 3) myosins (rose); 4) the 14-3-3 adaptor proteins which modulate

the activity of binding partners in a wide variety of signaling pathways (purple); 5) a large number of guanine nucleotide-binding proteins (G proteins, which serve to modulate or transduce transmembrane signal systems), connected with several membrane-bound kinases and members of the Ras family (brown); 6) an association of proteins involved in nuclear processes including DNA damage repair and maintenance, cell cycle progression, nucleoside metabolism and nuclear chaperonins (light green); and 7) enzymes of sugar metabolism including the interrelated glycolysis/gluconeogenesis, fructose/mannose, pentose phosphate and pyruvate metabolic pathways (pink). Additional networks included nuclear transport (teal), mitochondrial electron transport (grey) and ATP synthesis (orange), and multiple DNA replication licensing factors of the highly conserved mini-chromosome maintenance proteins (MCM) involved in the initiation of eukaryotic genome replication (light blue). Notably, HSP90α sat at the center of the interconnected networks (red asterisks), closely flanked by HSP90β and other heat shock proteins.

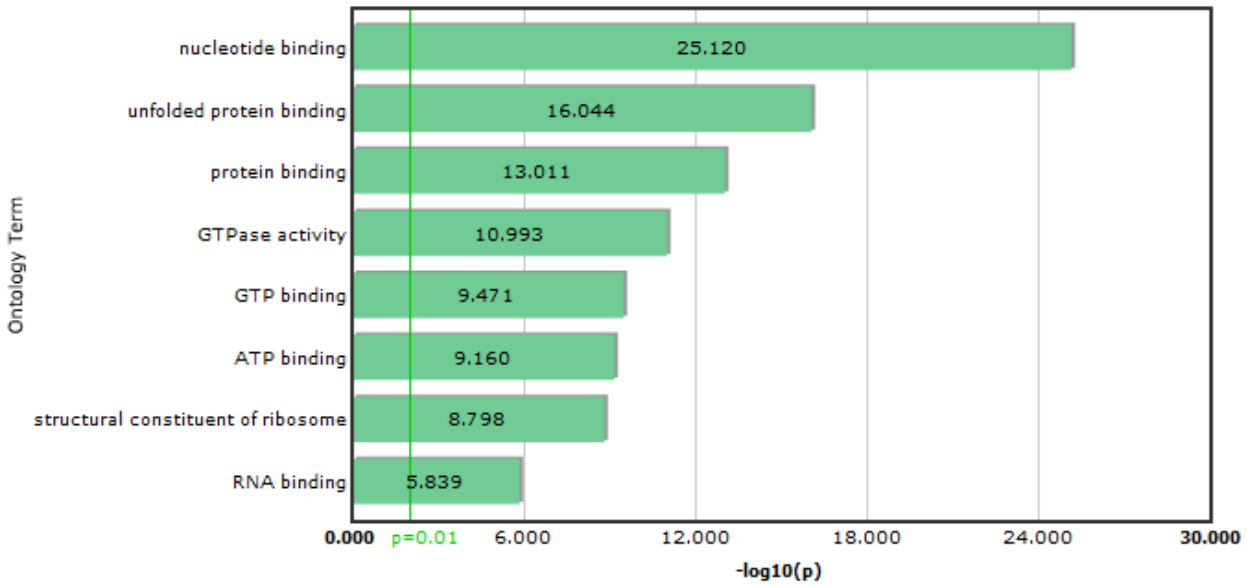

Figure 17 Enriched GO annotations of molecular function, sorted by corrected *p*-value. 197 proteins from high and medium confidences bore molecular function annotations and were tested with a Bonferroni and corrected Bonferroni test. At $p < 0.01$, recovered proteins were most enriched in proteins that bind nucleotides, unfolded proteins and other proteins, proteins with GTPase activity and those binding GTP or ATP, proteins of the ribosome and those which bind RNA.

Term	*Identified of Total Existing*	*% of total in list*	*p-value*	*Corr. p-value*
nucleotide binding	73 of 1066 annotated in Human	20.92	1.10e-30	7.59e-26
unfolded protein binding	21 of 88 annotated in Human	6.02	1.31e-21	9.04e-17
protein binding	106 of 3178 annotated in Human	30.37	1.42e-18	9.75e-14
GTPase activity	22 of 164 annotated in Human	6.30	1.48e-16	1.02e-11
GTP binding	25 of 257 annotated in Human	7.16	4.92e-15	3.38e-10
ATP binding	43 of 794 annotated in Human	12.32	1.01e-14	6.92e-10
structural constituent of ribosome	19 of 146 annotated in Human	5.44	2.32e-14	1.59e-09
RNA binding	23 of 312 annotated in Human	6.59	2.11e-11	1.45e-06

Table 7 Enriched GO annotations of molecular function. Tabular data to Figure 17. Sorted by corrected Bonferroni *p*-value.

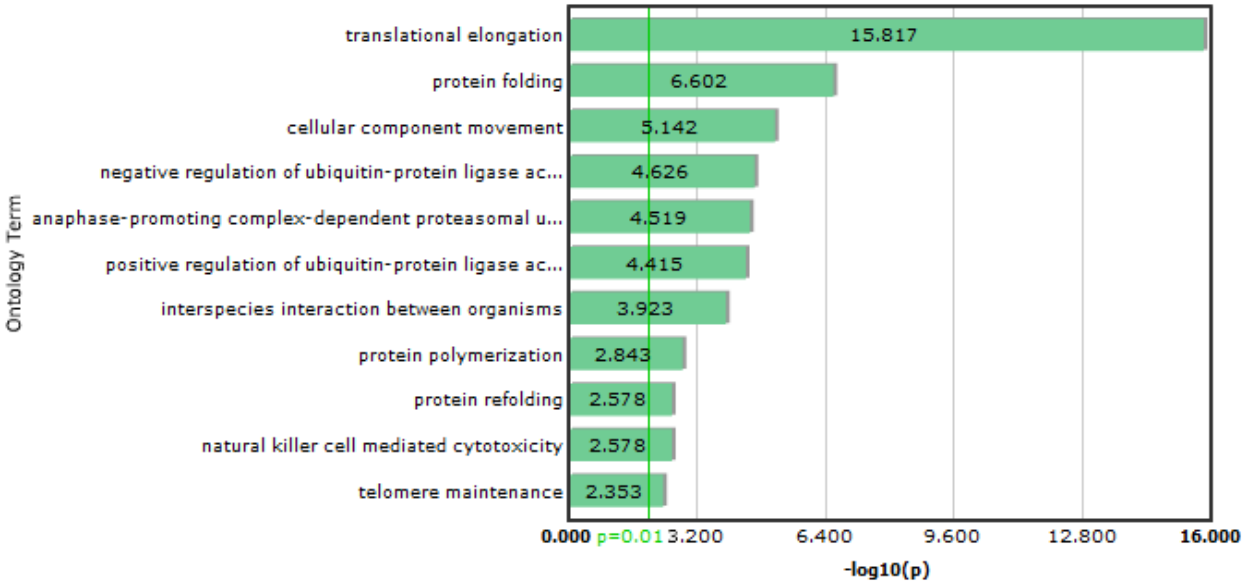

Figure 18 Enriched GO annotations of biological process, sorted by corrected *p*-value. 194 proteins from high and medium confidences bore cellular component annotations and were tested with a Bonferroni and corrected Bonferroni test. At $p < 0.01$, recovered proteins were most enriched in proteins involved with transitional elongation; protein folding, refolding and polymerization; cellular component movement; several ubiquitin-dependent proteasome processes; and telomere maintenance. See also Table 8 for complete descriptions.

Term	*Identified of Total Existing*	*% of total in list*	*p-value*	*Corr. p-value*
translational elongation	21 of 90 annotated in Human	6.02	2.25e-21	1.53e-16
protein folding	15 of 110 annotated in Human	4.30	3.70e-12	2.50e-07
cellular component movement	11 of 65 annotated in Human	3.15	1.07e-10	7.21e-06
negative regulation of ubiquitin-protein ligase activity during mitotic cell cycle	9 of 43 annotated in Human	2.58	3.50e-10	2.37e-05
anaphase-promoting complex-dependent proteasomal ubiquitin-dependent protein catabolic process	9 of 44 annotated in Human	2.58	4.47e-10	3.03e-05
positive regulation of ubiquitin-protein ligase activity during mitotic cell cycle	9 of 45 annotated in Human	2.58	5.68e-10	3.84e-05
interspecies interaction between organisms	14 of 142 annotated in Human	4.01	1.76e-09	1.19e-04
protein polymerization	6 of 23 annotated in Human	1.72	2.12e-08	1.44e-03
protein refolding	3 of 4 annotated in Human	0.86	3.90e-08	2.64e-03
natural killer cell mediated cytotoxicity	3 of 4 annotated in Human	0.86	3.90e-08	2.64e-03
telomere maintenance	4 of 9 annotated in Human	1.15	6.55e-08	4.43e-03

Table 8 Enriched GO annotations of biological process. Tabular data to Figure 18. Sorted by corrected Bonferroni *p*-value.

Figure 19 Functional and protein-protein interaction networks within identified fatty-acylated proteins of both high and medium confidences. A STRING[216] analysis of interactions at a high confidence level (≥0.876) revealed highly interconnected associations of three large protein complexes including the ribosome (circled in blue); heterogeneous nuclear ribonucleoprotein complexes (hnRNPs, yellow); and the proteasome (green). Seven other major networks were also apparent involving: interrelated cytoskeleton components including 1) the tubulins in particular as well as their regulatory molecules (highlighted in red); 2) actins and their regulatory molecules (periwinkle), and 3) myosins (rose); 4) the 14-3-3 adaptor proteins which modulate the activity of binding partners in a wide variety of signaling pathways (purple); 5) a large number of guanine nucleotide-binding proteins (G proteins, which serve to modulate or transduce transmembrane signal systems), connected with several membrane-bound kinases and members of the Ras family (brown); 6) an association of proteins involved in nuclear processes including DNA damage repair and maintenance, cell cycle progression, nucleoside metabolism and nuclear chaperonins (light green); and 7) enzymes of sugar metabolism including the interrelated glycolysis/gluconeogenesis, fructose/mannose, pentose phosphate and pyruvate metabolic pathways (pink). Additional networks included nuclear transport (teal), mitochondrial electron transport (grey) and ATP synthesis (orange), and multiple DNA replication licensing factors of the highly conserved mini-chromosome maintenance proteins (MCM) involved in the initiation of eukaryotic genome replication (light blue). Note the presence of HSP90α at the center of the interconnected networks (red asterisks), closely flanked by HSP90β and other heat shock proteins.

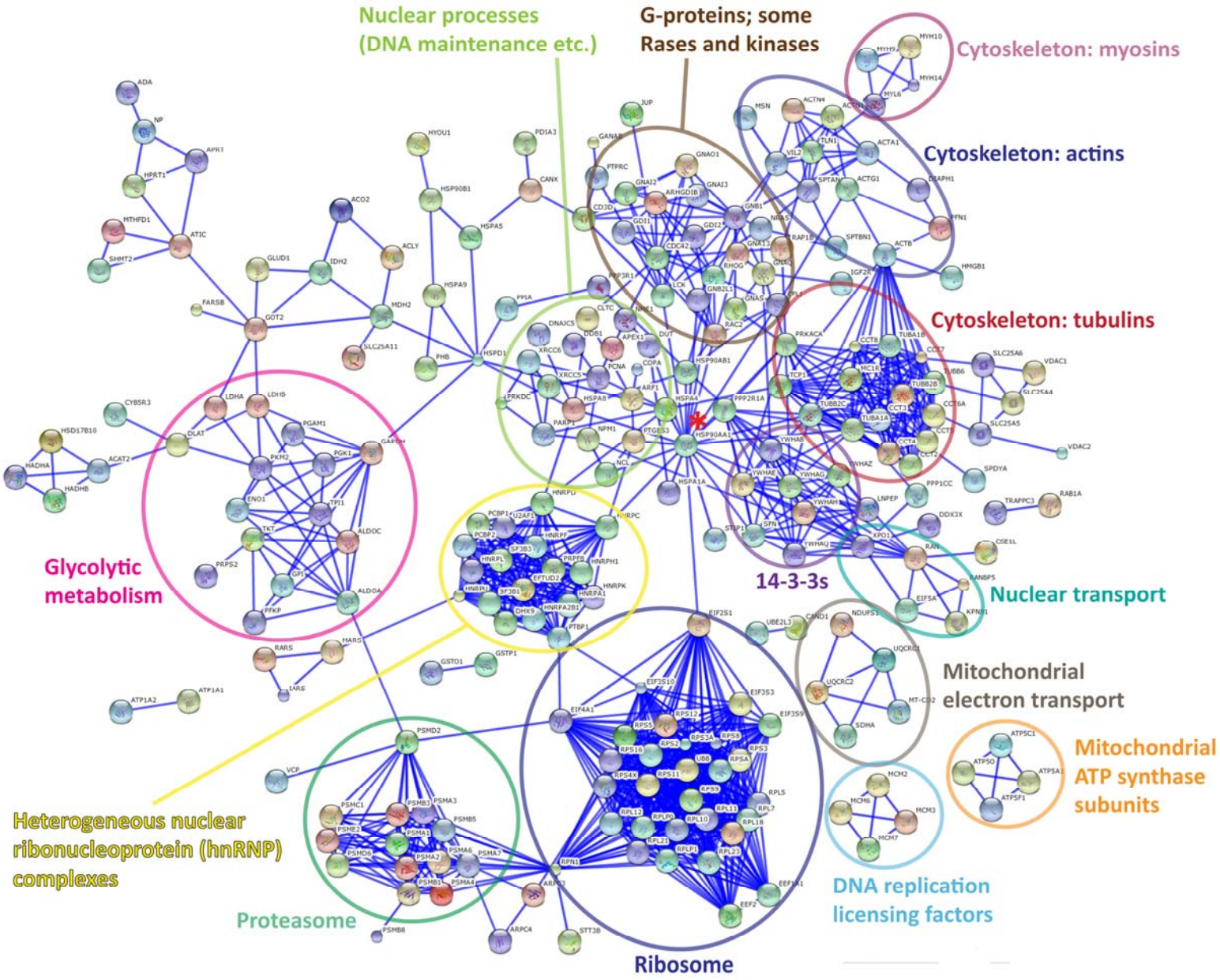
Nuclear processes
(DNA maintenance etc.)
G-proteins; some
Rases and kinases
Cytoskeleton: myosins
Cytoskeleton: actins
Cytoskeleton: tubulins
Glycolytic
metabolism
14-3-3s
Nuclear transport
Mitochondrial
electron transport
Mitochondrial
ATP synthase
subunits
Heterogeneous nuclear
ribonucleoprotein (hnRNP)
complexes
Proteasome
Ribosome
DNA replication
licensing factors

Correlation of fatty-acylation amd protein cysteine content

Examination of the relationship between MS spectral counts and cysteine content of proteins identified in either positive fractions or negative fractions for both high and medium confidence levels revealed no correlation ($R^2 < 0.1$) (Figure 20). Proteins with no or very low cysteine content were found to have relatively large numbers of spectral counts in both positive and negative enrichments. Likewise, proteins with higher cysteine contents exhibited both high and low signal in both enrichment sets.

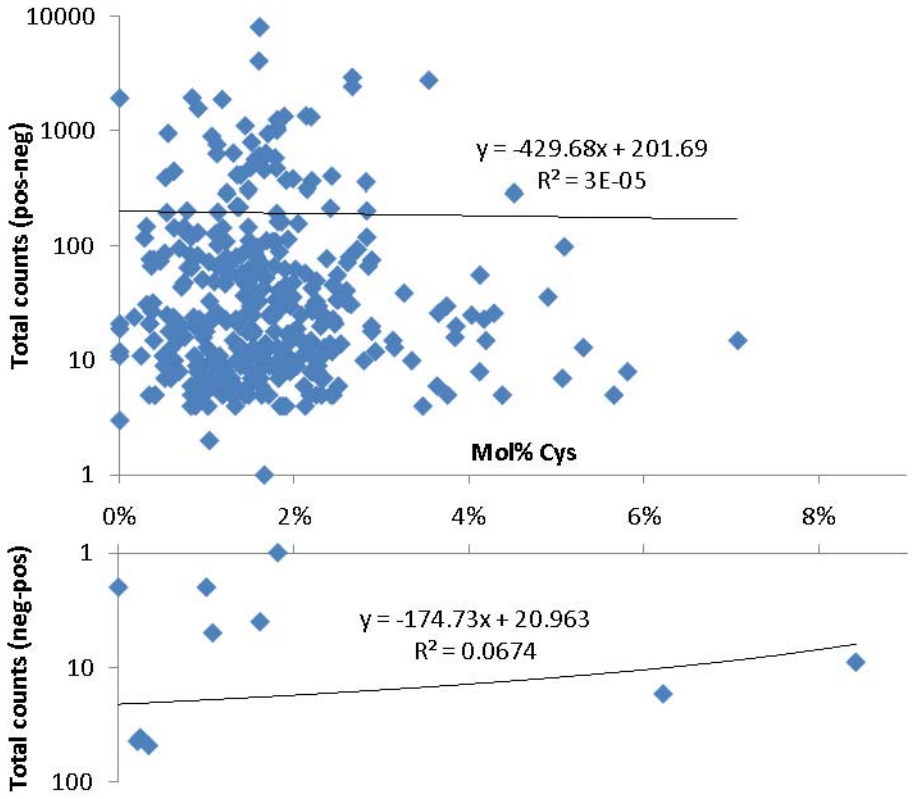

Figure 20 Total observed counts for proteins identified in high and medium confidences as a function of cysteine content. Top chart: proteins identified enriched in positive fractions, log scale. Bottom chart: proteins identified enriched in negative fractions, log scale, inverted. No significant correlation exists between cysteine content and total observed counts for either group. The insignificant correlation which does exist is negative for counts enriched in positive fractions, reflecting decreased counts with increased cysteine content, and likewise positive for counts enriched in negative fractions, reflecting decreased counts with increased cysteine content.

Discussion

Unraveling the diversity of fatty-acylated proteins and the underlying regulatory mechanisms of protein fatty-acylation in eukaryotes is a challenging task. In this work, the large-scale identification of fatty-acylated proteins from mammalian cells has been performed using azide/alkyne-functionalized fatty acids from an unbiased, fully solubilized protein preparation. The enrichment and proteomic analysis of proteins targeted by fatty acid reporters has revealed 57 known fatty-acylated proteins as well as 109 new candidate proteins (by gene symbol) with high confidence that may be regulated by protein fatty-acylation; extending the list to include high and medium confidence, this study identified 191 new candidate proteins and shared 154 identifications (Figure 15B and C). The comparison of azide- and alkynyl-fatty acid chemical reporters of various chain lengths highlights the utility of both classes of lipid analogs for detecting fatty-acylated proteins as well as the selectivity of protein fatty-acylation in cells.

Mechanisms of fatty-acylation

The mechanism of fatty-acylation for proteins identified in our survey including histone H3 could be due to chemical *S*-acylation (background reactivity, Figure 21A), substrate-mediated *S*-acylation (auto- or self-acylation, Figure 21B), enzyme-catalyzed *S*-acylation (i.e. DHHC-PATs, Figure 21C), or some combination of these factors (Figure 21). At sufficient concentrations, coenzyme A activated fatty acids are capable of spontaneous chemical *S*-acylation on cysteine residues of proteins (GAPDH[217]; SNAP-25[218]; tubulin[219,220]; rhodopsin[221]; G protein α subunits[222]; myelin proteolipid protein (MPP)[223]; actin, lactate dehydrogenase, fetuin[224]; Bet3[225]) and also short peptides containing the natural site of protein palmitoylation[224,226]. Many of the proteins demonstrated to undergo chemical acylation are also substrates for PATs (SNAP-25[227]; tubulin

and G protein subunits[220]; rhodopsin[221]) and many also undergo catalytic self-palmitoylation (GAPDH[228], SNAP-25[218], MPP[223], Bet3[225]). Likewise, DHHC-PATs load themselves prior to palmitoyl transfer through an auto-acylation event[229]. Auto-*S*-palmitoylation can occur in a regulated fashion such as in response to fatty acid levels (GAPDH[217]) or protein-protein interactions (SNAP-25 palmitoylation is 100-fold greater when bound in the SNARE complex[218]; likewise, the presence of $G_{\beta\gamma}$ enhances G_{α} palmitoylation[222]). This combination of mechanisms has complicated analysis of the regulation of *S*-palmitoylation.

S-acylation depends on two factors: the concentration of activated CoA ester and the relative reactivity of the cysteine. Reactivity depends on chemical accessibility and the concentration of thiolate anion capable of a nucleophilic attack, which is enhanced by physical proximity to basic residues[225,230-232] (Figure 21B and C). For DHHC-PATs, mutation of the cysteine-proximal basic residues (aspartic acid and histidine) sharply reduces or abrogates transferase activity[229,233]. Local concentration of fatty acid-CoA, and thus acylation, is favored by hydrophobic residues near a site of modification[230,234]; similarly, DHHC-PATs can place a bound fatty acid at a specific residue. Within mammalian cells, the global concentration of activated free fatty acids is kept to low nanomolar concentrations by the presence of acyl-CoA binding protein (ACBP)[235,236]. Because most studies of chemical acylation have not included ACBP and have extended the concentration of activated fatty acids even into the millimolar range, their results must be interpreted cautiously. Upon the inclusion of ACBP, chemical acylation of peptides and proteins can be eliminated; this buffering does not affect DHHC-PAT activity[224,235,237] and the effect on self-palmitoylating proteins has generally not been studied.

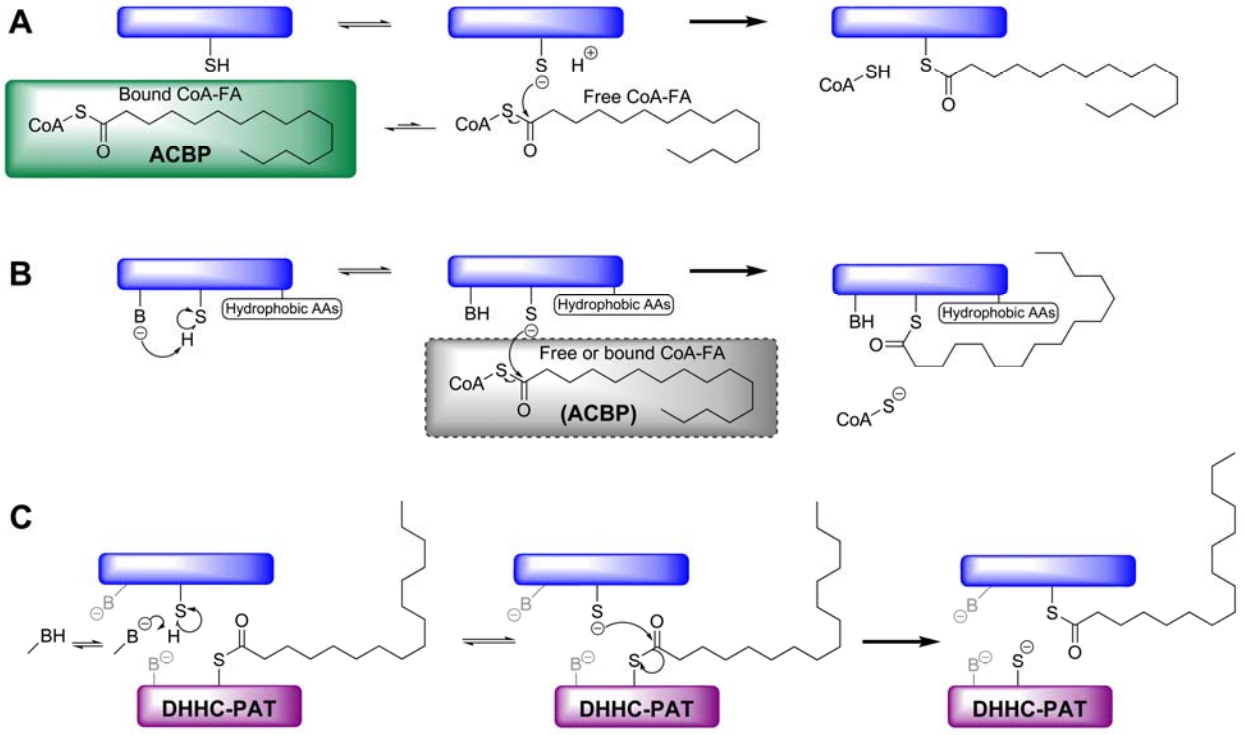

Figure 21 Mechanisms of protein *S*-acylation (palmitoylation). Mechanisms are not exclusive and may occur simultaneously. A) Chemical modification between coenzyme A activated fatty acids and cysteine-containing proteins (blue) can occur at sufficiently high concentration of fatty acid-CoA. In most of the cell, acyl-CoA binding protein (ACBP, green) normally buffers activated fatty acids to the low nanomolar range, quenching this mechanism. However, in mitochondria, chemical modification may play a greater role. B) Catalytic substrate-mediated (or auto- or self-acylation) occurs for a number of proteins, including DHHC-PATs, where the reaction prepares the PAT for palmitoyl transfer to other proteins. *S*-acylation is assisted by cysteine proximity to basic residues, which favor formation of a thiolate anion, and proximity to hydrophobic residues, which favor increase local concentration of fatty acid-CoA. DHHC-PAT activity is uninfluenced by ACBP; the effect of ACBP on other self-acylating proteins has not been studied. Protein-protein interactions can greatly influence the rate of auto *S*-acylation. C) Enzymatic DHHC-PAT-mediated palmitoylation likely occurs via a similar mechanism and many proteins that show self-modification are PAT substrates. A catalytic base is shown and might belong to either the DHHC-PAT (purple) or substrate protein. PAT specificity results from distinct PAT-protein interactions. The exact mechanism of DHHC-PAT-mediated palmitoylation remains a topic of study.

Other possible mechanisms of fatty-acylation

In addition to the cellular mechanisms of Figure 21, post-lysis acylation could result from disrupting ACBP binding, releasing activated fatty acids, and the simultaneously exposure of buried free cysteines such as C110 of H3 variants. The extent of this reaction will depend on the concentration of CoA activated fatty acid; in the case of click chemistry analysis, the relative concentrations of clickable and native fatty acids; the concentrations of protein; the relative concentration of other thiols such as glutathione; and finally the time and temperature before small molecules are removed from lysate proteins, e.g. by precipitation. No studies of protein fatty-acylation to date have addressed this possible mechanism and specific strategies to elucidate its potential contribution are described below in Future Directions.

Fatty-acylation does not correlate to protein cysteine content

While post-lysis modification with fatty acids cannot be excluded without additional experimentation, the prevalence of such a mechanism would favor higher recovery of proteins with high cysteine content. No significant correlation was found between cysteine content and MS counts ($R^2 < 0.1$) (Figure 20). The poor correlation that does exists for positive counts in excess of negative is negative, reflecting a decreased overall signal with increased cysteine content, and the small correlation between negative counts in excess of positive is positive, reflecting decreased signal in negative samples with increasing cysteine content. Cysteine content alone is thus unpredictive of enriched peptide counts, suggesting that post-lysis does not significantly contribute to recovered signal. However, this represents and overall trend and in particular for proteins such as H3, in which a free sulfhydryl is known to be maintained and which is present in large quanti-

ty, exceptions may be present. Further experimentation will shed light on this possibility (see Future Directions).

Possibility of "in vivo *chemical fatty-acylation"*

In addition to the mechanisms of Figure 21 and *ex vivo* post-lysis chemical acylation, the possibility for a sort of "*in vivo* chemical palmitoylation" exists for enzymes with highly reactive functional groups, in particular (but not exclusively) cysteine sulfhydryls. Such reactive functional groups are abundant in enzymes with oxidoreductase activity, such as the peroxiredoxins, and are also present in enzymes subject to redox control like the serine/threonine protein phosphatase-1 subfamily[238]. The active nature of these sulfhydryls presents the possibility of an almost immediate reaction with any nearby molecules of activated CoA esters; if depalmitoylation is kinetically slower, a palmitoylated state would be favored. Such "background" chemical acylation might be purposeful, as for the regulation of GAPDH activity, or alternatively might represent true background chemical reaction within the cell cleared either by intrinsic activity or an extrinsic enzyme. Notably, five of six peroxiredoxins were identified in this dataset, multiple members of the protein phosphatase-1 family and over 20 proteins bearing annotations of redox activity (see Table 9). One of the few proteins found to be common to four studies, thioredoxin domain-containing protein 1, was also identified, suggesting this mechanism could be widespread. Most of these proteins displayed a preference for fatty acid chain length, either long or short, and while this behavior would be unexpected in the denatured state, such preferences can be easily interpreted as the result of unique protein properties such steric accessibility or size and layout of hydrophobic and electrostatic interactions. Many of these proteins or their relatives were also detected in ABE experiments performed on rat brain tissue (Appendix Table 3), sug-

gesting that detection of such reactive proteins is not unique to cell culture or click chemistry. However, as with post-lysis modification, analysis of the possibility of *in vivo* chemical modification of reactive proteins will require further experimentation. The question would best be addressed by monitoring possible a reaction *in vitro* between purified proteins, such as those of Table 9, and a traceable fatty acid analog CoA-ester (radioactive or clickable) at low concentration preferably in the presence and absence of ACBP. Increased modification with time would present strong evidence that this mechanism occurs *in vivo*. Modification to unity would reflect extrinsic de-acylation while an equilibrium state of partial fatty-acylation indicates the proteins have an intrinsic de-acylation activity.

Table 9 Proteins identified in this work annotated to have redox function.

Protein name	Symbol
APEX nuclease (multifunctional DNA repair enzyme)	APEX1
C-1-tetrahydrofolate synthase, cytoplasmic	MTHFD1
Cytochrome c oxidase subunit II	COX2
D-3-phosphoglycerate dehydrogenase	PHGDH
Glutamate dehydrogenase (NAD(P)+)	GLUD1
Hydroxyacyl-Coenzyme A dehydrogenase, type II	HADH2
Isocitrate dehydrogenase [NADP], mitochondrial	IDH2
Lactate dehydrogenase B	LDHB
Malate dehydrogenase, mitochondrial	MDH2
NADH-ubiquinone oxidoreductase 75 kDa subunit, mitochondrial	NDUFS1
Peroxiredoxin-1	PRDX1
Peroxiredoxin-2	PRDX2
Peroxiredoxin-3	PRDX3
Peroxiredoxin-4	PRDX4
Peroxiredoxin-5, mitochondrial	PRDX5
Protein disulfide-isomerase	PP4HB
Protein disulfide-isomerase A3	PDIA3
Succinate dehydrogenase complex, subunit A, flavoprotein (Fp)	SDHA
Synaptic vesicle membrane protein VAT-1 homolog	VAT1
Thioredoxin domain-containing protein 1	TXNDC1
Trifunctional protein alpha-subunit	HADHA

Chain length preference in fatty-acylation

Preference for particular fatty acid chain lengths was seen dramatically for proteins such as ARFs, RAS or coronin 1A (Figure 12), but not for others such as VCP or Lck. Several factors likely combine to result in such biases. Enzymatically, both NMTs and DHHC PATs have been shown to have relatively broad substrate recognition centered on myristic acid (14 carbons[176]) and somewhere around palmitic and stearic acids (16 – 18 carbons[216]), respectively. Especially in

the case of dual myristoylation and palmitoylation, such as for Lck, no particular chain length preference is expected and none was observed. Likewise, for proteins bearing a sole myristoylation, as for the ARFs, a strong preference for myristic acid analogs is expected and was observed (Figure 12). In the case of palmitoylation by DHHC-PATs, while substrate chain length preference has been observed in competition experiments[216], the unknown enzyme structure and modification mechanism leaves multiple questions for the many mammalian transferases. First, the fatty acid substrate specificity of distinct PATs remains unknown and may be PAT-specific, perhaps controlled at their loading step. Second, the protein substrate specificity of loaded PATs remains unresolved. Thus, the chain length preference shown by Ras could be explained by modification with one or more PAT preferring a longer chain length, while likewise, the lack of specificity seen for VCP could reflect modification with PATs showing reduced specificity, or even modification by PATs with enhanced recognition of shorter chain lengths. Third, in addition to the affinities between PATs and their protein substrates, the protein to be acylated could interact with the specific fatty acid loaded on the transferase to foster or discourage binding and thus *S*-acylation. For example, by sterically protruding into a region filled by longer, but not shorter, fatty acids, protein substrates could be preferentially modified by binding PATs bearing shorter length fatty acids. Analogous interactions might exist for preference of longer chain lengths. PAT protein substrates may thus themselves provide an additional level of chain length preference in addition to the preference of the modifying PAT(s). For auto-acylation including PAT loading, hydrophobic, electrostatic, hydrogen bonding and steric interactions will govern substrate binding and result in energetic preference for some particular chain length; in the case of desaturation or similar chain length, preference may be very close, as previously described[216]. Finally, fatty-acylation of all types will be subject to simple stoichiometry: given a large enough

excess of a non-ideal chain length, incorporation of that fatty acid will be favored even in the presence of better substrates.

Metabolic modification of fatty-acid analogs

Due to the terminal position of their functionalization, both alkyne and azido fatty acid analogs are likely subject to catabolic and anabolic processes. Over time, these processes may alter the *in vivo* composition of analog chain length. This possibility is supported by the detection of many known myristoylated proteins after overnight incubation with alk-16[122]. Likewise, ARF modification with palmitic or stearic acid analogs was detected in this work (Figure 12), although with substantially reduced signal. Both enzyme substrate tolerances and metabolic processes could explain these observations. However, the strong influence of analog chain length on recovered signal for proteins like the ARFs indicates that metabolic exchange did not equalize the chain lengths of added analogs within the experimental timescale. The exact nature of fatty acid metabolism may be complex and will depend on time and metabolic state. For example, catabolism will be favored under conditions of limited energy or high metabolic demand. Similarly, given sufficient energy, added analog chain length will likely be subject redistribution towards the fatty acid chain length equilibrium of the cell. Other sources of fatty acids, such as from cell culture sera, will also influence this redistribution. Thus, outwardly similar experimental conditions may yield potentially unexpected differences in metabolism. However, within study of protein fatty-acylation, the effect of metabolism may be minor: given sufficient sensitivity, the reduced yet present incorporation of non-optimal chain lengths for a given fatty acid transferase will always be observed and the substrate tolerance of myristoylation and palmitoylation machinery[216176] indicates that the biological effect of two more or two less carbons is not substantial. This may be

especially true for fatty-acylation: in contrast to incorporation of amino acids or nucleotides, fatty acids from 12-20 carbons have relatively similar properties within an aqueous environment. In addition, because lipidated proteins often bear multiple lipid modifications, the effect of small differences in chain length will often be diluted. The chain length preferences of NMTs and PATs may thus not reflect overall requirements of hydrophobicity but rather the evolution of systems of control (constitutive and dynamic). Teasing out the contribution of metabolism on added fatty acid analogs will be most easily accomplished by MS analysis of the modified peptides to establish the fatty acid composition. Such detail will also provide insight into the proportion of modification. Until such experimentation, at least within the conditions of this work, the observation of substantial chain length preference of particular proteins for both short and long chains indicates that metabolic exchange did not equalize the concentration of myristic to stearic acid analogs and all proteins predicted to be myristoylated with high or medium confidence fell within the groups modified by myristic acid (Figure 11).

General implications for fatty-acylation and its study

Given the unbiased approach of this survey and the discovery of fatty-acylated proteins throughout diverse cellular compartments, the best conclusion might well be “What does it mean?” and the next perhaps “What is the next study?” These questions can be neither quickly dismissed nor quickly addressed, and their accurate answer lies in much future experimental work. However, contrasting Figure 2 and Figure 19, we begin to gain some insight into the full implications of this work.

Figure 2 represents the prevailing view of fatty-acylation: the modification, which can be dynamic in the case of palmitoylation, results in membrane association of proteins from a wide variety of membrane-related processes and regulates protein function by controlling subcellular location. This view is not incorrect and, in Figure 19, is reflected in the tight networks of G-proteins and 14-3-3 adapters. Both protein families are known to be heavily involved in signaling and signal modulation at the membrane. Despite these two similarities, Figure 2 and Figure 19 are strikingly different. In particular, Figure 2 bears no mention of the cytoskeleton, which must interface by some mechanism with membranes throughout the cell; it illustrates the nucleus but reports no role for fatty-acylation in any nuclear process, and likewise it shows no role of myristoylation or palmitoylation in metabolism[ii] or protein complexes, in particular the ribosome and proteasome, nor within complexes of mitochondria. Statistical analysis of GO annotations shows that the proteins identified in this work support the networks of Figure 19. Enriched cellular component annotations include cytosolic, nuclear, mitochondrial, ribosomal and ribonuclear proteins (Figure 16 and Table 6; note that cytoskeletal proteins are annotated as cytosolic), in good agreement with the networked clusters. Correspondingly, enriched biological process annotations include translational elongation, protein polymerization, cellular movement (which includes cytoskeletal proteins and their regulators) and telomere maintenance (Figure 18 and Table 8). Protein folding and refolding processes were also statistically overrepresented, matching the central, chaperon-surrounded HSP90α hub of Figure 19 (marked with a red asterisks). Enriched molecular functions reflect these biological processes and include binding of nucleotides and RNA, proteins and unfolded proteins, ATP or GTP, as well as GTP hydrolysis (Figure 17 and Table 7). Thus, this

[ii] Notably, GAPDH has the largest number of connections within the metabolic network (10 spokes) and was found to be regulated by autocatalytic palmitoylation, which was proposed to have a regulatory role in the context of sugar metabolism[217].

work first suggests broader involvement of fatty-acylation in cellular processes and subcellular localizations than is currently appreciated.

Behind the disparity in overviews of Figure 2 and Figure 19 lies the influence and importance of sample preparation in the study of fatty-acylation: of the five current global studies of protein acylation, only this work analyzed fully solubilized cells while the other four employed membrane preparations, continuing a historical trend. For decades, membrane fractionation and mild detergent solubilization (RIPA, NP40, Brij, etc.) have been a common first step in the study of fatty-acylated proteins[239,240] despite the fact that both techniques leave behind large, undissolved and typically unanalyzed pellets. Data from the global proteomics survey of Jurkat T cells[210] yield a sense of the compositional difference between the lowly pellet and membrane fractionation. Within the 5381 proteins confidently identified, 25% were common to membrane and cytosolic fractions, 27% to membrane and nuclear fractions and only 14% were detected in all three fractionations. Well correlating to these proportions, 17% – 26% of fatty-acylated proteins were shared in common between this study and that of Cravatt[122] which employed a closely similar experimental approach with membrane fractionation of the same cell line as this study, and this study identified a total of 101 more proteins. Thus, this work secondly indicates the examination of proteins from membrane fractionation has left undetected large populations of proteins present in subcellular locations other than membranes. Discoveries have consequently converged on a membrane-centric view of the modification (Figure 2).

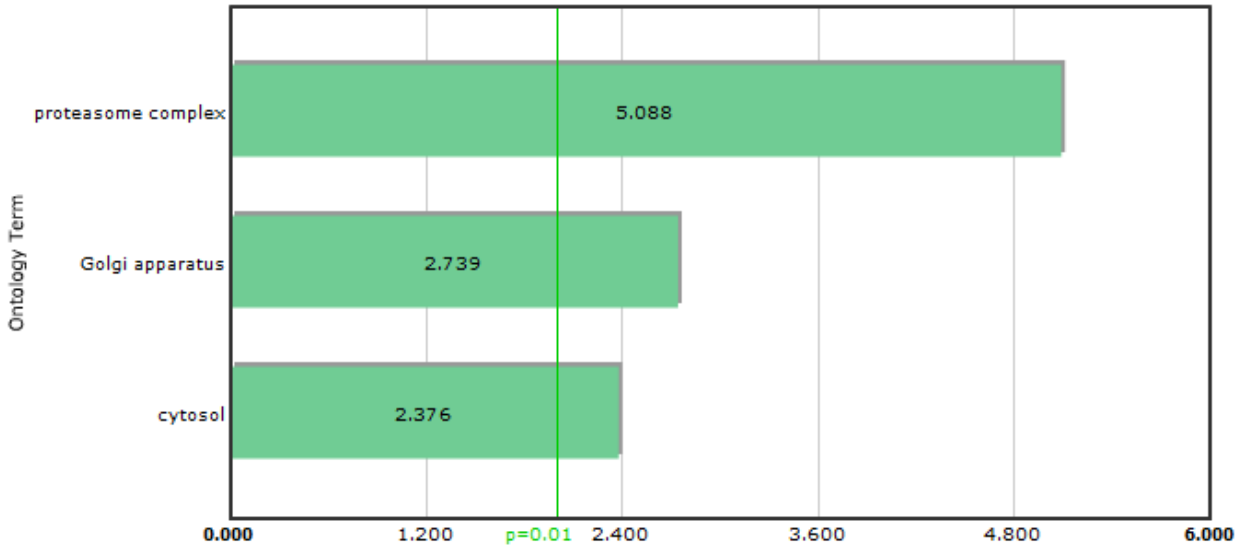

Figure 22 Enriched GO annotations of cellular component for full Cravatt dataset[122], sorted by corrected *p*-value. 133 proteins identified bore cellular component annotations and were tested with a Bonferroni and corrected Bonferroni test. Three components were enriched at $p < 0.01$.

Term	*Identified of Total Existing*	*% of total in list*	*p-value*	*Corr. p-value*
proteasome complex	7 of 28 annotated in Human	2.81	2.47e-10	8.17e-06
Golgi apparatus	19 of 462 annotated in Human	7.63	5.51e-08	1.82e-03
cytosol	24 of 735 annotated in Human	9.64	1.27e-07	4.20e-03

Table 10 Enriched GO annotations of cellular component for full Cravatt dataset[122]. Tabular data to Figure 22. Sorted by corrected Bonferroni *p*-value.

Supporting this conclusion, different sample preparations from the same cell line identified proteins from different cellular compartments and membrane fractionation yielded fewer statistically significant enrichments of cellular component. Repeating the analysis of Figure 16 and Table 6 for the full Cravatt dataset (Figure 22 and Table 10), three enrichments of cellular component were apparent versus nine for this work and the average statistically significance of enrichment was 16-fold lower (average corrected *p* value = 1.28 E -4 for this work vs. 2.01 E -3 for the Cravatt dataset). Only enrichments of cytosolic annotations were common to this study and compo-

nents of the membraneous Golgi apparatus were statistically overrepresented. The contrast in type and number of cellular component enrichment is first partially reflective of statistics. Within the proteins of this study, a similar yet smaller number of proteins were annotated to be part of the proteasome complex (5 vs. 7) and Golgi apparatus (15 vs. 19) but due to the lesser representation and the larger sample size of this dataset (361 vs. 260 proteins), these annotations did not reach statistical confidence. Second and more significantly, the differences in enrichment reflect the breadth and depth of sampling. Membrane preparation presents only the membrane-associated proteins of any given cellular component, hindering the identification of cellular components which contain protein members not bound to membranes. In the same way, the preparation favors enrichment of fully membraneous cellular components like the Golgi. For Jurkat T cells, these factors combined to yield a three-fold lower number of cellular component enrichments overall yet also new enrichments reflective of membrane preparation enrichment. Thus thirdly, this work suggests that analysis of the fraction(s) remaining after a membrane preparation could addess the bias of sample preparation while simultaneously maintaining enhanced detection of low-level membrane bound proteins.

A comparison of the 52 proteins shared in common between the two studies (or 82 considering possible subhit interpretations; see Appendix Table 3) to the dataset as a whole verifies the bias introduced by membrane fractionation. Compared to the full cohort (Figure 14F) in which 10% of proteins are predicted to be membrane bound and 50% were experimentally observed in membrane fractions, 14-18% of the shared 52-82 proteins are predicted to be membrane bound and 51-56% were experimentally observed (Figure 23). The skew towards a higher membrane composition is expected given the membrane preparation used in the comparison study. Cellular

component annotations of the common 52 proteins (Figure 24, Table 11) share statistical enrichment of cytosolic, cytoplasmic and ribosomal annotations with the full dataset; these annotations are often associated with membranes as shown by Figure 14 and Figure 23. However, distinctly missing from enriched annotations are non-membrane cellular components such as the nucleus and mitochondria. These differences are echoed by changed annotation enrichments of molecular function and biological processes (Figure 25, Figure 26, Table 12, Table 13): while often membrane-bound translational and ribosomal annotations remain enriched, others like cellular movement (i.e. cytoskeleton) are lost. Correspondingly, molecular functions like GTP binding and GTPase activity are no longer enriched but those common among membrane proteins, such as protein and nucleotide binding ubiquitous for G-protein subunits, remain. Due to the small sample size, multiple statistically significant enrichments are present for processes with small numbers of members. However, while the presence within 52 proteins of one member of a two-member annotation set is statistically significant (Figure 24, Figure 25, Figure 26, Table 11, Table 12, Table 13), meaning beyond the presence of fatty-acylation for that protein is tentative. Thus, the proteins shared with the Cravatt study are expectedly enriched in membrane bound proteins and often bear cytosolic and ribosomal annotations. Reflective of membrane selection, the common proteins lack cellular components, molecular functions and biological processes associated with the nucleus, cytoskeleton or mitochondria.

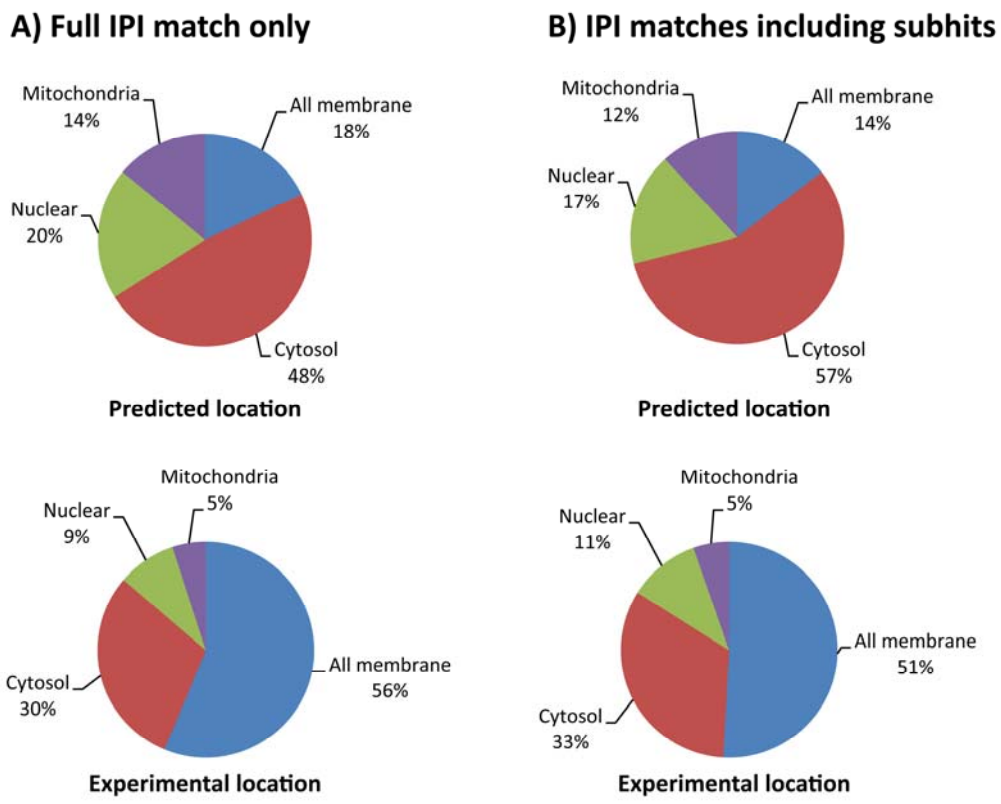

Figure 23 Predicted and observed subcellular location for proteins common to the data of this work and that of Cravatt[122]**.**

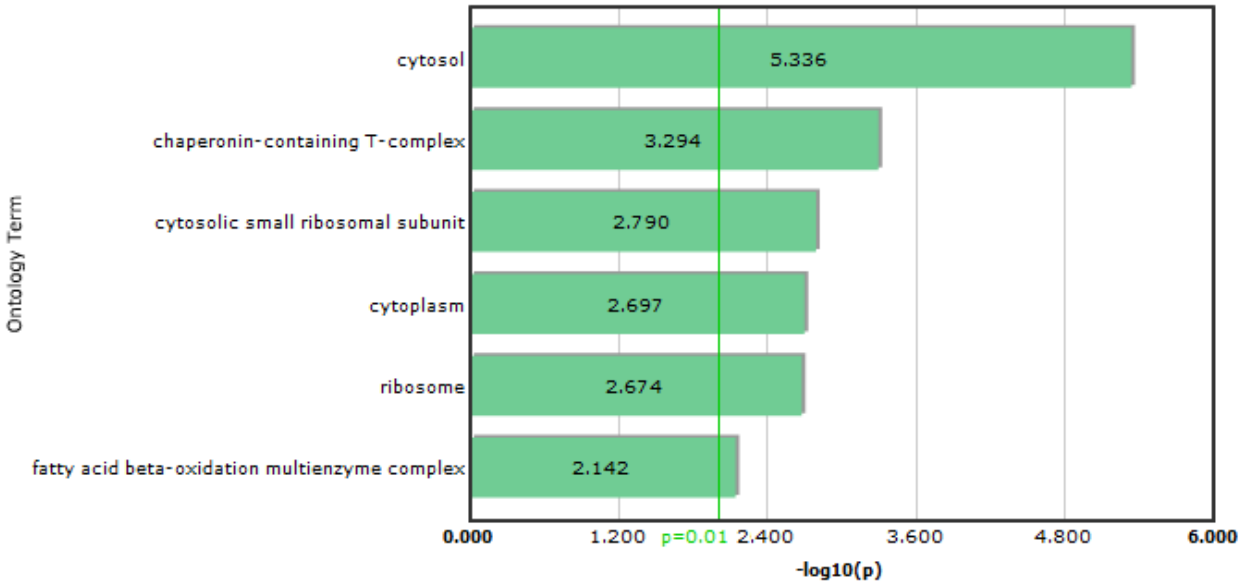

Figure 24 Enriched GO annotations of cellular component for the 52 proteins shared between this and the Cravatt studies, sorted by corrected *p*-value. 32 proteins identified bore cellular component annotations and were tested with a Bonferroni and corrected Bonferroni test. Six components were enriched at $p < 0.01$ including those of the cytoplasm and ribosome. Contrasting the full dataset, component annotations of mitochondria and nuclei are not longer present. Given the small sample size, components with small numbers of annotations are statistically significant if only one member of the set is present (see also Table 11). Such enrichments may or may not have biological meaning.

Term	*Identified of Total Existing*	*% of total in list*	*p-value*	*Corr. p-value*
cytosol	12 of 735 annotated in Human	23.08	2.78e-09	4.62e-06
chaperonin-containing T-complex	2 of 7 annotated in Human	3.85	3.05e-07	5.08e-04
cytosolic small ribosomal subunit	3 of 36 annotated in Human	5.77	9.74e-07	1.62e-03
cytoplasm	17 of 2445 annotated in Human	32.69	1.21e-06	2.01e-03
ribosome	5 of 165 annotated in Human	9.62	1.27e-06	2.12e-03
fatty acid beta-oxidation multienzyme complex	1 of 2 annotated in Human	1.92	4.34e-06	7.22e-03

Table 11 Enriched GO annotations of cellular component for the 52 proteins shared between this and the Cravatt studies. Tabular data to Figure 24. Sorted by corrected Bonferroni *p*-value.

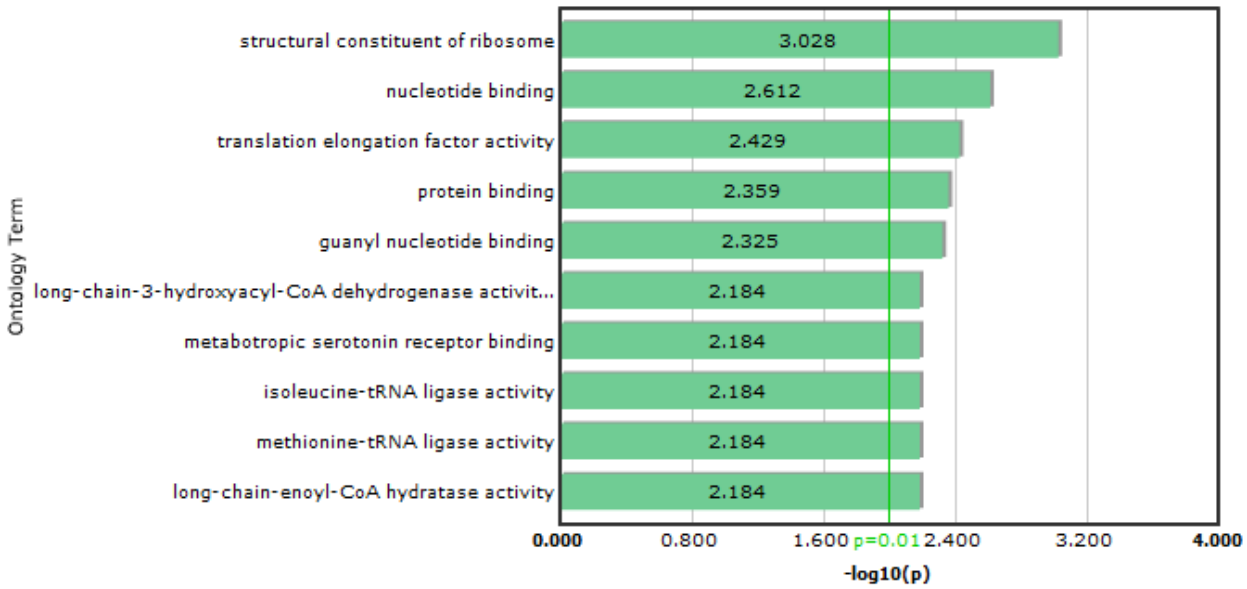

Figure 25 Enriched GO annotations of molecular function for the 52 proteins shared between this and the Cravatt studies, sorted by corrected *p*-value. 29 proteins bore molecular function annotations and were tested with a Bonferroni and corrected Bonferroni test. At $p < 0.01$, recovered proteins were most enriched in proteins that bind nucleotides and proteins, and those involved in translation including the ribosome. See also Table 12 and note regarding enrichment of annotations with few members in Figure 24.

Term	*Identified of Total Existing*	*% of total in list*	*p-value*	*Corr. p-value*
structural constituent of ribosome	5 of 146 annotated in Human	9.62	6.22e-07	9.38e-04
nucleotide binding	11 of 1066 annotated in Human	21.15	1.62e-06	2.44e-03
translation elongation factor activity	2 of 13 annotated in Human	3.85	2.47e-06	3.73e-03
protein binding	19 of 3178 annotated in Human	36.54	2.90e-06	4.38e-03
guanyl nucleotide binding	2 of 14 annotated in Human	3.85	3.14e-06	4.74e-03
long-chain-3-hydroxyacyl-CoA dehydrogenase activity	1 of 2 annotated in Human	1.92	4.34e-06	6.54e-03
metabotropic serotonin receptor binding	1 of 2 annotated in Human	1.92	4.34e-06	6.54e-03
isoleucine-tRNA ligase activity	1 of 2 annotated in Human	1.92	4.34e-06	6.54e-03
methionine-tRNA ligase activity	1 of 2 annotated in Human	1.92	4.34e-06	6.54e-03
long-chain-enoyl-CoA hydratase activity	1 of 2 annotated in Human	1.92	4.34e-06	6.54e-03

Table 12 Enriched GO annotations of molecular function for the 52 proteins shared between this and the Cravatt studies. Tabular data to Figure 25. Sorted by corrected Bonferroni *p*-value.

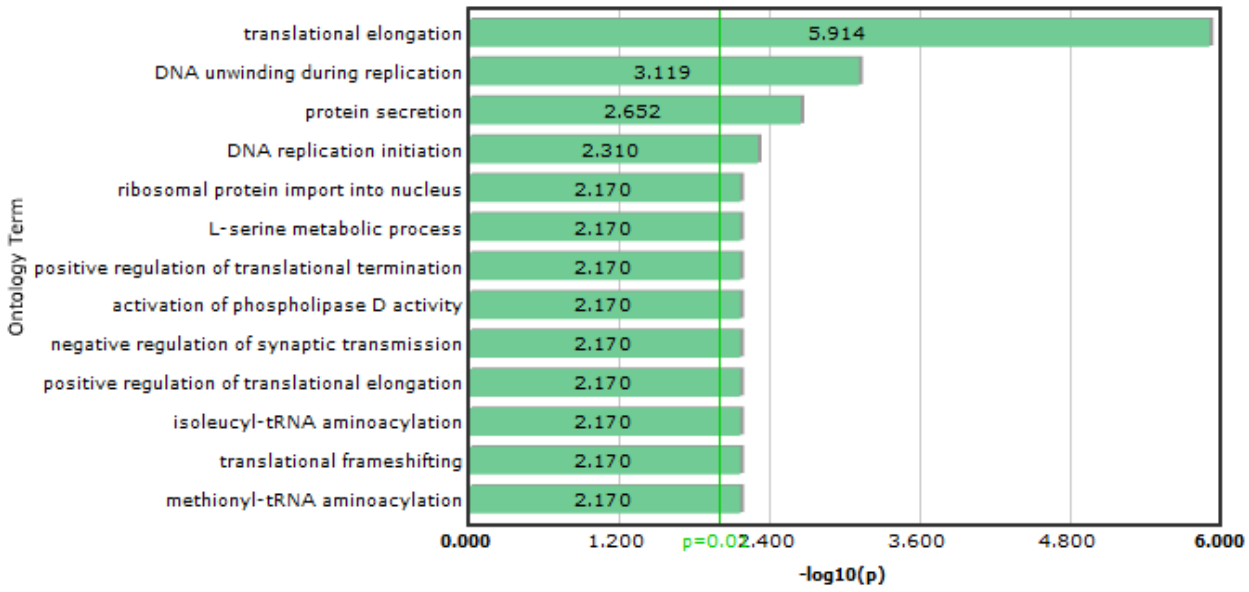

Figure 26 Enriched GO annotations of biological process for the 52 proteins shared between this and the Cravatt studies, sorted by corrected *p*-value. 30 proteins bore biological process annotations and were tested with a Bonferroni and corrected Bonferroni test. At $p < 0.01$, translational elongation remained. See also Table 13 and note regarding enrichment of annotations with few members in Figure 24.

Term	*Identified of Total Existing*	*% of total in list*	*p-value*	*Corr. p-value*
translational elongation	6 of 90 annotated in Human	11.54	7.81e-10	1.22e-06
DNA unwinding during replication	2 of 8 annotated in Human	3.85	4.88e-07	7.61e-04
protein secretion	2 of 11 annotated in Human	3.85	1.43e-06	2.23e-03
DNA replication initiation	2 of 14 annotated in Human	3.85	3.14e-06	4.90e-03
ribosomal protein import into nucleus	1 of 2 annotated in Human	1.92	4.34e-06	6.77e-03
L-serine metabolic process	1 of 2 annotated in Human	1.92	4.34e-06	6.77e-03
positive regulation of translational termination	1 of 2 annotated in Human	1.92	4.34e-06	6.77e-03
activation of phospholipase D activity	1 of 2 annotated in Human	1.92	4.34e-06	6.77e-03
negative regulation of synaptic transmission	1 of 2 annotated in Human	1.92	4.34e-06	6.77e-03
positive regulation of translational elongation	1 of 2 annotated in Human	1.92	4.34e-06	6.77e-03
isoleucyl-tRNA aminoacylation	1 of 2 annotated in Human	1.92	4.34e-06	6.77e-03
translational frameshifting	1 of 2 annotated in Human	1.92	4.34e-06	6.77e-03
methionyl-tRNA aminoacylation	1 of 2 annotated in Human	1.92	4.34e-06	6.77e-03

Table 13 Enriched GO annotations of biological process for the 52 proteins shared between this and the Cravatt studies. Tabular data to Figure 26. Sorted by corrected Bonferroni *p*-value.

In addition to sampeling proteins outside a membranous environment, the complete solubilization strategy employed here contributed in a second manner to the identification of previously unidentified fatty-acylated proteins and protein networks. Observation of fatty-acylation on highly abundant, often sticky proteins such as those of the ribosome, cytoskeleton and metabolic enzymes has often been obscured by difficulty in distinguishing genuine bound signal from background binding to beads. This limitation results from wash conditions insufficient to effectively remove plentiful proteins and can easily result in false negative assignments. Wash conditions typically present an experimental challenge: a balance must be struck between loss of proteins of interest and background binding. However, the combination of click chemistry with biotin capture presents one of the few experimental systems amenable to extreme stringency of wash. This harshly solubilizing detergent conditions used in this work during labeling and capture (0.5% – 4% SDS) combined with highly stringent washes (2% SDS, 8 M urea, 2.5 M NaCl and more) enabled reliable identification of abundant ribosomal, cytoskeletal and metabolic proteins. Under these conditions, weak but dectable background was still observable for abundant proteins like actins and tubulins, heat shock proteins and some metabolic enzymes (enolase and phosphoglycerate kinase, see Figure 11) but similar background was not observed for ribosomal, mitochondrial or proteasomal proteins. Western blotting for multiple proteins confirmed the lack of background binding and, in the case of HSP90, revealed MS detection of background binding to be more sensitivity than ECL at that exposure (Figure 11, Figure 12, Figure 13). Thus forthly, this work presents an experimental approach which enables distinction of true signal from high abundance proteins and has reliably detected fatty-acylation on highly abundant, sticky proteins.

As with all research, discoveries within fatty-acylation have flowed from the solubilized proteins of a sample. Major complexes and networks, in particular tightly-packed chromatin of the dense nucleus, as well as the cytoskeleton and others, are not brought into solution with typical approaches. They have thus remained largely or fully unexamined. In addition, the use of membrane preparations, while they enrich membrane-associated low-level proteins, has directed our view of fatty-acylation to a membrane-centric view. Multiple reviews summarize similarly to "Whereas kinase and phosphatase activity generally acts by directly modulating protein-protein interactions, palmitoylation is more likely to achieve its affects via regulation of protein-membrane interactions"[241] yet neglect to mention that other cell regions have been examined minimally at best. Overarchingly, the implication of this wok is that fatty-acylation is present throughout the cell, rather than one restricted to membrane-associated proteins, and plays a role in diverse processes from metabolism and energy production to protein maintenance and folding to the cell cycle.

If, then, fatty-acylation is so widespread, what is its role? We can best understand its broader implications first principles. Like hydrophobic sections of proteins, the addition of fatty acids can certainly serve to generate membrane affinities, but they can also serve to create intra- or inter-molecule affinities. Hydrophobic interactions underlie protein and protein-complex stability (including that of histone octamers) and lipidation, in particular dynamic palmitoylation, represents an efficient mechanism to modulate hydrophobicity. This modulation can change interactions within proteins, altering conformations and thus activities, as well as between proteins. In addition, lipid modifications alter chemical reactivity by capping a sulfhydryl, hydroxyl, amine or other functional groups; this change may result in alterations in catalytic activity of enzymes.

Thus, like phosphorylation, fatty-acylation and in particular dynamic palmitoylation is a regulatory PTM with the ability to modulate interactions and activities.

Many examples of fatty-acylation modulating hydrophobicity, altering interactions and changing activity are known. These examples extend to the generation of membrane affinity – for example, the catalytic efficiency of signaling cascades is effected by close physical proximity brought about by membrane-bound clustering – but are much more diverse. In the case of single proteins, constituitive *S*-acylation discovered crystallography on auto-palmitoylating Bet3 was shown to be essential to structure and function by providing internal, stabilizing hydrophobic interactions[225]. In contrast to a structural role, dynamic palmitoylation regulates protein activity of GAPDH in response to metabolic state[217]. Palmitoylation regulates protein-protein interactions outside effects on membrane association. Such effects have been studied in particular for the large network of tetraspanins. Abolishion of palmitoylation from integrin β4 diminished associations with tetraspanins CD9, CD81, and CD63, without changing behavior in membrane density fractionation, lipid raft association or detergent solubility[242]. Similarly, elimination of palmitoylation in CD151 had minimal influence on density fractionation and detergent solubility but resulted in significantly less association with CD9 and CD63[243]. Likewise, palmitoylation-deficient mutants of CD81 show impared interaction with CD9 and EWI-2[244]. In contrast, palmitoylation of CD9 actually inhibits association with EWI-2 and unmodified proteins are preferentially bound[245]. Palmitoylation is therefore required for the correct assembly and structure of the large tetraspanin network often coined the “tetraspanin web”[243]. While this network is localized to the cell surface, note should be made that palmitoylation does not appear to cause or alter membrane association. Fatty-acylation status also regulates N-type calcium channel activity

through modulation of protein-protein interactions. Palmitoylated splice variants of regulatory β subunits are stimulated by G_q while unmodified forms are inhibited by the same protein[246]. The function of palmitoylation thus extends far beyond simple membrane affinity, although this effect remains important. Modification by palmitic acid can modulate protein activity; can modulate intraprotein interactions altering stability and conformation; and can modulate protein-protein intereactions of quartenary structures by either enhancing or inhibiting binding.

While the tetraspanins represent a very large, if diffuse, complex, the role palmitoylation plays in spatiotemporal regulation of other large, multi-member and dynamic protein complexes remains a tantilizing area of future research. Most notable in Figure 19 is the preponderance of such networks and assembelies. Representation is extensive and includes the ribosome, proteasome and cytoskeleton; metabolic and mitochondrial complexes; and multiple assembelies with DNA and RNA association such as DNA replication licensing factors and heterogeneous nuclear nibonucleoprotein complexes. Each of these assemblies undergoes dramatic changes depending on cellular state and fatty-acylation likely plays a major role in their dynamic nature. However, the study of such protein networks and complexes will warrent techniques outside genetic mutation: the number of proteins and possible sites of modification combine exponentially to make a brute force approach of this strategy intractable. Further investigation will also likely reveal multiple roles for activity regulation by fatty-acylation as has been shown for GAPDH. Given the intimate connection between fatty-acids and key metabolic intermediates, as well as the presence of many glyclytic enzymes in this and other datasets (see Figure 11, Figure 14 and Figure 19), palmitoylation probably also regulates the activity of multiple metabolic enzyme. Overall, fatty-acylation and palmitoylation will increasingly be shown to have major roles in intra- and intre-

protein interactions, and in control of catalytic activity, particularly in the regulation of metabolism.

Histone H3 fatty-acylation

The discovery of S-fatty-acylation on histone H3 variants represents a new type of histone modification whose implications will require further study. In particular, mechanism of fatty-acylation (Figure 21), dynamics, stability and overall function remain open questions. Cys110 of H3 variants lies buried deep within the nucleosome at the end of the H3 α-2 helix, occupying the center of a four-helix bundle at the H3-H3' interface between the two H3-H4 dimers of the $(H3\text{-}H4)_2$ tetramer. Through hydrophobic interactions and hydrogen bonds, this region alone causes tetramer formation[247-250]. Disrupting the hydrophobic surfaces with a C110E mutation results in obligatory H3-H4 dimers[251]. Without denaturation, C110 is chemically inaccessible to a wide variety of sulfhydryl reactive reagents conditions[252-255]. The involvement of this residue in chromatin structure has been long discussed in the context of an H3-H3 disulfide[256,257]. However, four separate crystallographic studies, including one under oxidative conditions, have shown intersulfur distances in assembled nucleosomes to be incompatible with a disulfide linkage[247-250]. Indeed, this residue has been shown to become chemically accessible only during active gene transcription[258-260]. Additionally, in HPLC histone purifications, small quantities of hydrophobic (late-eluting) species are observed after the main H3 peak[261], possibly representing the presence of fatty-acylated H3 species.

Cytosolic H3 modification including acetylation or methylation by early acting enzymes prior to chromatin incorporation has been demonstrated[262,263] and given the ER and perinuclear localiza-

tion of multiple DHHC-PATs[264], it is possible H3 variants are modified before nuclear incorporation, during nuclear breakdown or possibly at the periphery of the nucleus during specific regulatory events (Figure 27). The lack of chain length dependence (Figure 11 and Figure 12) could be reflective of the broad substrate specificity of DHHC-PATs.

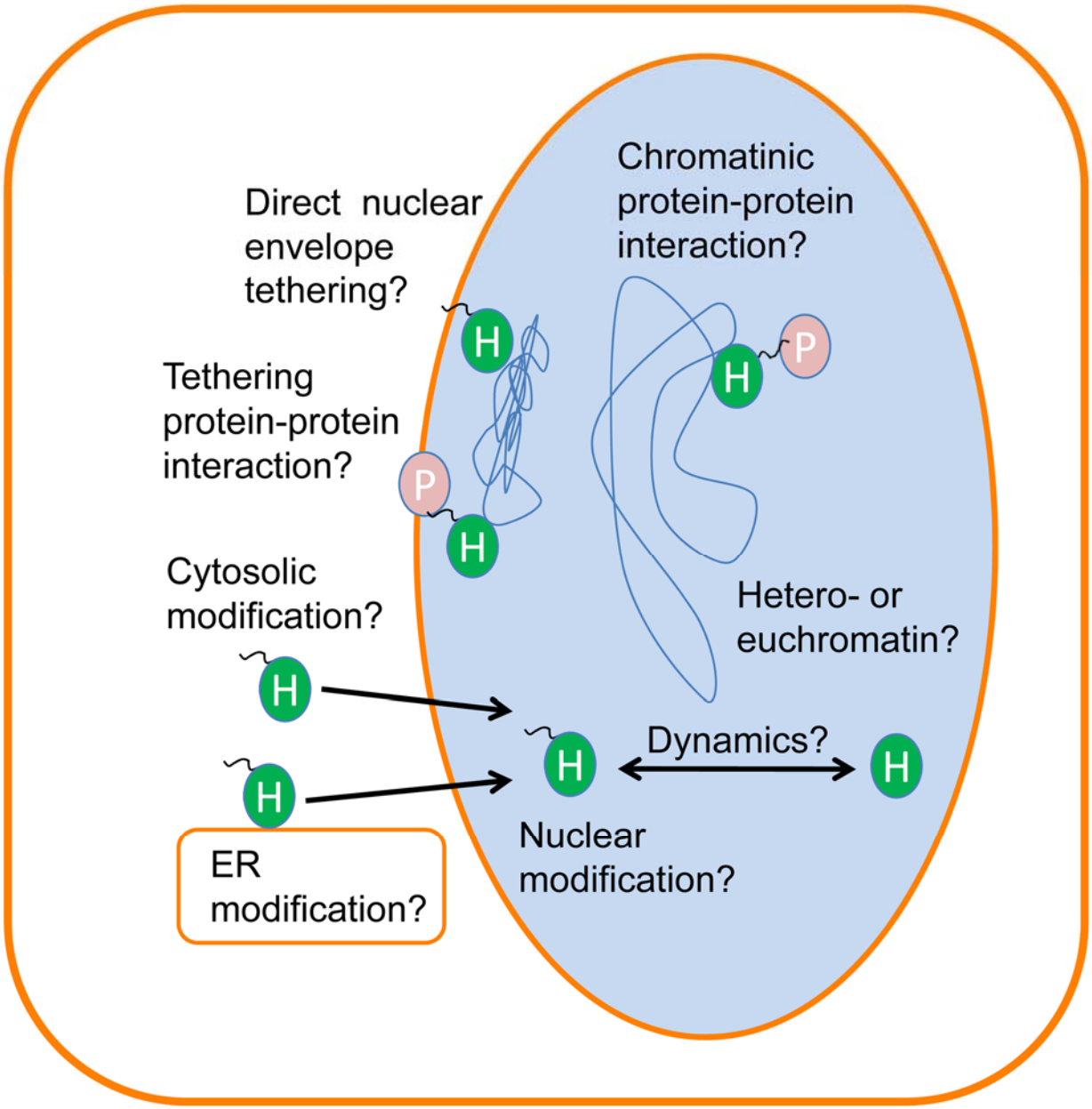

Figure 27 Possible roles of histone H3 acylation. The function of histone H3 acylation remains to be determined and for heterochromatin, might be involved in direct tethering to the nuclear envelope or tethering through a new protein-protein interaction. If involved in euchromatin, H3 acylation might play a role in a new protein-protein interaction. The dynamics, mechanism and cellular location of modification remain to be determined.

Functionally, the S-fatty-acylation of histone H3 variants might, like methylation and acetylation[265], alter nuclear events by establishing a binding platform for effector proteins like histone chaperones (Figure 27). Alternatively, *S*-palmitoylation could affect the properties of chromatin itself, perhaps resulting in new, stabilizing hydrophobic interactions within one or between several nucleosomes, or nucleosomes and other chromatin proteins. Palmitoylation might also play a role in the sub-organellular structure of the nucleus including spatial and functional compartmentalization of proteinaceous nuclear bodies, and chromatin domains and territories[266,267]. PTMs including methylation and acetylation show distinct nuclear localization, which can change with tissue type, cellular state and cell cycle[268]. Such PTMs are well established to modulate gene activity by changing higher-order nuclear organization. For example, the addition of active chromatin marks like H3K9 acetylation or H3K4me2 results in chromatin decondensation and the formation of chromatin loops[269]. Whether S-palmitoylation is involved in the regulatory protein-protein interactions of subnuclear organization remains to be seen. Particularly tempting is the potential involvement of S-palmitoylation in perinuclear tethering of chromatin to the nuclear envelope (Figure 27), a localization generally associated with inactive heterochromatin and gene silencing[266,267]. Indeed, H3 variants are enriched in the nuclear shell fraction of HeLa cells[270]. While such localization might involve interaction with the nuclear membranes, it also could be protein specific. H3 has been shown to interact with membrane-bound lamin B-receptor (LBR)[271] and BAF (barrier-to-autointegration factor)[272], which in turn bind multiple inner nuclear membrane proteins[273,274]. In addition, carboxyl-terminal tails of nuclear lamins bind H3[275]. Given the dynamic nature of S-palmitoylation[20], it will be interesting to determine the status of C110 palmitoylation (and potentially H3.1 C96) in conjunction with other PTMs, through the

cell cycle and under various states, as well as the relative levels of modification between the H3 variants and their localizations.

Conclusion

Deciphering the function, regulation and meaning of protein fatty-acylation will be an exciting field for years to come. This survey of proteins and others demonstrate that many more cellular proteins are modified with fatty acids than previously appreciated. Using fully solubilized mammalian cells, we discovered S-acylation of histone H3 variants. The highly conserved Cys110 was determined by site-directed mutagenesis to be the site of modification for H3.2; the function of this PTM remains to be elucidated and may be involved in perinuclear chromatin silencing. The large-scale identification of fatty-acylation sites on proteins remains a significant challenge and will be essential for dissecting the functional roles of protein fatty-acylation in various cellular pathways. The characterization of specific acyltransferases and lipases responsible for individual fatty-acylated proteins will be key to determining their functions.

DIRECT VISUALIZATION OF CHOLESTEROL

Introduction

In humans and other vertebrates, cholesterol is essential to life and plays a critical role in disease and healthy physiology[276]. Eukaryotic cells have complex mechanisms to sense cholesterol levels and regulate its synthesis and trafficking[277]. Defects in cholesterol homeostasis are responsible for diseases such as familial hypercholesterolemia or atherosclerosis[278], and neurological conditions like Niemann-Pick disease[276]; low brain cholesterol is also associated with autism spectrum disorders[279]. Within membranes, cholesterol regulates permeability, fluidity and mechanical strength, and it is a major component of detergent-resistant microdomains (lipid-rafts)[276,280,281]. Cholesterol content in membranes affects protein sorting and activity of membrane proteins[276,280,281]. Cholesterol is a ligand for some proteins and many of its derivatives are signaling molecules (e.g. steroid hormones). The major lipid component of the brain is cholesterol, especially in myelin, where it functions as an insulator and enables the efficient transmission of action potential signals[282]. Cholesterol is a post translational modification (PTM) on the C-terminus of sonic hedgehog (Shh), where it restricts the spatial diffusion of the morphogen to generate the gradients that control vertebrate development in tissues[27]. Cholesterylation defective mutants of Shh show gross mispatterning and embryonic lethality[27]. Cholesterol sensing, trafficking and protein modification are critical to physiology and disease yet their underlying mechanisms are not fully understood.

Several techniques have been developed to investigate cholesterol and all have limitations[42,79]. Radioactive cholesterol is the most faithful reporter but is limited by speed of detection and cannot be easily combined with other analyses such as immunohistochemistry (IHC). Indirect methods to detect cholesterol include enzymatic assays (cholesterol oxidase), cholesterol-binding proteins (the cholesterol-binding region of perfringolysin O or anti-cholesterol antibodies) and polyene dyes that fluoresce when bound to cholesterol (filipin in particular). These methods can suffer from inaccessibility to cholesterol, giving false negative signal, and may have affinity for other substances, resulting in false positive signal. Direct visualization methods using fluorescent cholesterol analogs provide convenient tools to monitor lipid trafficking[42,79], but the fusion of large fluorophores to cholesterol may perturb structural features necessary for its biologically activity (Figure 32) or interfere with specific cholesterol recognition by endogenous mechanisms[27,283]. The naturally occurring, intrinsically fluorescent sterol dehydroergosterol (DHE) provides a more faithful fluorescent reporter[42,79]. However, DHE suffers from low quantum yield, rapid bleaching and ultra-violet (UV) excitation and emission requiring specialized, UV-transparent imaging equipment[42,79]. The two-step bioorthogonal method presented here circumvents many of these disadvantages. Cells or animals are labeled with a biologically active cholesterol reporter, 25-azidonorcholesterol (**az-chol**) (Figure 30), which has minimal structural change and exhibits similar metabolism and distribution to cholesterol *in vivo*[181,284]. Following metabolic incorporation, az-chol can be reacted with a fluorescent dye best suited to experimental design via Cu^{I}-catalyzed [3+ 2] azide-alkyne cycloaddition (CuAAC)[94], often termed "click chemistry" (Figure 30a). This approach allows the use of standard imaging equipment and is easily combined with common analyses and workflows such as IHC. We show that this bioorthogonal tech-

nique robustly images from protein cholesterylation to *in vivo* cholesterol trafficking in cells and organs.

Figure 28 Cholesterol, 25-azidonorcholesterol (az-chol) and other cholesterol reporters. Accurate and effective reporting of cholesterol requires an analog to 1) be non-toxic to cells; 2) be incorporated by cells like cholesterol; and 3) have little or no change in biological activity compared to the native molecule. Most analogues perturb the structural features essential to the biological activity of cholesterol (a) including: a free 3□-hydroxyl (highlighted in red), the planar tetracyclic ring system (brown) including the □5(6) double bond (magenta), angular methyl groups (green) and the 17□-octyl side chain (pink); modifications to these characteristics can cause substantially altered behavior; for example 22 and 25 NBD-cholesterol orient themselves "up-side-down" with the 3□-hydroxyl in the interior of the membrane. (b) 25-azidonorcholesterol (az-chol) maintains all these key features, simply replacing methyl 26 with an azide (blue). (c) Intrinsically fluorescent cholesterol analogs exhibit similar and nonidentical physiochemical behavior to cholesterol; they retain some of the most faithful biological activity. Both differ from cholesterol by desaturation of their □7(8), □9(11) and in the case of dehydroergosterol, its □22(23) double bond and an additional methyl group at C24. (d) Spin-labeled 25-doxylnorcholesterol exhibits biophysical membrane properties that closely match cholesterol, demonstrating that the octyl chain can tolerate modification. (e) Many fluorescent cholesterol analogs exist; all have significantly modified structure from (a). (f) Multiple crosslinking analogs are available and also exhibit strong structural deviations from (a).

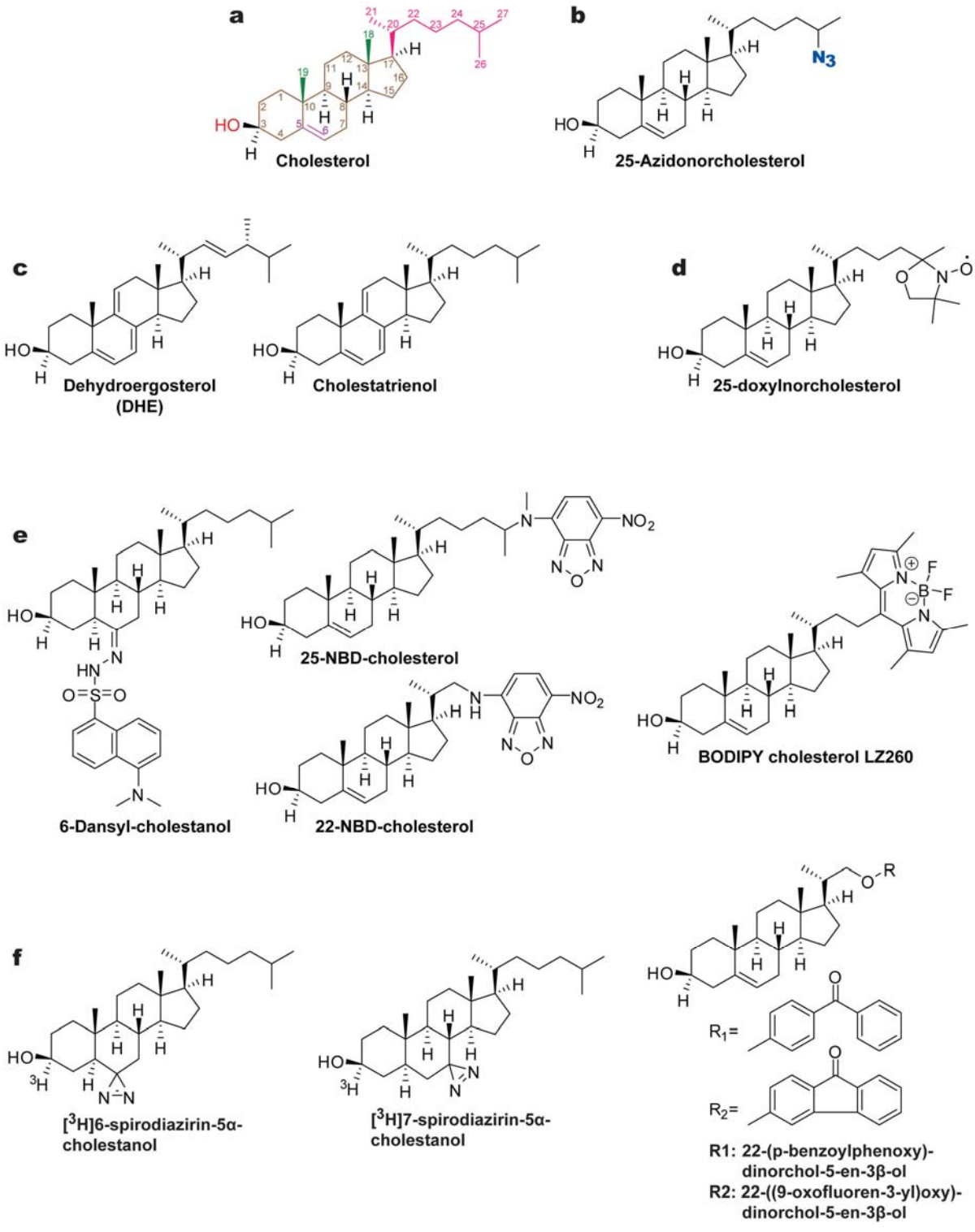
a
Cholesterol
b
25-Azidonorcholesterol
c
Dehydroergosterol (DHE)
Cholestatrienol
d
25-doxylnorcholesterol
e
6-Dansyl-cholestanol
25-NBD-cholesterol
22-NBD-cholesterol
BODIPY cholesterol LZ260
f
[3H]6-spirodiazirin-5α-cholestanol
[3H]7-spirodiazirin-5α-cholestanol
R1: 22-(p-benzoylphenoxy)-dinorchol-5-en-3β-ol
R2: 22-((9-oxofluoren-3-yl)oxy)-dinorchol-5-en-3β-ol

Az-chol was evaluated as a cholesterol analog for photocrosslinking over three decades ago[181,284] and exhibits minimal structural perturbation, as the replacement of a methyl group with an azide maintains the key features[80] of biologically active cholesterol (Figure 28). The azide does not substantially alter size or hydrophobicity, does not add charge and is biologically compatible. Isotope labeling experiments show that az-chol is incorporated into the membranes of baby hamster kidney 21 (BHK-21) cells in place of cholesterol and is sensed by HMG-CoA (3-hydroxy-3-methyl-glutaryl-CoA reductase, the key regulatory enzyme in the cholesterol biosynthetic pathway), and causes inhibition of *de novo* cholesterol synthesis[181,284]. Incorporation kinetics of radioactively labeled cholesterol and az-chol are nearly identically from 5 to 25 μg/mL (12 – 60 μM)[181]. Cells supplemented with cholesterol or az-chol show no significant differences in cell growth, DNA, RNA or protein synthesis[181]. Az-chol does not alter cell morphology after application up to 96 hours[181]. After intravenous injection in rats, az-chol is transported to the liver and, as cholesterol, distributes to all subcellular fractions[284]. Az-chol upregulates acyl-CoA:cholesterol O-acyltransferase activity *in vivo* and, as in cells, downregulates HMG-CoA[284]. Esterified az-chol products were also found in the blood and liver[284]. Az-chol has thus been shown to have biological activity very similar to cholesterol in cells and animals.

Results

Given the biological activity of az-chol[284] and usefulness of chemical reporters and bioorthogonal methods to study protein lipidation[93,94,285,286] and lipid trafficking[86,287], we synthesized az-chol[181] (Figure 29) and applied it to study cholesterol localization, trafficking and protein modification (Figure 30, Figure 31). We began by verifying az-chol incorporation onto Shh, a known cholesterylated protein[27]. Cholesterylation of Shh is an autocatalytic processing event of the 45 kDa precursor protein cleaving a 19 kDa N-terminal domain that must also be palmitoylated for proper activity[27]. We metabolically labeled human embryonic kidney (HEK) 293T cells that inducibly overexpress Shh[288] (293T-Shh) with az-chol and immunopurified Shh. The isolated morphogen was then reacted with alkynyl-rhodamine via CuAAC and the modification was imaged by in-gel fluorescence scanning (Figure 30b). Because Shh is N-terminally palmitoylated, we also labeled 293T-Shh cells with an azido-palmitate reporter (az-15)[93,94] as a control for protein labeling. Both az-chol and az-15 were incorporated onto mature Shh, indicating that az-chol correctly reports protein cholesterylation (Figure 30b). Az-15 labeling and rhodamine modification alone did not introduce a significant mobility shift, while az-chol labeling induced a noticeable increase in the apparent molecular weight of Shh (Figure 30b lanes 1 – 3). Dual metabolic labeling with az-15 and az-chol imparted a yet further decease in Shh mobility (Figure 30b, lane 4). Notably, we observe other az-chol-modified proteins in total cell lysates (Figure 31 lanes 1 – 2), echoing the original autoradiographic evidence that cholesterol modification exists on proteins other than Shh[26,27]. Az-chol thus serves as an efficient chemical reporter for protein cholesterylation and we anticipate it will be useful in elucidating the identity and function of modified proteins.

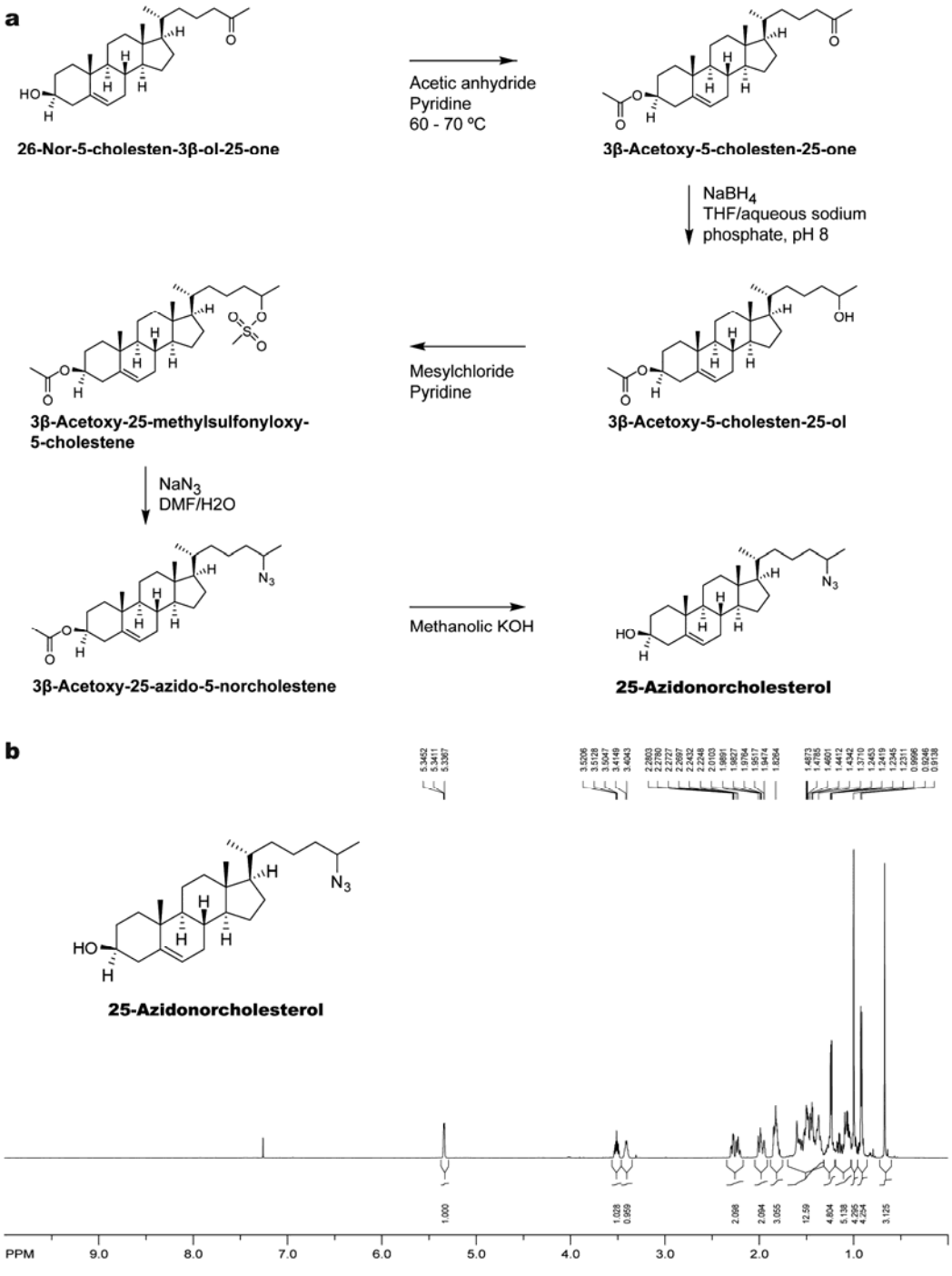

Figure 29 Synthesis and characterization of az-chol. (a) Az-chol was synthesized as previously described with the exception that final product was purified by silica gel chromatography. (b) Proton NMR.

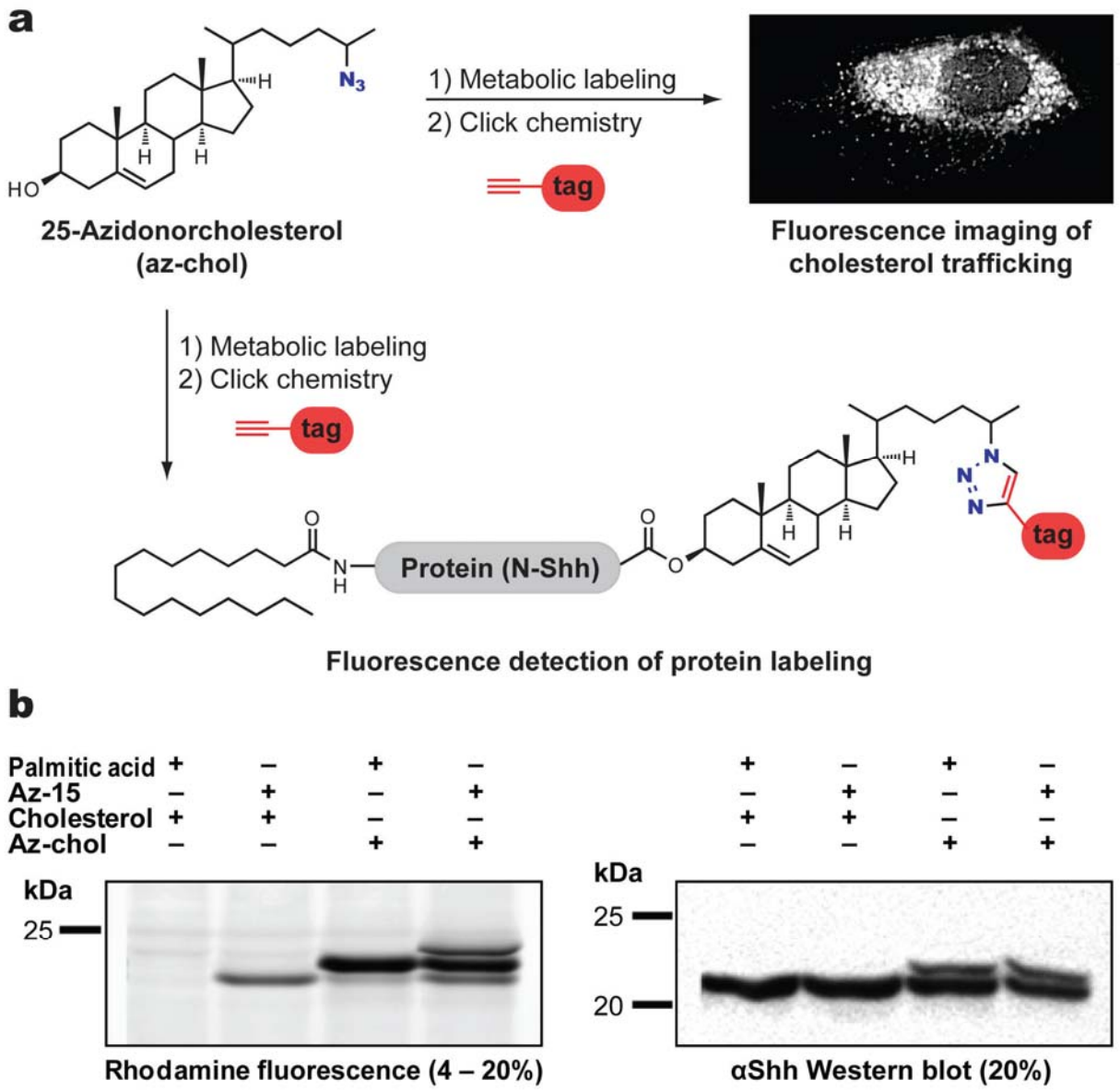

Figure 30 25-azidonorcholesterol (az-chol) labeling. (a) Az-chol is first metabolically incorporated in cell culture or in utero. Subsequently, az-chol can be visualized by conjugation to rhodamine through click-chemistry. (b) In-gel fluorescence and Western blot analysis of Shh labeled with lipids and their clickable analogs. Both az-chol and az-15 were incorporated onto N-Shh and imparted gel mobility shifts. Modification with rhodamine conjugates of az-15 alone show the least shift (lane 2, left-hand panel), followed by az-chol (lane 3); their combination imparted the greatest apparent increase in molecular weight (lane 4). Due to transfer efficiency, a 20% gel was used for Western blotting which condensed the band bearing both lipid analogs (lane 4, right-hand panel).

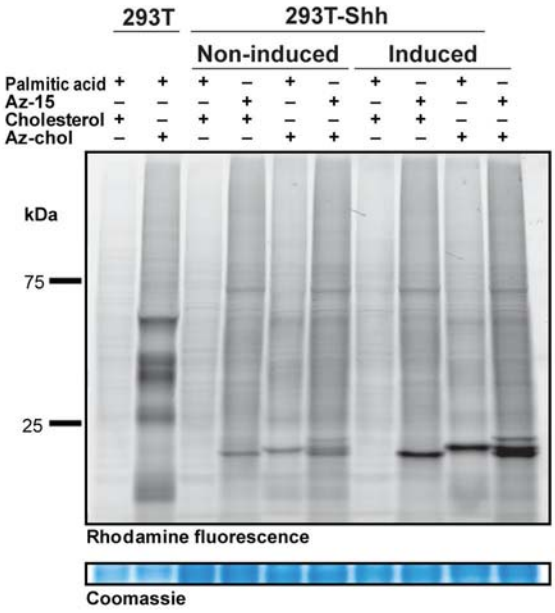

Figure 31 Shh induction and validation of lipid PTMs. Fluorescence profiles of 293T cells with and without Shh overexpression. 293T cells and Shh overexpressing cells incorporate az-chol and dominant signal is present at ~19 kDa and upregulated by overexpression; 293T cells lacking Shh show incorporation onto unknown proteins. Different band shifts are apparent with each modification or combinations thereof.

We then evaluated az-chol as a reporter for cholesterol distribution in mammalian cells by fluorescence microscopy. For these experiments we used Chinese hamster ovary (CHO) cells and M12 mutant CHO cells that carry a deletion of the NPC1 locus[289]. Defects in this gene result in Niemann-Pick disease type C, an autosomal recessive lipid storage disorder characterized by the accumulation of cholesterol in enlarged endosomal-lysosomal storage compartments[290,291]. These filipin-positive perinuclear organelles have been used in NPC disease diagnosis for years[292] and we sought to compare filipin staining with az-chol imaging. We first verified that application of az-chol did not alter fine cell morphology of wild-type CHO or M12 cells compared to choles-

terol by electron microscopy (Figure 32). For fluorescence imaging, cells were metabolically labeled with az-chol or cholesterol, fixed (and, in the case of antibody staining, permeabilized with 1% Tween-20), reacted with alkyne-rhodamine via CuAAC, simultaneously co-stained with filipin and imaged by fluorescence microscopy. Az-chol labeled CHO and M12 cells exhibited bright rhodamine fluorescence in intracellular vesicles and cellular membranes; signal was distributed throughout the cell though attenuated in the nucleus (Figure 33). Rhodamine but not filipin fluorescence was absent in cholesterol-treated samples (Figure 33a and b far right; Figure 34a). Staining patterns for az-chol and filipin were similar and distinct (Figure 33). Fluorescence overlap was extensive (Pearson's coefficient 0.5 – 0.7), particularly in the cholesterol storage organelles of M12 cells, but some filipin positive regions (organelles or lipid droplets) showed no az-chol signal; the opposite was also true (Figure 33a and b inserts). Particularly notable was labeling in the vicinity of the cell membrane: although both techniques labeled the cell membrane, az-chol tended to outline filipin staining (Figure 33a and b, arrowheads).

Figure 32 Electron microscopy analysis of CHO cells reveals no morphological changes. CHO cells (a) and M12 cells (b) show no difference in gross or fine morphology when cultured with either cholesterol (top rows) or az-chol (bottom rows) as determined by EM. Note the prominent, enlarged endosomal-lysosomal lipid storage organelles in (b).

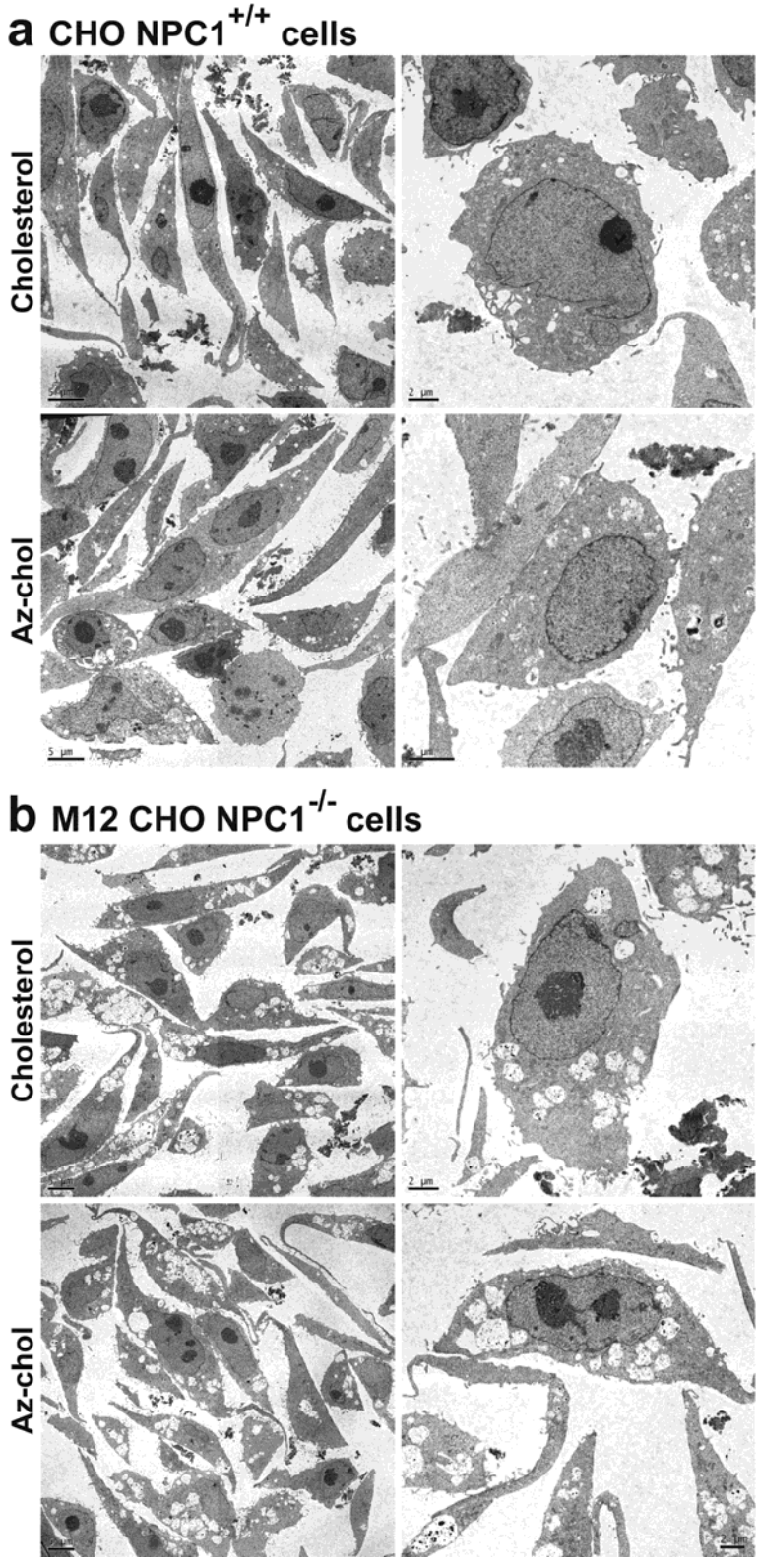
a CHO NPC1+/+ cells
Cholesterol
Az-chol
2 µm
5 µm
b M12 CHO NPC1-/- cells
Cholesterol
Az-chol
2 µm

Figure 33 Az-chol and filipin labeling of normal and Niemann Pick type C disease model cells with and without MβCD cholesterol depletion. False-color representation of (**a**) normal CHO $NPC^{+/+}$ and (**b**) CHO M12 $NPC^{-/-}$ cells. Scale bars are 10 μm (main), 2.5 μm (insert). Overlap between filipin and az-chol signal is substantial yet different. Some regions are filipin positive and az-chol negative; the reverse is also true (a, b). Az-chol signal tended to outline filipin staining of the plasma membrane (insert arrowheads). Az-chol and filipin both localize to M12 cholesterol-rich lipid droplets but show distinct localization (b). MβCD cholesterol depletion virtually eliminates az-chol signal but leaves filipin signal for both cells and lipid-rich structures (a, b); cholesterol controls show no az-chol labeling (a, b and Figure 34a) and all signal from either technique is abrogated with methanol lipid extraction (Figure 34). (**c**) NPC cholesterol and lipid storage compartments are generally encircled by LAMP-1 signal.

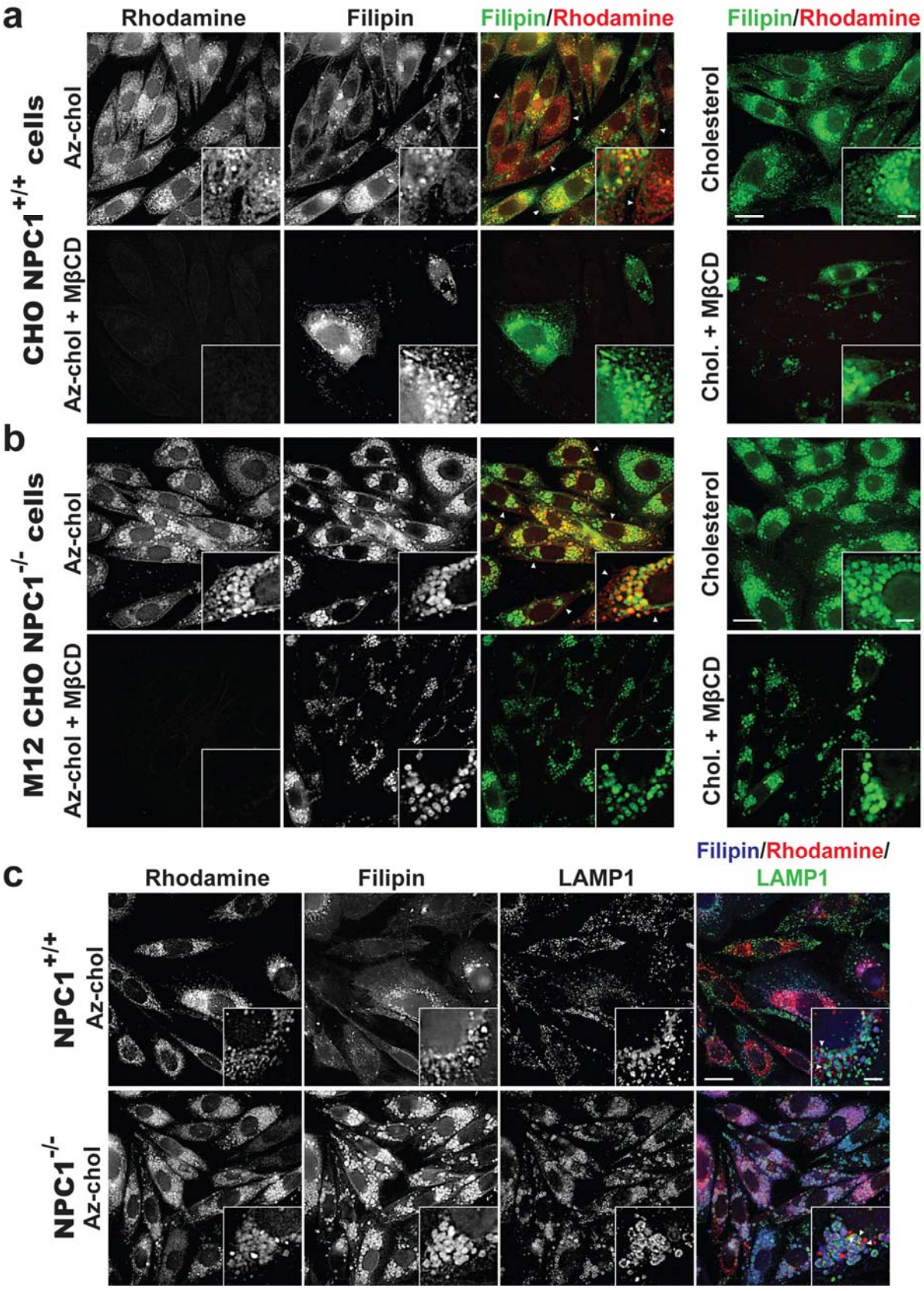
a
Rhodamine
Filipin
Filipin/Rhodamine
Filipin/Rhodamine
CHO NPC1+/+ cells
Az-chol
Cholesterol
Az-chol + MβCD
Chol. + MβCD
b
M12 CHO NPC1-/- cells
Az-chol
Cholesterol
Az-chol + MβCD
Chol. + MβCD
c
Rhodamine
Filipin
LAMP1
Filipin/Rhodamine/
LAMP1
NPC1+/+
Az-chol
NPC1-/-
Az-chol

To shed light on the differences between az-chol and filipin staining, we evaluated both imaging techniques after lipid extraction and also examined colocalization with subcellular markers. As expected, az-chol signal was almost entirely abrogated by cholesterol extraction with methyl-β-cyclodextran (MβCD) (Figure 33a and b). This contrasted with filipin, where signal remained for some CHO cells and many M12 cells, particularly in their lipid storage compartments (Figure 33a, b). In contrast, general lipid extraction with methanol completely eliminated fluorescence staining for both methods (Figure 34b). We examined the subcellular distribution of az-chol and filipin with markers for ER (calreticulin), Golgi apparatus (Golgin 97), early endosomes (EEA1), lysosomes (LAMP-1) and GM1-gangliosides often found in lipid rafts (cholera toxin B). As previously reported[293], az-chol and filipin stained lysosomal storage compartments encircled by LAMP-1 positive vacuolar membranes; these compartments are significantly more pronounced in M12 cells compared to wild type (Figure 33c and Figure 35). Notably, multiple compartments could be seen with an az-chol rich core surrounded by a filipin positive layer and outlined by LAMP-1 signal (Figure 33, insert arrowheads). Az-chol and filipin colocalization with GM1-ganglioside staining was pronounced in M12 storage compartments (Figure 36), as previously observed[294]. We found minimal az-chol colocalization with other subcellular markers (Pearson's coefficients 0.0 – 0.3), probably reflective of the broad distribution of cholesterol throughout cellular organelles, and az-chol did not appear to alter the localization of subcellular markers (**Figs. S7 – S9**). Az-chol thus enables imaging of cholesterol distribution in cells similar to filipin and filipin also stains methanol soluble, MβCD-resistant lipids.

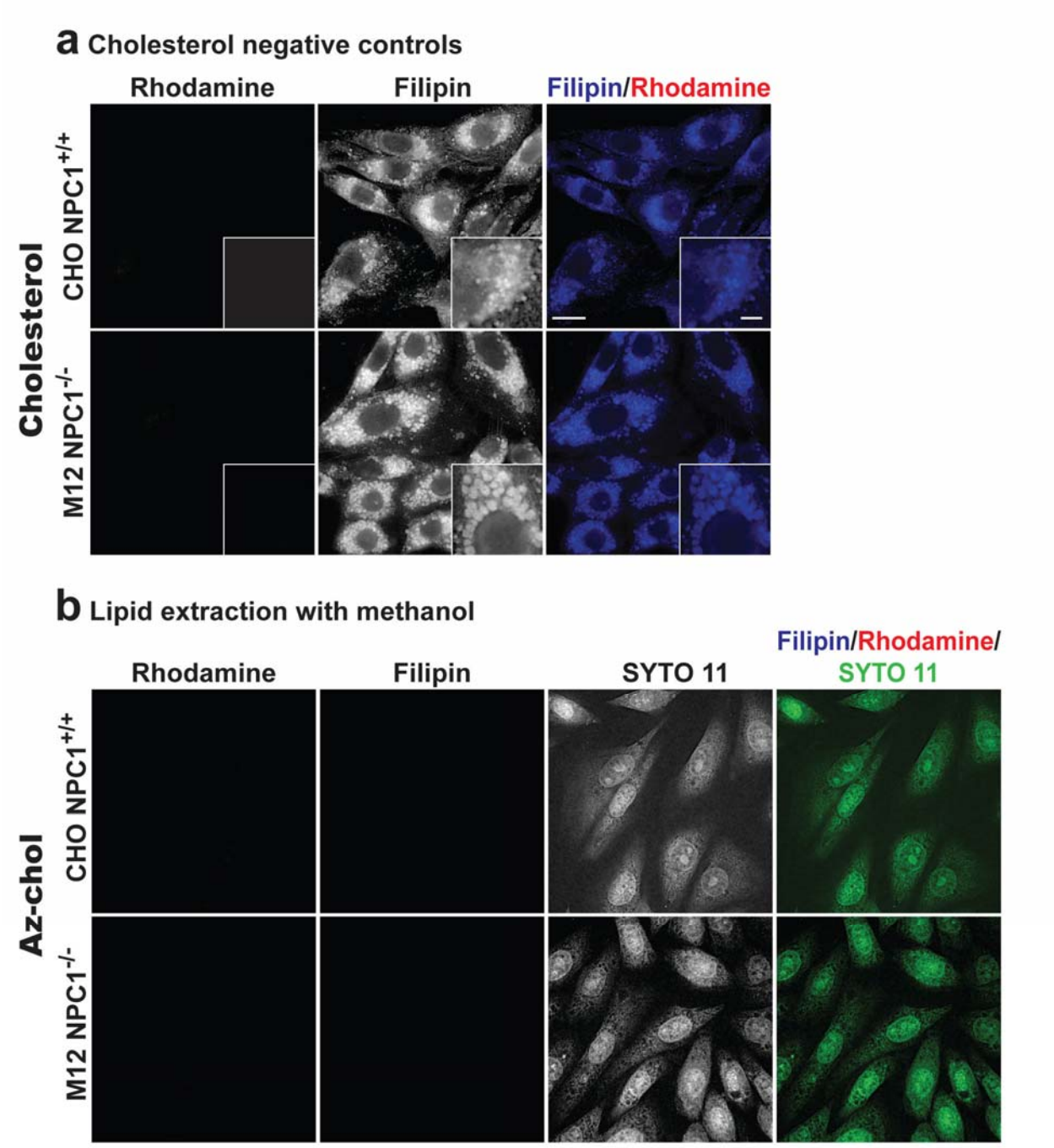

Figure 34 Absence of az-chol signal with cholesterol and elimination of lipid staining with methanol lipid extraction. (a) For CHO or M12 cells cultured with cholesterol, background staining was minimal and filipin staining unchanged. (b) Lipid extraction with methanol eliminated all signal for both az-chol and filipin. Cell presence was verified by SYTO 11 staining.

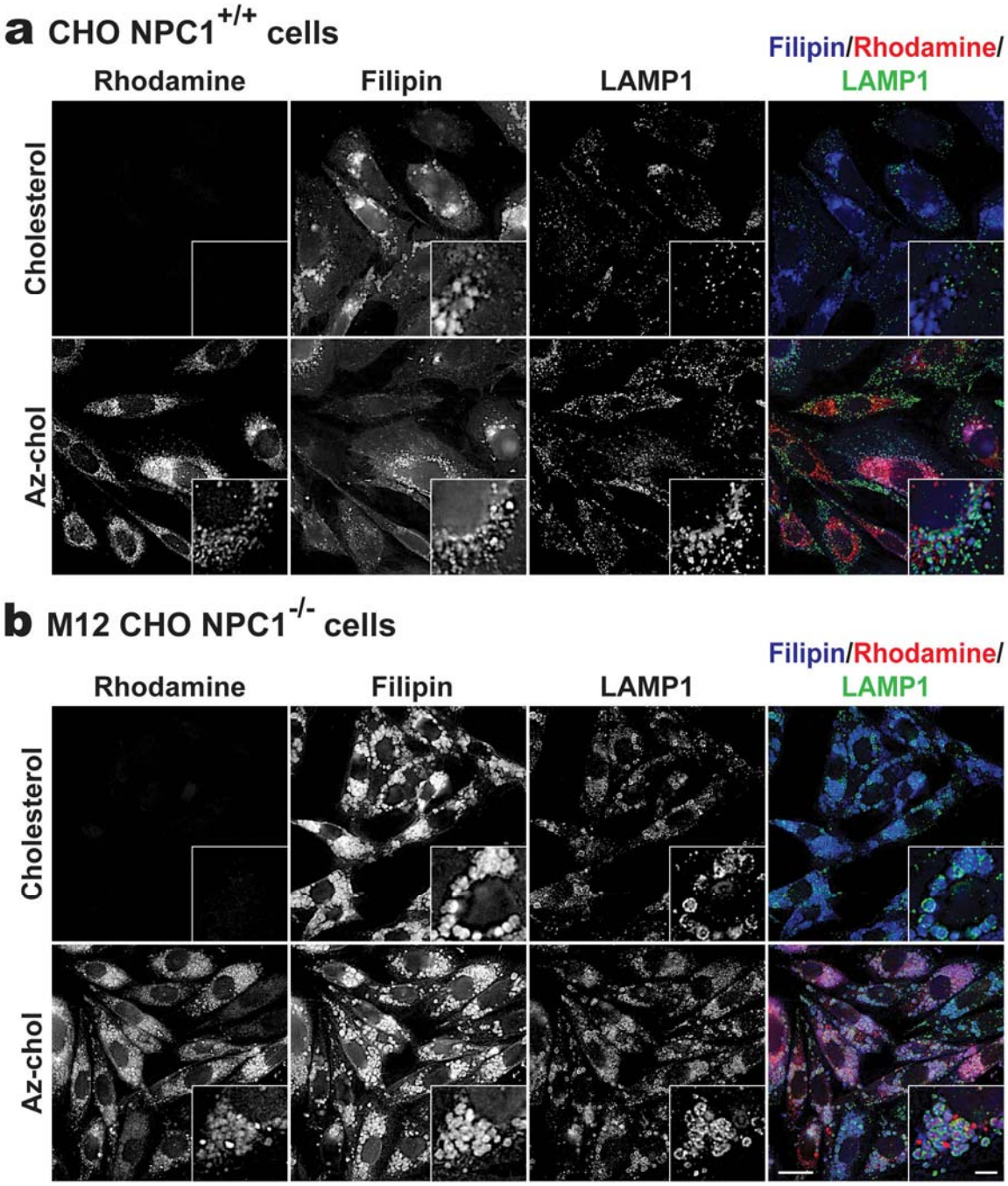

Figure 35 LAMP-1 signal encircles small late endosomal/lysosomal organelles in CHO cells (a) and much larger cholesterol storage compartments in M12 cells (b). Cholesterol controls show no rhodamine signal.

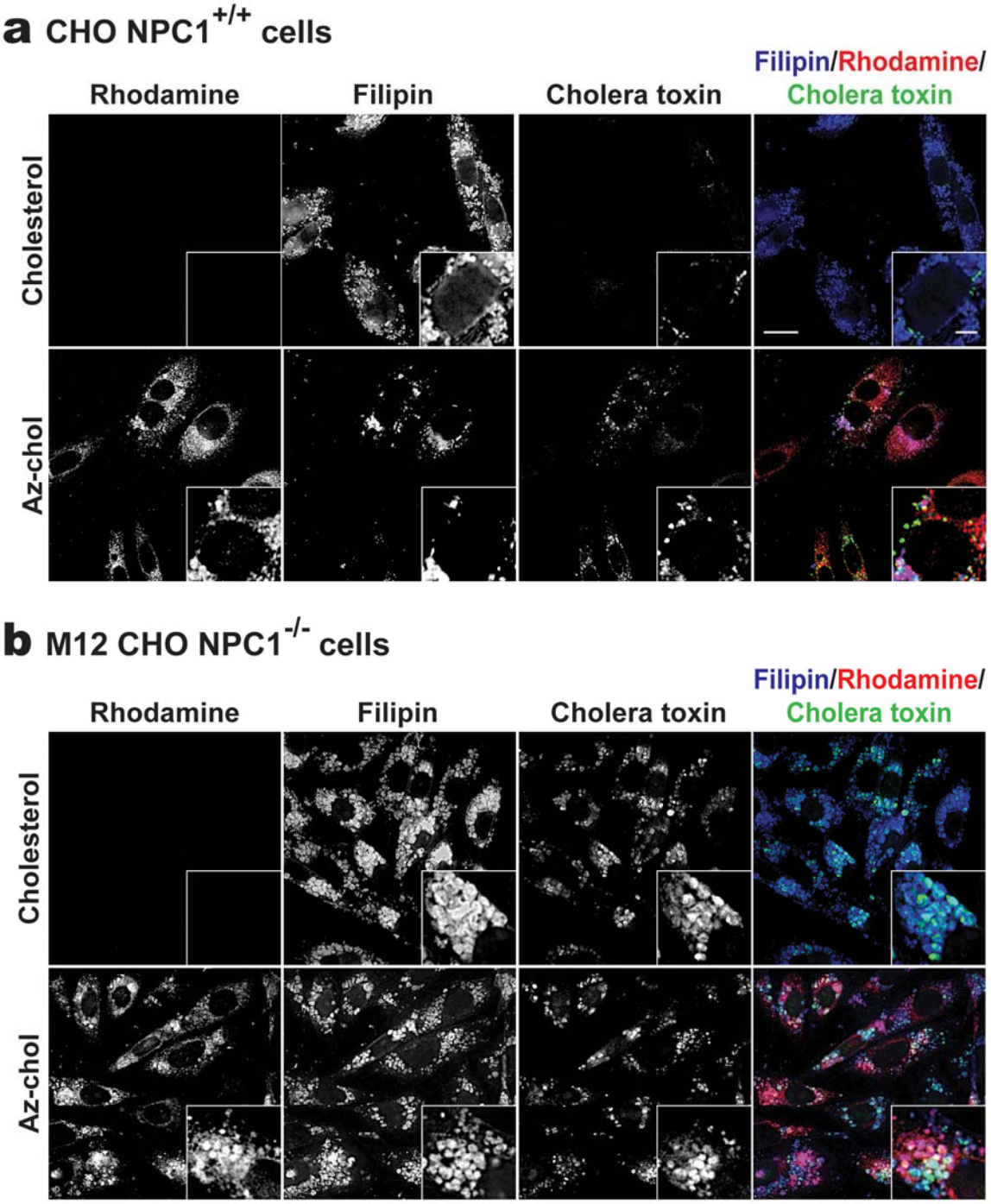

Figure 36 GM1-ganglioside binding FITC-cholera toxin B shows little signal and no pronounced colocalization with az-chol in CHO cells (**a**). Az-chol, filipin and cholera toxin staining was pronounced in the cholesterol storage organelles of M12 cells (**b**).

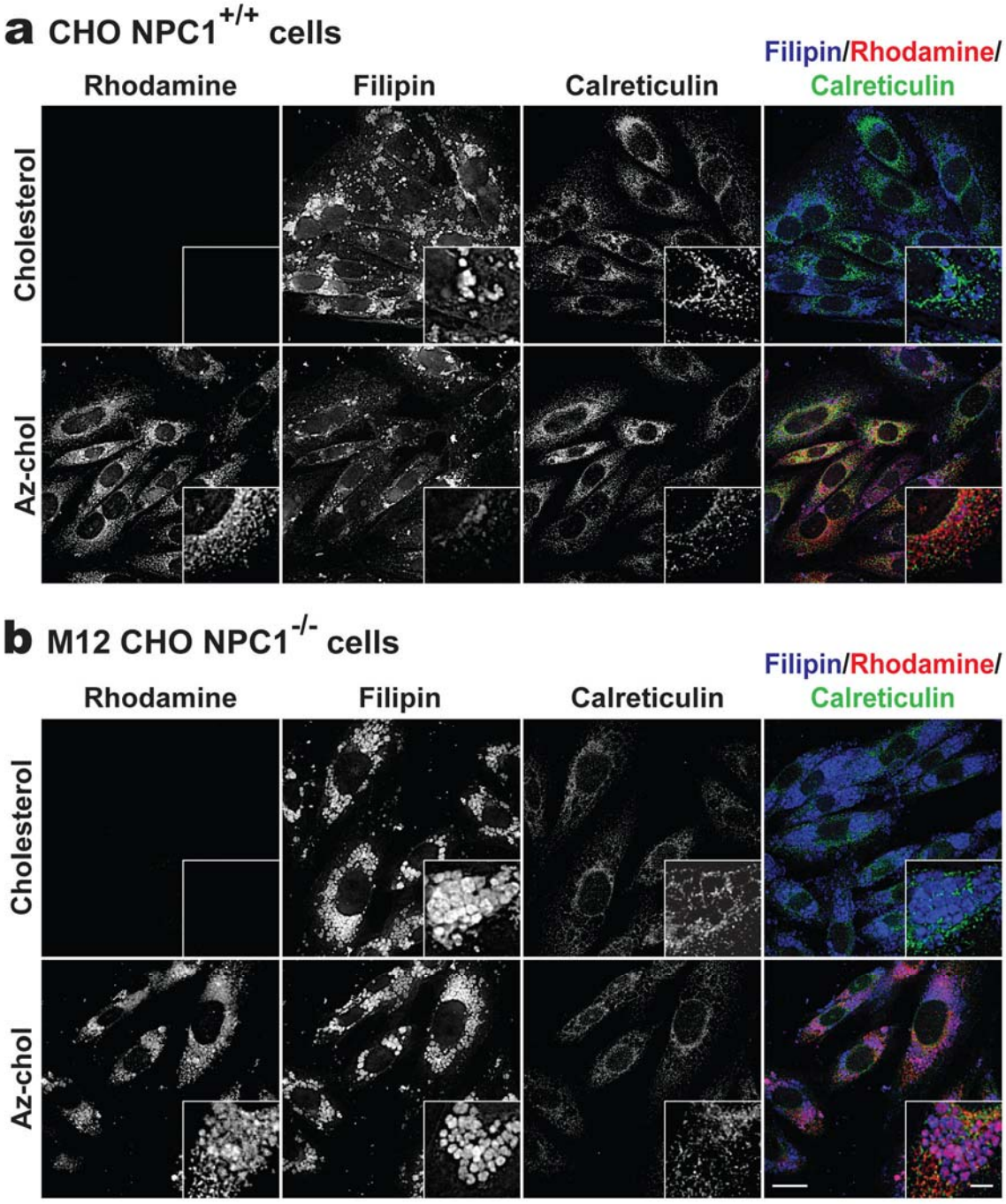

Figure 37 ER marker calreticulin shows no pronounced colocalization with Az-chol in CHO (a) or M12 cells (b).

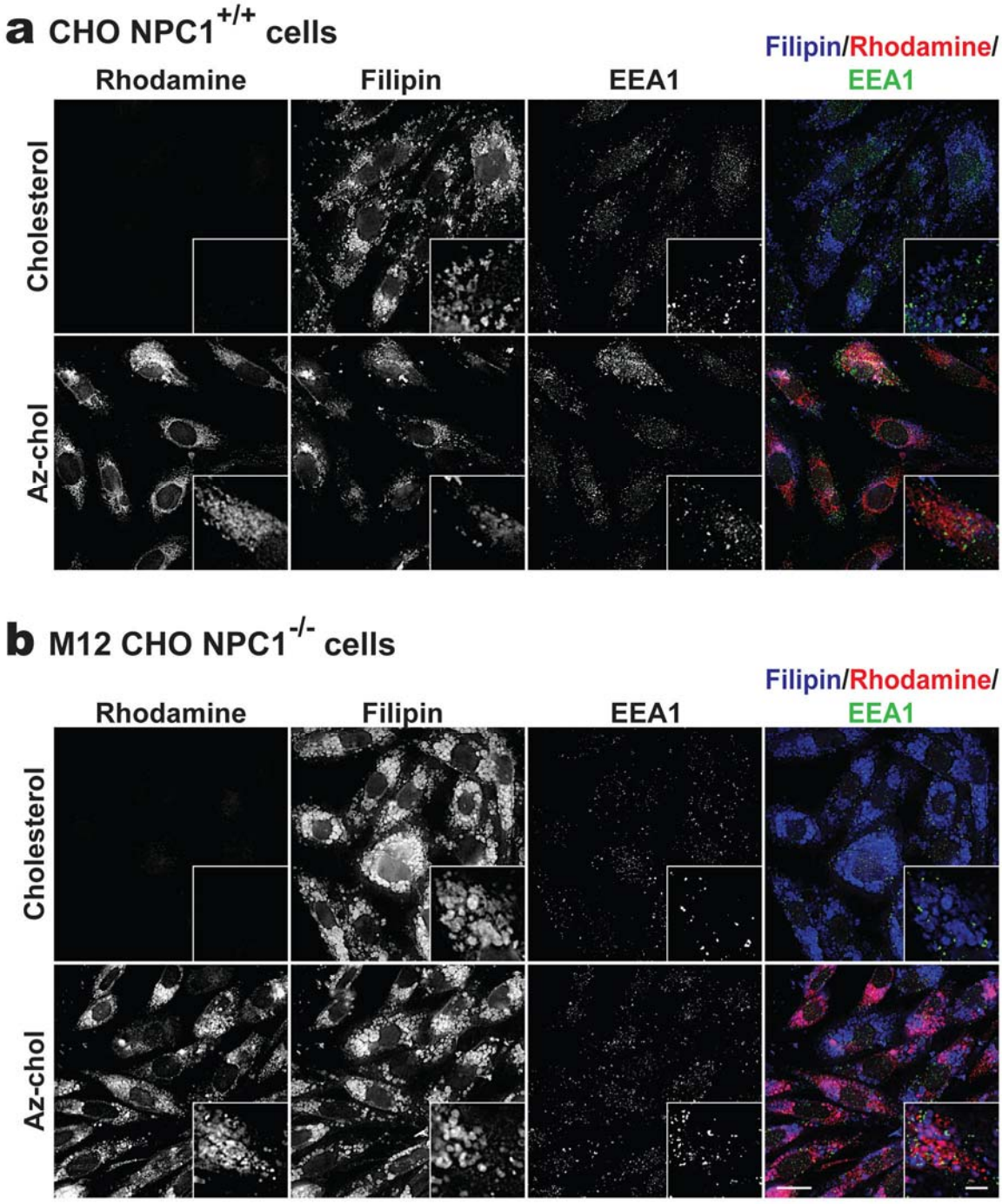

Figure 38 Early endosome marker EEA1 shows no pronounced colocalization with Az-chol in CHO (**a**) or M12 cells (**b**).

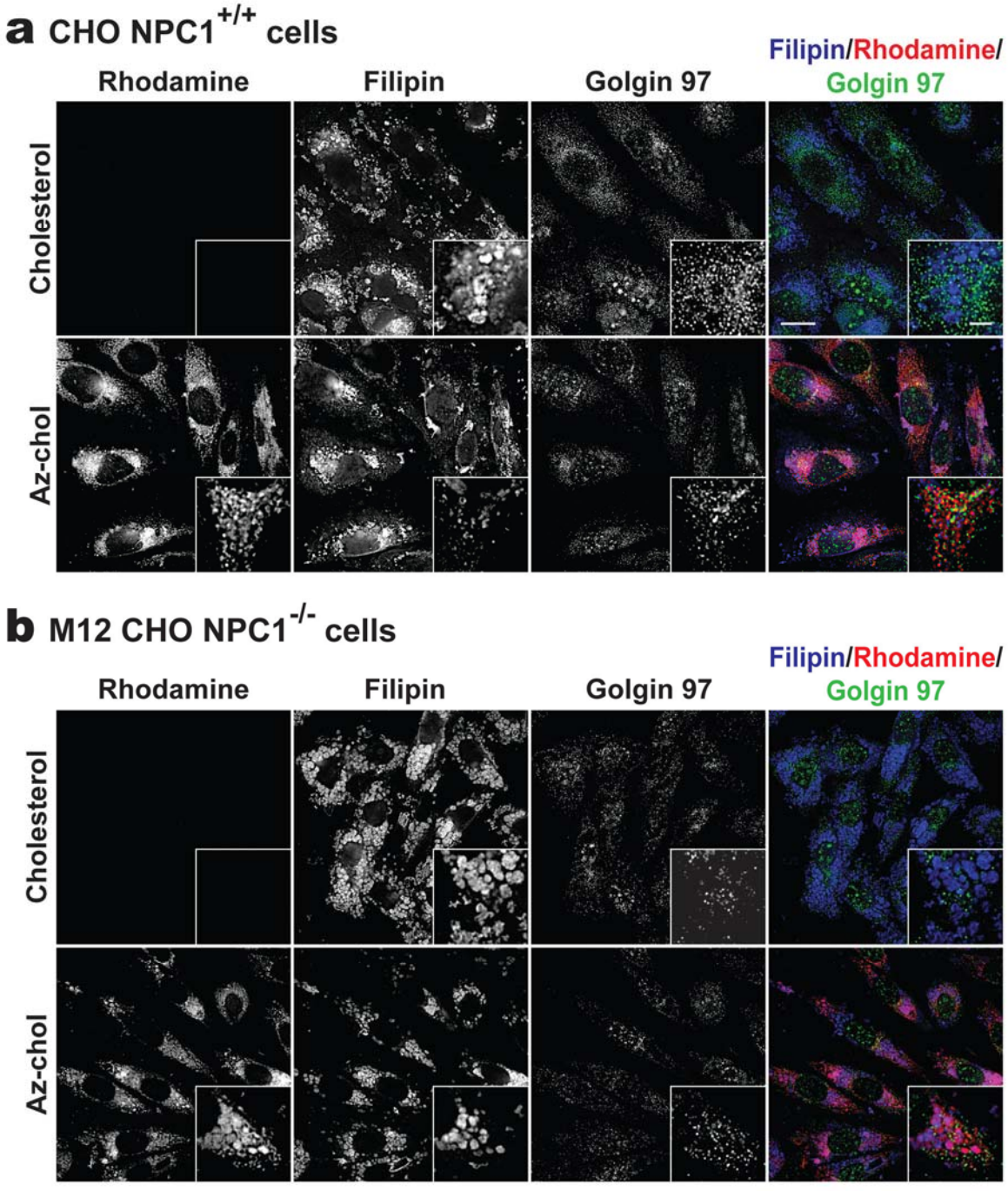

Figure 39 Golgi marker Golgin 97 shows no pronounced colocalization with Az-chol in CHO (**a**) or M12 cells (**b**).

We then explored the utility of az-chol for imaging cholesterol distribution *in vivo*. With only ~2% of body weight yet nearly a quarter of total cholesterol, the brain is the most cholesterol rich organ[282]. Defects in brain cholesterol homeostasis have dramatic consequences from development on and often involve the Purkinje cells of the cerebellum: a hallmark of NPC disease is Purkinje cell degeneration[282,289] and cerebellar hypoplasia is observed in Smith Lemli-Opitz syndrome that results from a defect in the last step of cholesterol synthesis[295]. Purkinje cells are also a major site of neurosteroid synthesis[296] and brain cholesterol turnover via cholesterol 24-hydroxylase[282]. We thus imaged cholesterol distribution in the cerebellum of a developing mouse embryo. Because maternal cholesterol is poorly absorbed and cholesterol is excluded by the blood-brain-barrier[282], az-chol was directly injected into the lateral ventricle of an E12.5 mouse embryo. Sagittal sections at low and high magnification revealed an asymmetrical cholesterol distribution (Figure 40). At low magnification, nascent neurons were more intensely labeled, likely a reflection of high cholesterol content (Figure 40a, magenta arrowheads). This trend continued in the inferior colliculus where cells with neural morphology displayed prominent az-chol labeling (Figure 40a, labeled IC, magenta arrowheads). In addition, the apical surfaces of the cerebellum and inferior colliculus appeared to be enclosed by a cholesterol-rich envelope; the pial surface of the inferior colliculus displayed the same layer (Figure 40a and inserts, white arrowheads). Higher magnification revealed distinct plasma membrane az-chol labeling as well as cell polarization with az-chol enriched toward the apical surface (Figure 40b and inserts, magenta arrows); this pattern continued throughout the layers of the pseudostratified neuroepithelium. The thick az-chol–rich layer at the apical surface of the cerebellum was pronounced under high magnification (Figure 40b and inserts, white arrows). This could be reflective of a "sealant" membrane providing proper containment of cerebrospinal fluid (CSF) and might be composed

either of polarized surface cells or an extracellular deposition. Alternatively, the cholesterol-rich layer could provide a binding platform for lipophilic hormones and factors circulating in CSF. Az-chol is thus useful for *in vivo* imaging of cholesterol distribution in embryos and organs.

Figure 40 Cholesterol localization in the developing mouse brain. Cholesterol was asymmetrically distributed in the cerebellum (**C**) and inferior colliculus (**IC**) of the E12.5 developing mouse brain. Scale bars are 50 μm (main), 25 μm (insert). (**a**) Under low magnification, an az-chol–rich envelope (white arrowheads) surrounded the apical surface (**AS**) of the cerebellum and inferior colliculus. These apical surfaces interface the cerebrospinal fluid (CSF) filled ventricles (**V**). The pial surface (**PS**) of the inferior colliculus also exhibited an exterior az-chol band. Az-chol signal was pronounced in nascent neurons (magenta arrowheads; see also inserts), likely reflecting high cholesterol content. Rhodamine signal was absent in littermate controls. (**b**) Higher resolution revealed the structure of the thick apical envelope in the cerebellum (white arrowheads). Scale bars are 10 μm (main), 2.5 μm (insert). Az-chol distinctly labeled plasma membranes of neural progenitors and tended to show apical localization (magenta arrowheads). Apical polarization of az-chol signal was observed many cells deep into the neuroepithelium.

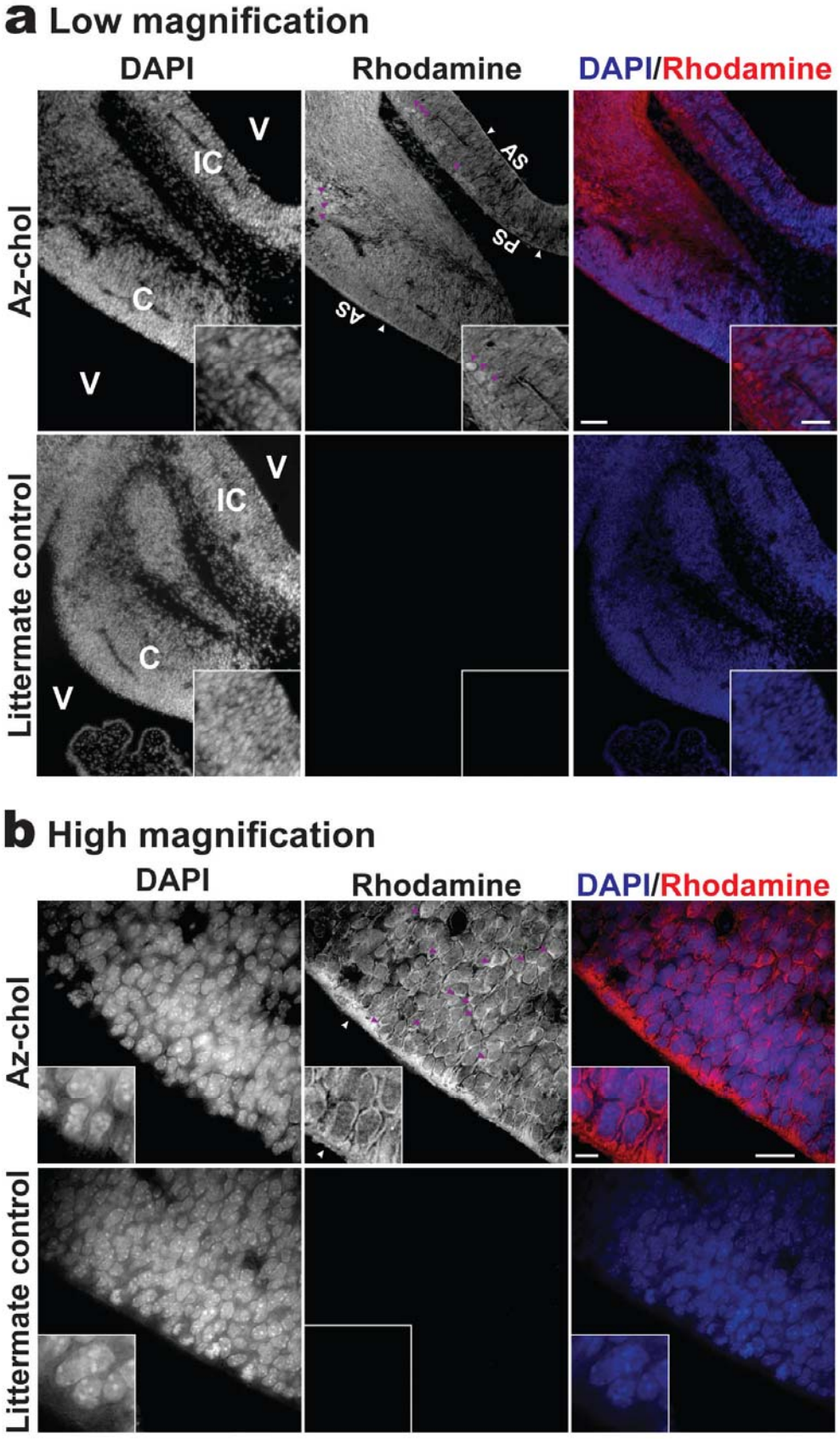
a Low magnification
DAPI
Rhodamine
DAPI/Rhodamine
Az-chol
Littermate control
V
IC
C
V
AS
PS
AS
V
IC
C
V
b High magnification
DAPI
Rhodamine
DAPI/Rhodamine
Az-chol
Littermate control

Discussion

Cholesterol has long been difficult to image. External factors other than cholesterol can alter the results of indirect assays: cholesterol oxidase results depend on membrane composition and location, fixing technique and a host of other aspects[79,297]. Likewise, perfringolysin O derivatives only bind regions with high (>20-25 mol%) cholesterol content and may be influenced by membrane properties[79]. Echoing the results here, filipin has been previously reported to yield false positive signal after cholesterol predepletion with MβCDs and can report the opposite of perfringolysin O staining[79]. Filipin false negatives have also been observed for multiple organelles[297], depending on clathrin content[298], and in smooth muscle plasma membrane[299]. The persistence of filipin signal after MβCD but not methanol for normal and M12 cells (above and Figure 34) indicates filipin has substantial lipid affinities outside of cholesterol.

Direct imaging of cholesterol has also presented challenges. All but a few cholesterol analogs have significant structural changes that perturb key features essential to the biologically activity of cholesterol[42,71,79] (above). Some of these changes radically alter cholesterol behavior, resulting in an "upside down" orientation (with the free 3□-hydroxyl pointing into the membrane interior) or disrupting cholesterol-induced phospholipid membrane condensation[42,68]. Intrinsically fluorescent sterols like DHE and cholestatrienol, despite their similarity in biological behavior, are limited by their requirement of UV compatible instrumentation and may face a high background from tissue autofluorescence. The two-step labeling approach described here involves the metabolic incorporation of a biologically active cholesterol reporter, az-chol, which has minimal structural perturbation compared to cholesterol, traffics like it and is nontoxic *in vivo*. Subsequently, fluorescent dyes are installed using bioorthogonal ligation methods for direct imaging.

This approach can be applied from a single protein to a whole organism and represents an excellent option for rapid, easily accessible and multimodal cholesterol imaging. We anticipate bioorthogonal cholesterol reporters like az-chol will aid in the study of cholesterol function in physiology and disease.

FUTURE DIRECTIONS

The identification of a new class of histone PTMs raises many interesting questions about biological significance including the mechanism of modification, stability, dynamics and regulation, effect on structure and chromatin stability, as well as effect on histone localization. These questions represent exciting possibilities for future experimental work.

Validation of in-vivo modification

As illustrated in Figure 21, of the three potential mechanisms for fatty-acylation of histone H3, the possibility of *in vivo* chemical modification is unlikely due to the low concentration of activated fatty acids resulting from acyl-carrier binding proteins (ACBPs). In addition, the chemical inaccessibility of intact histones precludes reaction. However, there exists the chance that acylation occurs as a post-lysis artifact, when both ACBPs and nucleosomes are denatured exposing both the formerly unreactive cysteine and releasing activated CoA esters. Thus, this possibility should be examined prior to other research.

Validation of in-vivo modification by manipulation of activated CoA and sulfhydryl reactivity

Two straightforward experiments can quickly answer this answer. In the first approach, the reaction between endogenous activated fatty-acid ester and free thiols is chemically modified. After metabolic labeling with alkyne or azido palmitic acid, cells can be split into three equal fractions. One fraction will be subject to rapid lysis (Polytron) in the presence of a large excess (e.g.100 mM) of a reduced thiol such as mercaptoethanol or cysteamine, providing a sink for activated fatty acids. As the total cellular concentration of activated acyl-CoA esters lies in the range of 5 –

160 μM [300], this 600 – 20,000-fold excess will substantially reduce if not prevent post-lysis fatty-acylation. The second fraction will be likewise lysed in an excess of a thiol capping reagent, such as iodoacetamide, also in high concentration (e.g. 50 mM). Under such conditions, newly exposed thiols are likely to be immediately capped, rather than potentially acylated. The third fraction serves as a control and can be lysed without change from previous experiments. After lysis, thiol, thiol capping reagent and any remaining CoA intermediates will be removed by simple methanol precipitation; previous experiments indicate click chemistry is unaffected after either thiol capping or after reduction with mercaptoethanol, as long as such reagents are removed by precipitation. Following protein pellet resuspension and the addition of cleavable affinity tag, the capture and retrieval can be repeated as previously. Parallel Western blot analysis will reveal if histone H3 fatty-acylation is reduced or eliminated by excess free thiol or thiol capping compared to control levels. This approach offers the advantage that cellular concentrations of both small molecules (excepting added reagents) and proteins remain unmodified. Both thiol capping and a thiol sink represent a mechanism to control post-lysis fatty-acylation, should it be occurring.

Validation by addition of marked activated CoA-palmitate

Mirroring this approach but monitoring the presence rather than lack of reaction, a potential chemical modification can be determined by the inclusion of a marked activated fatty acid, either radioactive or stable isotope, or the addition of a marked protein, either bearing a tag or likewise isotopically marked, which is present during lysis. In the first case, [^{13}C]-palmitic acid available from multiple suppliers can be activated as described [301] and added at physiologically relevant concentrations (e.g. 5, 50 and 100 μM) to cells during histone extraction lysis. Isolated histones

can then be dually digested sequentially with trypsin and GluC, which will produce a peptide TNLCAIHAK of monoisotopic mass 969.507 when unmodified. This size is well within the range of MS peptide analysis. The relatively uncomplicated protein composition of a histone extraction allows infusion and monitoring of a particular m/z, circumventing the possibility that lipidated peptides are lost on a reverse phase column. Alternatively, a different stationary phase such as a HILIC (hydrophilic interaction liquid chromatography) column which elutes similar to a normal phase could be employed. In either case, the m/z of the peptide alone, likely as a doubly charged species, and the peptide modified by palmitic acid, palmitic acid analogs, or isotopically tagged palmitic acid can be followed. The reaction of added activated esters resulting in [^{13}C]-palmitoylated histone peptides suggests a post-lysis artifact. However, to properly interpret results, this experimental setup requires exact knowledge of the concentration of endogenous activated esters as the two and a half log variation in concentration will substantially change extent of reaction: observation of a newly modified species at 100 μM might not reflect the mechanism of palmitoylation if endogenous concentrations are 10 μM or less.

Validation by addition of marked H3

Because exact endogenous concentration of activated fatty acids may be difficult to ascertain, a more straightforward approach is the addition of tagged histone H3 during lysis. This tag can be genetic, such as the his-tagged H3 variants employed here, or it could be marked by stable isotope labeling. The most interpretable data would be generated by addition of a purified histone and the myc-his-tagged H3 variants employed here provides a convenient mechanism of purification (IMAC). Alternatively, an isotopically marked H3 could be purified by histone extraction and immunoprecipitation (Figure 13). Whole cell lysates from co-lysis of cell pellets of either

genetically or isotopically marked, together with cells metabolically labeled with clickable precursors, represents another possible approach. However, in this case the levels of small molecule are uncertain, and competing, possibly differentially labeled, activated fatty acid esters could complicate results. While concentrations could be assumed to be equivalent in cells cultured simultaneously, e.g. with the same concentration of [^{13}C]-lysine and [^{12}C]-lysine, the fact that alkyne-fatty acids in particular modify fatty acid metabolism makes this assumption precarious. Additionally, for genetically tagged, overexpressed H3, the relative protein concentrations will be unknown and are likely difficult to control.

In all configurations, the lysis buffer would contain a known quantity of histone, preferably matched to endogenous levels (equalize by Western blotting). After a native, non-reducing gel to check that the cysteine is still free (no H3 dimers), the purified protein would be dissolved in the same volume of lysis buffer and the cells lysed with this solution as before. The check for disulfide status could also be done on purified proteins via a colorimetric assay (Ellman's reagent) but is essential to ensure free sulfhydryls due to the lack of disulfide reactivity. Alternatively, the same number of metabolically labeled wild-type cells and genetically tagged, H3-expressing cells could be copelleted and lysed. Analysis can be by Western, looking for H3 itself (which in the myc-his-H3 is shifted by the myc-his tag), by an antibody against the myc epitope or by both antibodies, simultaneously, sequentially or in two membrane stripes. In the case of myc-his-H3s used here, after purification of palmitoylated proteins as described from native cells lysed in the presence of myc-his-H3s, the presence of a myc tag from clickable fatty acid analogs indicates post-lysis reaction has occurred.

A final experimental setup would examine the presence of newly (chemically) palmitoylated, isotopically marked peptides. In this arrangement, lysis by histone extraction would take place with simultaneous inclusion of purified isotopically marked histone H3, for example labeled with [^{13}C]-cysteine, again in a roughly equivalent concentration to endogenous levels). Chemically modified, isotopically marked peptides can then be detected after codigestion with trypsin and GluC as described above. For all cases in which histone extraction is used, it must be noted that HPLC separations of histones are well established. Thus, after knowing the chromatographic properties of a palmitoylated standard, HPLC can allow for both enrichment as well as detection. Such a standard can be made by incubating reduced, purified H3 with a large concentration of CoA-palmitate (e.g. 0.1 – 1 mM) using e.g. methyl-beta-cyclodextrin and/or organics to maintain solubility; the established HPLC separation methods allow purification for additional experimental investigation described below.

Future experimental analysis of palmitoylated H3

After verification that histone modification is not an artifact of post-lysis chemical reaction, experiments can address the possible influences of fatty-acylation on nuclear location; dynamics and regulation of histone palmitoylation throughout the cell cycle and relationship to other histone PTMs; mechanism of modification; effect on nucleosome stability; effect on nucleosome structure; and the possibility of palmitoylated H3 selectively preferring particular DNA sequences.

Subnuclear localization

The effect of palmitoylation on subnuclear localization can be easily addressed in two experimental approaches. First, immunohistochemical techniques employing an anti-myc antibody can examine the localization of myc-his tagged H3 and the tagged C→A mutant. Various cell lines can be transfected as described, protein allowed to be expressed for e.g. 12 hours, fixed, permeabilized, and visualized with anti-myc antibody. Predigestion with a nuclease (e.g. Benzonase) may be required for optimal signal and neighboring untransfected cells serve as negative controls. This approach, while direct, may suffer from limited selectivity due to the low stoichiometry of modification. To combat this limitation, as nucleosomal histones have been shown to translocate across cell membranes into the nucleus[302], exogenously supplied H3 – both fully palmitoylated and reduced – can be applied externally. Nuclear trafficking of purified, epitope-labeled histone H3 can be imaged by IHC. Alternatively, the fatty-acylated and unmodified H3 can be marked with a fluorophore by either genetic means (e.g. GFP) or chemical reaction (e.g. dansyl chloride, sulfo-NHS-rhodamine) and imaged during and after incorporation. This approach allows live imaging but the behavior of the modified histone must be validated by comparison to a less perturbed system. One of the best approaches for a validation would be application of an H3 variant palmitoylated *in vitro* with a clickable analog to cells grown otherwise without clickable analogs. Visualization with the click reaction in combination with subcellular markers would then reveal localization, such as preferential association with the nuclear envelope. Ideally, this technique will also be combined with analysis of cell cycle as described below.

Cell cycle dynamics of H3 palmitoylation and palmitoylation relationship to other histone PTMs

Many histone PTMs vary throughout the cell cycle and this may also be the case for histone H3 palmitoylation. The possibility can be easily examined through a combination of cell synchronization and metabolic labeling; by analyzing both state of protein modification and cellular localization, insight can be gleaned as to the possible cycle-dependent effects of palmitoylation on protein trafficking. Analysis of time points selected to fall within each point of the cell cycle should be performed after double thymidine block, thymidine-nocodazole block or serum starvation. In each case, cells can be metabolically labeled with alkyne or azido fatty acids for a constant incubation of 1-12 hrs, likely optimally at 4-6 hrs, before the sample is lysed. Samples can then be parallel purified for fatty-acylated proteins and analyzed by Western blotting. Alternatively, purified samples may be analyzed by mass spectrometry after digestion with various combinations of proteases both for relative abundance and information of PTMs present on palmitoylated histone peptides. This could be done in a label-free manner, but would be best performed by protein level labeling with iTRAQ. Following iTRAQ labeling, samples of various time points can be combined and purified in a single purification. Labeled proteins can subsequently be digested and analyzed in one run, eliminating sample preparation variability, and mass spectrometric analysis would yield information of both the relative abundance and identity of accompanying, possibly varying PTMs throughout the cell cycle. The analysis of co-occurring PTMs is of course also possible without cell synchronization, however it makes the most sense in that context. Antibodies to various histone PTMs and Western blotting of purified palmitoylated proteins represent an alternative method to detect combinations of PTMs linked to histone palmitoylation. For both detections, dynamics would be reflected by a change in relative palmitoylated abundance throughout various time points in the cell cycle. In order to properly inter-

pret the results, a required control is knowledge of total H3 levels; this can be obtained by a Western of input material before fractionation or likewise analysis by MS and iTRAQ signal after digestion.

Mechanism of modification

After ruling out chemical modification during lysis, the remaining possibilities of autocatalytic modification and enzyme-mediated fatty-acylation can be tested with two simple experiments. While autocatalytic modification is unlikely, a consequence of the known buried and unreactive state of H3 sulfhydryl in assembled nucleosomes, it cannot be ruled out a priori: auto-modification might for example occur in rout to the nucleus prior to quaternary structure. To experimentally address this possibility, purified H3 (IMAC purification for his-tagged H3 variants, immunoprecipitation or HPLC from native sources, or a combination of these strategies) can be incubated with activated palmitoyl-CoA esters of either radiolabeled or clickable fatty acids in the presence and absence of acyl-carrier binding protein. In the former case, detection is by autoradiography and in the latter, in-gel fluorescence after click chemistry with a fluorophore. In the absence of ACBP, reaction at high (e.g. mM levels) of activated ester is expected; such levels are unreflective of cellular condition, reflect simple chemical modification and serve as a positive control. Note that solubility in the absence of ACBP may be an issue and may require the presence of MBCD. Self-palmitoylation such as the loading step of DHHC-PATs takes place in the presence of fatty-acid binding proteins and palmitoylation of H3 in the presence of ACBP at reasonable concentration (e.g. 5 – 250 μM) suggests autocatalytic modification. In this case, further studies of enzyme kinetics are warranted. For both autocatalytic and enzyme-mediated modification, the C→A mutant generated in this work should be included as a negative control.

If autocatalytic modification is absent, enzymatic modification by DHHC-PATs can be assayed by the co-overexpression of H3 variants with DHHC-PATs (in pools or individually); an empty vector transfection serves as a negative control. Detection is as above, either click chemistry and subsequent in-gel fluorescence or autoradiography, both after metabolic incorporation of respective analogs. The simplest readout is an SDS-PAGE gel looking for a H3 signal noticeably upregulated by the cotransfection of one or more PATs. Alternatively, a more precise result can be obtained by isolation of fatty-acylated proteins, followed by Western detection as described. In the case, the same anti-myc can be used for detection, or as described above, alternatively the anti-H3 antibody looking either for the shifted histone signal, or the endogenous signal, which in the presence of an active DHHC-PAT would also be expected to increase in abundance. The possible identification of a PAT modification of H3 begs additional questions such as the location of modification and its timing, questions which would be addressed by experiments.

Effect of H3 palmitoylation on nucleosome composition and stability

H3 palmitoylation might modify the stability of histone octamers, possibly strikingly: as the buried cysteines already form a region of hydrophobic yet reversible[259,260] hydrophobic interaction, palmitoylation of one or both H3 cysteines could foster an especially stable interaction, as has been observed in and which is required for activity of Bet3[303,304]. This interaction could be between two palmitate residues, or alternatively between a native and modified H3. Experimental analysis of these questions requires purification of H3 and other core histones, which is most easily done in an appropriate scale by HPLC[261] from cell lines or native sources. Chicken erythrocytes have historically been heavily employed and protocols employing that protein source have

been developed for nucleosome reconstitution[305] and crystallization[247]. In addition, because a C→A mutant can be generated in vitro by Raney nickel dethiolation of cysteine[306], this likely represents the best material for biochemical experiments.

After purification of core histones from chicken erythrocytes, dethiolation of a portion of H3, palmitoylation of another portion of H3 as described above under "Validation by addition of marked H3," and validation of identity, purity and extent of reaction (SDS-PAGE and mass spectrometry or Western blotting or both), core histones can be reconstituted by established methods [305]. Histone octamer reconstitution can be validated by gel filtration chromatography, analytical centrifugation and native non-reducing gels. Reconstitution of the nucleosomes with palmitoylated H3 may require experimental optimization such as alterations in chaotrope (thiourea or guanidinium chloride might for example be substituted for urea), changes in dialysis such as times, chaotrope concentrations, temperatures or chaotrope substitutions; these experimental modifications must be empirically determined.

Reconstitutions should be attempted with native, fully palmitoylated and dethiolated H3. In addition, a reconstitution should be performed with an equimolar mix of palmitoylated and native or dethiolated H3 to addresses the preference of acylated H3 within the environment of the nucleosome. To determine this preference, nucleosome subunits should be fully chemically crosslinked[307], the different variations of nucleosome composition isolated by HPLC and the sulfhydryl content of fractions determined (e.g. Ellman's reagent). While a somewhat heterogeneous set of products is expected due to crosslinking, a predominant fraction with one free cysteine per 262 kDa nucleosome reflects preference of a palmitoylated H3 for native H3. In conjunction

with this approach, H3 modified with a clickable palmitic acid analog can be reacted with a fluorophore and the molar equivalent of fatty acid per fraction determined by absorbance or fluorescence; specific radioactivity can be employed in an analogous manner.

Octamer stability of reconstitutions from native, dethiolated and fatty-acylated octamer can most easy be compared by non-reducing urea gradient gels; this provides a direct, side-by-side comparison of dissociations. Alternatively, analytical ultracentrifugation of octamer with different concentrations of chaotrope or salt can determine the relative equilibrium of subunit and assembled nucleosome. Finally, reconstituted octamers can be combined with DNA[308] and the resulting pellet exposed to gradually increasing salt concentrations[309]. Decreased stability results in the increased release of histone monomers into the supernatant at lower salt concentrations (gel).

Effect of H3 palmitoylation on chromatin and nucleosome structure

The possibly different chromatin structure resulting different states of H3 acylation in nucleosomes can be explored by many techniques such as digestion, gel-shift and supercoiling assays. However, such reconstitution is subject to influence by a wide variety of variables including DNA:histone ratio, possibly ATP-dependent assembly machinery and others[310]. These parameters must be empirically explored. At the single nucleosome level, established crystallization conditions can be attempted after successful reconstitution in either the presence or absence of DNA; the addition of one or two palmitates could however result in substantially changed crystallization conditions.

Palmitoylated H3 protein and DNA sequence selectively

In addition to possible effects that altered nucleosome structure could have overall on chromatin, H3 palmitoylation might affect the proteins which bind octamers. Changes in both preferred protein binding partner and sequence can be determined by combining metabolic labeling and purification of lipidated proteins with a myc-his tagged H3. Both analyses begin as described for the identification of palmitoylated H3 with overexpression and simultaneous metabolic labeling. A modified chromatin IP (ChIP) is employed for identification of DNA binding sites in which cells are fixed in formaldehyde, nuclei are isolated and disrupted followed by micrococcal nuclease digestion to nucleosomes[311]. These crosslinked nucleosome are subjected under denaturing conditions (urea and/or SDS) to serial isolation of the his-tag (IMAC) followed by capture of palmitoylated proteins as described. The flow through must be examined to determine the absence of biotinylated, palmitoylated proteins for the accurate comparison of differences in binding sequence of H3 modification. Both unmodified H3 proteins of the flow-through and the $Na_2S_2O_4$ eluted, palmitoylated H3 can be matched in protein concentration and subjected to protease K digestion. DNA is then extracted (chloroform/methanol), gel purified and sequenced to reveal differences in DNA sequence preference[311].

Proteins interacting with H3 of different states of fatty-acylation can be determined in an analogous manner but leaving protein not DNA. In this case, chromatin is prepared as above but crosslinked with a cleavable crosslinker such as BSOCOES (base cleavable), DSP, DTSSP or DTBP (thiol cleavable; see caution below), or DST (periodate cleavable) in place of formaldehyde. After denaturation (SDS/urea), benzonase is used to fully digest DNA. IMAC under denaturing conditions can then isolate his-tagged H3 and palmitoylated H3 is subsequently purified on

beads as described but not eluted with $Na_2S_2O_4$. Rather, the release agent for the cleavable cross-linker is applied, releasing proteins bound to palmitoylated H3. Similarly, the flow through from fatty-acylated H3 purification can be re-applied to another IMAC column and the bound, cross-linked proteins released by the necessary cleaving reagent. Note that while sodium dithionite is reasonably tolerant to sulfhydryls (analysis of labeled proteins by reducing SDS-PAGE is possible), storage of samples in BME, even at – 80 C, resulted in loss of signal, indicating that elution with thiol will require optimization of time and concentration on model systems. Likewise, IMAC is sensitive to pH and the redox state of nickel; conditions will require optimization. The eluted H3 crosslinked fractions can then be analyzed by mass spectrometry (in-gel or in-solution).

Analysis of in-vivo effect

After H3 palmitoylation has been verified to take place *in vivo* and studied *in vitro*, the modification can be studied *in vivo* in mice. This will involve either kockin of H3.1, H3.2 and H3.3 each bearing C→A mutations, followed by subsequent crossing, or kockout of two of the three followed by crosslink with the remaining mutant. According to the Mouse Genome Database, no knockouts exist for any H3 variant, and the first experiment would involve determination of viability for knockouts of H3 variants.

CONCLUSION

Like science upon which they are based, these new techniques represent stepping stones and the most interesting work lies ahead: what is the function of histone palmitoylation and what else is ubiquitous, ancient, essential yet potentially harmful cholesterol doing? Many histone PTMs have no phenotype; would this one? Here at Rockefeller the Allfrey lab discovered this buried histone residue to be opened up during active transcription[260]. Could palmitoylation serve to anchor necessary protein complexes – more or less the major role lipids serve on proteins – during this process? Likewise, this work discovered many ribosomal proteins to be lipidated, work later validated by the Freeman lab, and revealed fatty-acylation of may multi-protein complexes. What else have we been missing in the role of lipids to organize cellular processes? It will be exciting to see what biology falls out of unbiased screens such as this one, and this study is another stark reminder of how much sample preparation influences results. Lipids and in particular cholesterol seem to be prominently involved in factors essential to the development of organisms and to me, they have always seemed to be a sort of a "gentle anchor"; this is particularly apparent in Shh distribution of cholesterylation null mutants. With the ability to visualize the presence and distributions of lipidated proteins, the door opens to the study of such low-level factors (as has already started[99]), allowing us to finally decipher why so many secreted factors are lipidated.

REFERENCES

1 Brown, H. A. & Murphy, R. C. Working towards an exegesis for lipids in biology. *Nat Chem Biol* **5**, 602-606, doi:nchembio0909-602 [pii] 10.1038/nchembio0909-602 (2009).

2 DiNitto, J. P., Cronin, T. C. & Lambright, D. G. Membrane recognition and targeting by lipid-binding domains. *Sci STKE* **2003**, re16, doi:10.1126/stke.2132003re16 2003/213/re16 [pii] (2003).

3 Shimizu, T. Lipid mediators in health and disease: enzymes and receptors as therapeutic targets for the regulation of immunity and inflammation. *Annu Rev Pharmacol Toxicol* **49**, 123-150, doi:10.1146/annurev.pharmtox.011008.145616 (2009).

4 Kojima, M. *et al.* Ghrelin is a growth-hormone-releasing acylated peptide from stomach. *Nature* **402**, 656-660 (1999).

5 Resh, M. D. Trafficking and signaling by fatty-acylated and prenylated proteins. *Nat Chem Biol* **2**, 584-590 (2006).

6 Eaton, S. Multiple roles for lipids in the Hedgehog signalling pathway. *Nat Rev Mol Cell Biol* **9**, 437-445, doi:nrm2414 [pii] 10.1038/nrm2414 (2008).

7 Hancock, J. F., Magee, A. I., Childs, J. E. & Marshall, C. J. All ras proteins are polyisoprenylated but only some are palmitoylated. *Cell* **57**, 1167-1177 (1989).

8 Nagar, B. *et al.* Structural basis for the autoinhibition of c-Abl tyrosine kinase. *Cell* **112**, 859-871 (2003).

9 Hantschel, O. *et al.* A myristoyl/phosphotyrosine switch regulates c-Abl. *Cell* **112**, 845-857 (2003).

10 Tian, L. *et al.* Palmitoylation gates phosphorylation-dependent regulation of BK potassium channels. *Proc Natl Acad Sci U S A* **105**, 21006-21011 (2008).

11 Farazi, T. A., Waksman, G. & Gordon, J. I. The biology and enzymology of protein N-myristoylation. *J Biol Chem* **276**, 39501-39504 (2001).

12 Zha, J., Weiler, S., Oh, K. J., Wei, M. C. & Korsmeyer, S. J. Posttranslational N-myristoylation of BID as a molecular switch for targeting mitochondria and apoptosis. *Science* **290**, 1761-1765 (2000).

13 de Jonge, H. R., Hogema, B. & Tilly, B. C. Protein N-myristoylation: critical role in apoptosis and salt tolerance. *Sci STKE* **2000**, PE1 (2000).

14 Yu, X., Wang, L., Luo, Y. & Roeder, R. G. Identification and characterization of a novel OCA-B isoform. implications for a role in B cell signaling pathways. *Immunity* **14**, 157-167 (2001).

15 Siegel, R. *et al.* Nontranscriptional regulation of SYK by the coactivator OCA-B is required at multiple stages of B cell development. *Cell* **125**, 761-774 (2006).

16 Resh, M. D. Palmitoylation of ligands, receptors, and intracellular signaling molecules. *Sci STKE* **2006**, re14 (2006).

17 Smotrys, J. E. & Linder, M. E. Palmitoylation of intracellular signaling proteins: regulation and function. *Annu Rev Biochem* **73**, 559-587, doi:10.1146/annurev.biochem.73.011303.073954 (2004).

18 DeMar, J. C., Jr. & Anderson, R. E. Identification and quantitation of the fatty acids composing the CoA ester pool of bovine retina, heart, and liver. *J Biol Chem* **272**, 31362-31368 (1997).
19 Liang, X. *et al.* Heterogeneous fatty acylation of Src family kinases with polyunsaturated fatty acids regulates raft localization and signal transduction. *J Biol Chem* **276**, 30987-30994, doi:10.1074/jbc.M104018200 M104018200 [pii] (2001).
20 Linder, M. E. & Deschenes, R. J. Palmitoylation: policing protein stability and traffic. *Nat Rev Mol Cell Biol* **8**, 74-84 (2007).
21 Tsutsumi, R., Fukata, Y. & Fukata, M. Discovery of protein-palmitoylating enzymes. *Pflugers Arch* (2008).
22 Zhou, F., Xue, Y., Yao, X. & Xu, Y. CSS-Palm: palmitoylation site prediction with a clustering and scoring strategy (CSS). *Bioinformatics* **22**, 894-896 (2006).
23 Glomset, J. A., Gelb, M. H. & Farnsworth, C. C. Prenyl proteins in eukaryotic cells: a new type of membrane anchor. *Trends Biochem Sci* **15**, 139-142 (1990).
24 Zhang, F. L. & Casey, P. J. Protein prenylation: Molecular mechanisms and functional consequences. *Annual Review of Biochemistry* **65**, 241-269 (1996).
25 Benetka, W., Koranda, M. & Eisenhaber, F. Protein Prenylation: An (Almost) Comprehensive Overview on Discovery History, Enzymology, and Significance in Physiology and Disease. *Monatshefte für Chemie / Chemical Monthly* **137**, 1241-1281, doi:10.1007/s00706-006-0534-9 (2006).
26 Porter, J. A., Young, K. E. & Beachy, P. A. Cholesterol modification of hedgehog signaling proteins in animal development. *Science* **274**, 255-259 (1996).
27 Mann, R. K. & Beachy, P. A. Novel lipid modifications of secreted protein signals. *Annual Review of Biochemistry* **73**, 891-923, doi:DOI 10.1146/annurev.biochem.73.011303.073933 (2004).
28 Hall, T. *et al.* Crystal structure of a hedgehog autoprocessing domain: Homology between hedgehog and self-splicing proteins. *Cell* **91**, 85-97 (1997).
29 Paulick, M. G. & Bertozzi, C. R. The glycosylphosphatidylinositol anchor: a complex membrane-anchoring structure for proteins. *Biochemistry* **47**, 6991-7000, doi:10.1021/bi8006324 (2008).
30 Takeda, J. & Kinoshita, T. GPI-anchor biosynthesis. *Trends Biochem Sci* **20**, 367-371, doi:S0968-0004(00)89078-7 [pii] (1995).
31 Hillenkamp, F., Karas, M., Beavis, R. C. & Chait, B. T. Matrix-assisted laser desorption/ionization mass spectrometry of biopolymers. *Anal Chem* **63**, 1193A-1203A (1991).
32 Fenn, J. B., Mann, M., Meng, C. K., Wong, S. F. & Whitehouse, C. M. Electrospray ionization for mass spectrometry of large biomolecules. *Science* **246**, 64-71 (1989).
33 Sims, P. J., Waggoner, A. S., Wang, C. H. & Hoffman, J. F. Studies on Mechanism by Which Cyanine Dyes Measure Membrane-Potential in Red Blood-Cells and Phosphatidylcholine Vesicles. *Biochemistry* **13**, 3315-3330 (1974).
34 Stauffer, T. P., Ahn, S. & Meyer, T. Receptor-induced transient reduction in plasma membrane PtdIns(4,5)P2 concentration monitored in living cells. *Curr Biol* **8**, 343-346, doi:S0960-9822(98)70135-6 [pii] (1998).
35 Coniglio, J. G., Anderson, C. E. & Robinson, C. S. The absorption and distribution of labeled fatty acids in the rat. *Proc Soc Exp Biol Med* **75**, 666-669 (1950).

36 WHITEHOUSE, M., GURIN, S. & STAPLE, E. CATABOLISM IN VITRO OF CHOLESTEROL .2. FURTHER STUDIES ON OXIDATION OF CHOLESTEROL BY RAT LIVER MITOCHONDRIA. *J Biol Chem* **236**, 68-& (1961).
37 Brady, R. O. & Gurin, S. The biosynthesis of radioactive fatty acids and cholesterol. *J Biol Chem* **186**, 461-469 (1950).
38 Becker, W. & Bruce, A. in *Prog Lipid Res* Vol. 24 325-346 (1985).
39 Schlesinger, M. J., Magee, A. I. & Schmidt, M. F. Fatty acid acylation of proteins in cultured cells. *J Biol Chem* **255**, 10021-10024 (1980).
40 Stein, O., Stein, Y., Goodman, D. S. & Fidge, N. H. in *J Cell Biol* Vol. 43 410-431 (1969).
41 Peseckis, S. M., Deichaite, I. & Resh, M. D. Iodinated fatty acids as probes for myristate processing and function. Incorporation into pp60v-src. *J Biol Chem* **268**, 5107-5114 (1993).
42 Wustner, D. Fluorescent sterols as tools in membrane biophysics and cell biology. *Chem Phys Lipids* **146**, 1-25, doi:S0009-3084(06)00197-6 [pii] 10.1016/j.chemphyslip.2006.12.004 (2007).
43 Blumenthal, R., Gallo, S. A., Viard, M., Raviv, Y. & Puri, A. Fluorescent lipid probes in the study of viral membrane fusion. *Chem Phys Lipids* **116**, 39-55, doi:S0009308402000191 [pii] (2002).
44 Maier, O., Oberle, V. & Hoekstra, D. Fluorescent lipid probes: some properties and applications (a review). *Chem Phys Lipids* **116**, 3-18, doi:S0009308402000178 [pii] (2002).
45 Molotkovskii Iu, G. [Fluorescent lipid probes: properties and application]. *Bioorg Khim* **25**, 855-867 (1999).
46 Johnson, I. D., Kang, H. C. & Haugland, R. P. Fluorescent membrane probes incorporating dipyrrometheneboron difluoride fluorophores. *Anal Biochem* **198**, 228-237 (1991).
47 Pagano, R. E., Martin, O. C., Kang, H. C. & Haugland, R. P. A novel fluorescent ceramide analogue for studying membrane traffic in animal cells: accumulation at the Golgi apparatus results in altered spectral properties of the sphingolipid precursor. *J Cell Biol* **113**, 1267-1279 (1991).
48 Pagano, R. E., Longmuir, K. J., Martin, O. C. & Struck, D. K. Metabolism and intracellular localization of a fluorescently labeled intermediate in lipid biosynthesis within cultured fibroblasts. *J Cell Biol* **91**, 872-877 (1981).
49 Sparrow, C. P. *et al.* A fluorescent cholesterol analog traces cholesterol absorption in hamsters and is esterified in vivo and in vitro. *J Lipid Res* **40**, 1747-1757 (1999).
50 Chattopadhyay, A. Chemistry and biology of N-(7-nitrobenz-2-oxa-1,3-diazol-4-yl)-labeled lipids: fluorescent probes of biological and model membranes. *Chem Phys Lipids* **53**, 1-15, doi:0009-3084(90)90128-E [pii] (1990).
51 Huang, H. *et al.* in *J Lipid Res* Vol. 51 1157-1172 (2010).
52 Wiegand, V., Chang, T., Strauss, J., Fahrenholz, F. & Gimpl, G. Transport of plasma membrane-derived cholesterol and the function of Niemann-Pick C1 protein. *Faseb J* **17**, 782-+ (2003).
53 Ran, Y. & Fanucci, G. E. A dansyl fluorescence-based assay for monitoring kinetics of lipid extraction and transfer. *Anal Biochem* **382**, 132-134, doi:S0003-2697(08)00493-4 [pii] 10.1016/j.ab.2008.07.022 (2008).

54 Hoekstra, D., Deboer, T., Klappe, K. & Wilschut, J. Fluorescence Method for Measuring the Kinetics of Fusion between Biological-Membranes. *Biochemistry* **23**, 5675-5681 (1984).
55 Grechishnikova, I. V., Bergstrom, F., Johansson, L. B., Brown, R. E. & Molotkovsky, J. G. New fluorescent cholesterol analogs as membrane probes. *Biochim Biophys Acta* **1420**, 189-202, doi:S0005-2736(99)00088-7 [pii] (1999).
56 Stoffel, W. & Michaelis, G. Chemical syntheses of novel fluorescent-labelled fatty acids, phosphatidylcholines and cholesterol esters. *Hoppe Seylers Z Physiol Chem* **357**, 7-19 (1976).
57 Pownall, H. J. & Smith, L. C. Pyrene-labeled lipids: versatile probes of membrane dynamics in vitro and in living cells. *Chem Phys Lipids* **50**, 191-211 (1989).
58 Somerharju, P. Pyrene-labeled lipids as tools in membrane biophysics and cell biology. *Chem Phys Lipids* **116**, 57-74, doi:S0009308402000208 [pii] (2002).
59 Tanhuanpaa, K., Virtanen, J. & Somerharju, P. Fluorescence imaging of pyrene-labeled lipids in living cells. *Biochim Biophys Acta* **1497**, 308-320, doi:S0167-4889(00)00068-9 [pii] (2000).
60 Kao, Y. J., Doody, M. C. & Smith, L. C. Transfer of cholesterol and a fluorescent cholesterol analog, 3'-pyrenylmethyl-23,24-dinor-5-cholen-22-oate-3 beta-ol, between human plasma high density lipoproteins. *J Lipid Res* **27**, 781-785 (1986).
61 Lusa, S., Myllärniemi, M., Volmonen, K., Vauhkonen, M. & Somerharju, P. in *Biochem J* Vol. 315 (Pt 3) 947-952 (1996).
62 Antes, P., Schwarzmann, G. & Sandhoff, K. Distribution and metabolism of fluorescent sphingosines and corresponding ceramides bearing the diphenylhexatrienyl (DPH) fluorophore in cultured human fibroblasts. *Eur J Cell Biol* **59**, 27-36 (1992).
63 Kao, Y. J., Soutar, A. K., Hong, K. Y., Pownall, H. J. & Smith, L. C. N-(2-Naphthyl)-23,24-dinor-5-cholen-22-amin-3beta-ol, a fluorescent cholesterol analogue. *Biochemistry* **17**, 2689-2696 (1978).
64 Brunner, J. in *Meth Enzymol* Vol. 172 628-687 (1989).
65 Klausner, R. D. & Wolf, D. E. Selectivity of fluorescent lipid analogues for lipid domains. *Biochemistry* **19**, 6199-6203 (1980).
66 Kessel, A., Ben-Tal, N. & May, S. Interactions of cholesterol with lipid bilayers: the preferred configuration and fluctuations. *Biophys J* **81**, 643-658, doi:S0006-3495(01)75729-3 [pii] 10.1016/S0006-3495(01)75729-3 (2001).
67 Wang, T. Y. & Silvius, J. R. Different sphingolipids show differential partitioning into sphingolipid/cholesterol-rich domains in lipid bilayers. *Biophysical Journal* **79**, 1478-1489 (2000).
68 Scheidt, H. A., Muller, P., Herrmann, A. & Huster, D. The potential of fluorescent and spin-labeled steroid analogs to mimic natural cholesterol. *J Biol Chem* **278**, 45563-45569, doi:10.1074/jbc.M303567200 M303567200 [pii] (2003).
69 Kaiser, R. D. & London, E. Determination of the depth of BODIPY probes in model membranes by parallax analysis of fluorescence quenching. *Biochim Biophys Acta* **1375**, 13-22, doi:S0005-2736(98)00127-8 [pii] (1998).
70 Schroeder, F. Use of a Fluorescent Sterol to Probe the Transbilayer Distribution of Sterols in Biological-Membranes. *Febs Letters* **135**, 127-130 (1981).

71 Schroeder, F. Fluorescent sterols: probe molecules of membrane structure and function. *Prog Lipid Res* **23**, 97-113, doi:0163-7827(84)90009-2 [pii] (1984).
72 Wüstner, D., Mondal, M., Tabas, I. & Maxfield, F. R. in *Traffic* Vol. 6 396-412 (2005).
73 Mukherjee, S., Zha, X., Tabas, I. & Maxfield, F. R. in *Biophys J* Vol. 75 1915-1925 (1998).
74 Sklar, L. A., Hudson, B. S. & Simoni, R. D. Conjugated Polyene Fatty-Acids as Membrane Probes - Preliminary Characterization. *Proceedings of the National Academy of Sciences of the United States of America* **72**, 1649-1653 (1975).
75 Kuerschner, L. *et al.* in *Nat Methods* Vol. 2 39-45 (2005).
76 Mateo, C. R., Souto, A. A., Amat-Guerri, F. & Acuna, A. U. New fluorescent octadecapentaenoic acids as probes of lipid membranes and protein-lipid interactions. *Biophys J* **71**, 2177-2191, doi:S0006-3495(96)79419-5 [pii] 10.1016/S0006-3495(96)79419-5 (1996).
77 Liu, X. H. & Prestwich, G. D. Didehydrogeranylgeranyl (Delta Delta GG): a fluorescent probe for protein prenylation. *J Am Chem Soc* **124**, 20-21, doi:ja0119144 [pii] (2002).
78 Hao, M. M. *et al.* Vesicular and non-vesicular sterol transport in living cells - The endocytic recycling compartment is a major sterol storage organelle. *Journal of Biological Chemistry* **277**, 609-617, doi:DOI 10.1074/jbc.M108861200 (2002).
79 Gimpl, G. & Gehrig-Burger, K. Cholesterol reporter molecules. *Bioscience Reports* **27**, 335-358, doi:DOI 10.1007/s10540-007-9060-1 (2007).
80 Rog, T., Pasenkiewicz-Gierula, M., Vattulainen, I. & Karttunen, M. Ordering effects of cholesterol and its analogues. *Biochimica Et Biophysica Acta-Biomembranes* **1788**, 97-121, doi:DOI 10.1016/j.bbamem.2008.08.022 (2009).
81 Pöyry, S., Róg, T., Karttunen, M. & Vattulainen, I. in *J Phys Chem B* Vol. 112 2922-2929 (2008).
82 Bielawska, A., Crane, H. M., Liotta, D., Obeid, L. M. & Hannun, Y. A. Selectivity of Ceramide-Mediated Biology - Lack of Activity of Erythro-Dihydroceramide. *Journal of Biological Chemistry* **268**, 26226-26232 (1993).
83 Heyliger, C. E., Kheshgi, T. J., Murphy, E. J., Myers-Payne, S. & Schroeder, F. Fatty acid double bond orientation alters interaction with L-cell fibroblasts. *Mol Cell Biochem* **155**, 113-119 (1996).
84 Frolov, A. *et al.* High density lipoprotein-mediated cholesterol uptake and targeting to lipid droplets in intact L-cell fibroblasts - A single- and multiphoton fluorescence approach. *Journal of Biological Chemistry* **275**, 12769-12780 (2000).
85 Cornelius, A. S., Yerram, N. R., Kratz, D. A. & Spector, A. A. Cytotoxic effect of cis-parinaric acid in cultured malignant cells. *Cancer Res* **51**, 6025-6030 (1991).
86 Neef, A. B. & Schultz, C. Selective fluorescence labeling of lipids in living cells. *Angew Chem Int Ed Engl* **48**, 1498-1500, doi:10.1002/anie.200805507 (2009).
87 Saxon, E. & Bertozzi, C. R. Cell surface engineering by a modified Staudinger reaction. *Science* **287**, 2007-2010 (2000).
88 Soellner, M. B., Nilsson, B. L. & Raines, R. T. Reaction mechanism and kinetics of the traceless Staudinger ligation. *Journal of the American Chemical Society* **128**, 8820-8828, doi:Artn Ja060484k Doi 10.1021/Ja060484k (2006).

89 Lemieux, G. A., de Graffenried, C. L. & Bertozzi, C. R. A fluorogenic dye activated by the Staudinger ligation. *Journal of the American Chemical Society* **125**, 4708-4709, doi:Doi 10.1021/Ja029013y (2003).
90 Hangauer, M. J. & Bertozzi, C. R. A FRET-based fluorogenic phosphine for live-cell Imaging with the Staudinger ligation. *Angewandte Chemie-International Edition* **47**, 2394-2397, doi:DOI 10.1002/anie.200704847 (2008).
91 Prescher, J. A., Dube, D. H. & Bertozzi, C. R. Chemical remodelling of cell surfaces in living animals. *Nature* **430**, 873-877, doi:Doi 10.1038/Nature02791 (2004).
92 Dube, D. H., Prescher, J. A., Quang, C. N. & Bertozzi, C. R. Probing mucin-type O-linked glycosylation in living animals. *Proceedings of the National Academy of Sciences of the United States of America* **103**, 4819-4824, doi:DOI 10.1073/pnas.0506855103 (2006).
93 Hang, H. C. *et al.* Chemical probes for the rapid detection of Fatty-acylated proteins in Mammalian cells. *J Am Chem Soc* **129**, 2744-2745 (2007).
94 Charron, G. *et al.* Robust Fluorescent Detection of Protein Fatty-Acylation with Chemical Reporters. *Journal of the American Chemical Society* **131**, 4967-4975, doi:Doi 10.1021/Ja810122f (2009).
95 Kostiuk, M. A. *et al.* Identification of palmitoylated mitochondrial proteins using a bio-orthogonal azido-palmitate analogue. *Faseb J* **22**, 721-732 (2008).
96 Martin, D. D. *et al.* Rapid detection, discovery, and identification of post-translationally myristoylated proteins during apoptosis using a bio-orthogonal azidomyristate analog. *Faseb J* **22**, 797-806 (2008).
97 Heal, W. P., Wickramasinghe, S. R., Leatherbarrow, R. J. & Tate, E. W. N-Myristoyl transferase-mediated protein labelling in vivo. *Org Biomol Chem* **6**, 2308-2315 (2008).
98 Heal, W. P. *et al.* Site-specific N-terminal labelling of proteins in vitro and in vivo using N-myristoyl transferase and bioorthogonal ligation chemistry. *Chem Commun (Camb)*, 480-482 (2008).
99 Ching, W., Hang, H. C. & Nusse, R. Lipid-independent secretion of a Drosophila Wnt protein. *J Biol Chem* **283**, 17092-17098 (2008).
100 Nguyen, U. T. T. *et al.* Exploiting the substrate tolerance of farnesyltransferase for site-selective protein derivatization. *Chembiochem* **8**, 408-423, doi:DOI 10.1002/cbic.200600440 (2007).
101 Kho, Y. *et al.* A tagging-via-substrate technology for detection and proteomics of farnesylated proteins. *Proceedings of the National Academy of Sciences of the United States of America* **101**, 12479-12484, doi:DOI 10.1073/pnas.0403413101 (2004).
102 Chan, L. N. *et al.* A novel approach to tag and identify geranylgeranylated proteins. *Electrophoresis* **30**, 3598-3606, doi:DOI 10.1002/elps.200900259 (2009).
103 Rose, M. W. *et al.* Enzymatic incorporation of orthogonally reactive prenylazide groups into peptides using geranylazide diphosphate via protein farnesyltransferase: Implications for selective protein labeling. *Biopolymers* **80**, 164-171, doi:Doi 10.1002/Bip.20239 (2005).
104 Berry, A. F. H. *et al.* Rapid Multilabel Detection of Geranylgeranylated Proteins by Using Bioorthogonal Ligation Chemistry. *Chembiochem* **11**, 771-773 (2010).
105 Rose, M. W. *et al.* Evaluation of geranylazide and farnesylazide diphosphate for incorporation of prenylazides into a CAAX box-containing peptide using protein farnesyltrans-

ferase. *Journal of Peptide Research* **65**, 529-537, doi:DOI 10.1111/j.1399-3011.2005.00261.x (2005).
106 Vila, A. *et al.* in *Chem Res Toxicol* Vol. 21 432-444 (2008).
107 Bussink, A. P. *et al.* N-Azidoacetylmannosamine-mediated chemical tagging of gangliosides. *Journal of Lipid Research* **48**, 1417-1421, doi:DOI 10.1194/jlr.C700006-JLR200 (2007).
108 Lafont, D., Bouchu, M. N., Girard-Egrot, A. & Boullanger, P. Syntheses and interfacial behaviour of neoglycolipid analogues of glycosyl ceramides. *Carbohydrate Research* **336**, 181-194 (2001).
109 Sletten, E. M. & Bertozzi, C. R. Bioorthogonal chemistry: fishing for selectivity in a sea of functionality. *Angew Chem Int Ed Engl* **48**, 6974-6998 (2009).
110 Tornoe, C. W., Christensen, C. & Meldal, M. Peptidotriazoles on solid phase: [1,2,3]-triazoles by regiospecific copper(i)-catalyzed 1,3-dipolar cycloadditions of terminal alkynes to azides. *J Org Chem* **67**, 3057-3064, doi:jo011148j [pii] (2002).
111 Rostovtsev, V. V., Green, L. G., Fokin, V. V. & Sharpless, K. B. A stepwise Huisgen cycloaddition process: Copper(I)-catalyzed regioselective "ligation" of azides and terminal alkynes. *Angewandte Chemie-International Edition* **41**, 2596-+ (2002).
112 Meldal, M. & Tornoe, C. W. Cu-catalyzed azide-alkyne cycloaddition. *Chemical Reviews* **108**, 2952-3015, doi:Doi 10.1021/Cr0783479 (2008).
113 Best, M. D. Click Chemistry and Bioorthogonal Reactions: Unprecedented Selectivity in the Labeling of Biological Molecules. *Biochemistry* **48**, 6571-6584, doi:Doi 10.1021/Bi9007726 (2009).
114 Wu, P. & Fokin, V. V. Catalytic azide-alkyne cycloaddition: Reactivity and applications. *Aldrichimica Acta* **40**, 7-17 (2007).
115 Kolb, H. C., Finn, M. G. & Sharpless, K. B. Click chemistry: Diverse chemical function from a few good reactions. *Angewandte Chemie-International Edition* **40**, 2004-+ (2001).
116 Rodionov, V. O., Presolski, S. I., Diaz, D. D., Fokin, V. V. & Finn, M. G. Ligand-accelerated Cu-catalyzed azide-alkyne cycloaddition: A mechanistic report. *Journal of the American Chemical Society* **129**, 12705-12712, doi:Doi 10.1021/Ja072679d (2007).
117 Chan, T. R., Hilgraf, R., Sharpless, K. B. & Fokin, V. V. Polytriazoles as copper(I)-stabilizing ligands in catalysis. *Organic Letters* **6**, 2853-2855, doi:Doi 10.1021/Ol0493094 (2004).
118 Yap, M. C. *et al.* in *J Lipid Res* Vol. 51 1566-1580 (2010).
119 Wilson, J. P., Raghavan, A. S., Yang, Y. Y., Charron, G. & Hang, H. C. Proteomic analysis of fatty-acylated proteins in mammalian cells with chemical reporters reveals S-acylation of histone H3 variants. *Mol Cell Proteomics*, doi:M110.001198 [pii] 10.1074/mcp.M110.001198 (2010).
120 Zhang, M. M., Tsou, L. K., Charron, G., Raghavan, A. S. & Hang, H. C. in *Proc Natl Acad Sci USA* Vol. 107 8627-8632 (2010).
121 Hannoush, R. N. & Arenas-Ramirez, N. Imaging the lipidome: omega-alkynyl fatty acids for detection and cellular visualization of lipid-modified proteins. *ACS Chem Biol* **4**, 581-587 (2009).
122 Martin, B. R. & Cravatt, B. F. Large-scale profiling of protein palmitoylation in mammalian cells. *Nat Methods* **6**, 135-138 (2009).

123 Yount, J. S. *et al.* Palmitoylome profiling reveals S-palmitoylation-dependent antiviral activity of IFITM3. *Nature Chemical Biology* **6**, 610-614, doi:Doi 10.1038/Nchembio.405 (2010).
124 Wilson, J., Wilson, S., Charron, G. & Hang, H. Direct visualizaiton of cholesterol on proteins, in cells and in brains with click chemistry. *P Natl Acad Sci-Biol* **Under revision.** (2010).
125 Jao, C. Y., Roth, M., Welti, R. & Salic, A. in *Proc Natl Acad Sci USA* Vol. 106 15332-15337 (2009).
126 Smith, M. D. *et al.* Synthesis and convenient functionalization of azide-labeled diacylglycerol analogues for modular access to biologically active lipid probes. *Bioconjugate Chemistry* **19**, 1855-1863, doi:Doi 10.1021/Bc8001002 (2008).
127 Agard, N. J., Prescher, J. A. & Bertozzi, C. R. A strain-promoted [3+2] azide-alkyne cycloaddition for covalent modification of blomolecules in living systems. *Journal of the American Chemical Society* **126**, 15046-15047, doi:Doi 10.1021/Ja0449981 (2004).
128 Agard, N. J., Prescher, J. A. & Bertozzi, C. R. A new bioorthogonal ligation for labelling of azide-bearing glycoconjugates. *Glycobiology* **14**, 1197-1197 (2004).
129 Agard, N. J., Baskin, J. M., Prescher, J. A., Lo, A. & Bertozzi, C. R. A comparative study of bioorthogonal reactions with azides. *Acs Chem Biol* **1**, 644-648 (2006).
130 Baskin, J. M. *et al.* Copper-free click chemistry for dynamic in vivo imaging. *Proceedings of the National Academy of Sciences of the United States of America* **104**, 16793-16797 (2007).
131 Codelli, J. A., Baskin, J. M., Agard, N. J. & Bertozzi, C. R. Second-generation difluorinated cyclooctynes for copper-free click chemistry. *J Am Chem Soc* **130**, 11486-11493, doi:10.1021/ja803086r (2008).
132 Neef, A. B. & Schultz, C. in *Angew Chem Int Ed Engl* Vol. 48 1498-1500 (2009).
133 Fernandez-Suarez, M. *et al.* Redirecting lipoic acid ligase for cell surface protein labeling with small-molecule probes. *Nat Biotechnol* **25**, 1483-1487, doi:nbt1355 [pii] 10.1038/nbt1355 (2007).
134 Speers, A. E. & Cravatt, B. F. Profiling enzyme activities in vivo using click chemistry methods. *Chemistry & Biology* **11**, 535-546, doi:DOI 10.1016/j.chembiol.2004.03.012 (2004).
135 Speers, A. E. & Cravatt, B. F. A tandem orthogonal proteolysis strategy for high-content chemical proteomics. *J Am Chem Soc* **127**, 10018-10019 (2005).
136 Debets, M. F., van der Doelen, C. W. J., Rutjes, F. P. J. T. & van Delft, F. L. Azide: A Unique Dipole for Metal-Free Bioorthogonal Ligations. *Chembiochem* **11**, 1168-1184 (2010).
137 Hossain, M. B., Vanderhelm, D., Sanduja, R. & Alam, M. Structure of 6-Azidotetrazolo[5,1-Alpha)Phthalazine, C8h4n8, Isolated from the Toxic Dinoflaggelate Gymnodinium-Breve. *Acta Crystallographica Section C-Crystal Structure Communications* **41**, 1199-1202 (1985).
138 Ciesla, Z., Filutowicz, M. & Klopotowski, T. Involvement of the L-cysteine biosynthetic pathway in azide-induced mutagenesis in Salmonella typhimurium. *Mutat Res* **70**, 261-268, doi:0027-5107(80)90017-2 [pii] (1980).
139 Devadas, B. *et al.* in *J Biol Chem* Vol. 267 7224-7239 (1992).

140 Greenberg, G. R., Chakrabarti, P. & Khorana, H. G. in *Proc Natl Acad Sci USA* Vol. 73 86-90 (1976).
141 Quay, S. C., Radhakrishnan, R. & Khorana, H. G. Incorporation of photosensitive fatty acids into phospholipids of Escherichia coli and irradiation-dependent cross-linking of phospholipids to membrane proteins. *J Biol Chem* **256**, 4444-4449 (1981).
142 Chakrabarti, P. & Khorana, G. in *Biochemistry* Vol. 14 5021-5033 (1975).
143 Hibbs, A. R. & Marzuki, S. in *Biochim Biophys Acta* Vol. 862 445-450 (1986).
144 Hsu, T. L. *et al.* Alkynyl sugar analogs for the labeling and visualization of glycoconjugates in cells. *Proc Natl Acad Sci U S A* **104**, 2614-2619, doi:0611307104 [pii] 10.1073/pnas.0611307104 (2007).
145 Engstová, H. *et al.* in *J Biol Chem* Vol. 276 4683-4691 (2001).
146 Nicholls, D., Gescher, A. & Griffin, R. J. Medicinal azides. Part 8. The in vitro metabolism of p-substituted phenyl azides. *Xenobiotica* **21**, 935-943, doi:10.3109/00498259109039533 (1991).
147 Minto, R. E. & Blacklock, B. J. in *Prog Lipid Res* Vol. 47 233-306 (2008).
148 Dembitsky, V. M. Anticancer activity of natural and synthetic acetylenic lipids. *Lipids* **41**, 883-924 (2006).
149 Rooney, F. & Capon, R. J. Callyspongynes A and B: new polyacetylenic lipids from a southern Australian marine sponge, Callyspongia sp. *Lipids* **33**, 639-642 (1998).
150 Li, X. C. *et al.* Potent in vitro antifungal activities of naturally occurring acetylenic acids. *Antimicrob Agents Chemother* **52**, 2442-2448, doi:AAC.01297-07 [pii] 10.1128/AAC.01297-07 (2008).
151 Ben-Zvi, Z. & Danon, A. in *The Chemistry of Triple Bounded Functional Groupsw* (ed Saul Patal) Ch. 13, (John Wiley & Sons, Ltd, 1994).
152 Helvig, C. *et al.* Suicide inactivation of cytochrome P450 by midchain and terminal acetylenes. A mechanistic study of inactivation of a plant lauric acid omega-hydroxylase. *J Biol Chem* **272**, 414-421 (1997).
153 Zou, A. P. *et al.* Effects of 17-octadecynoic acid, a suicide-substrate inhibitor of cytochrome P450 fatty acid omega-hydroxylase, on renal function in rats. *J Pharmacol Exp Ther* **268**, 474-481 (1994).
154 Ortiz de Montellano, P. R. & Reich, N. O. Specific inactivation of hepatic fatty acid hydroxylases by acetylenic fatty acids. *J Biol Chem* **259**, 4136-4141 (1984).
155 Muerhoff, A. S. *et al.* Prostaglandin and fatty acid omega- and (omega-1)-oxidation in rabbit lung. Acetylenic fatty acid mechanism-based inactivators as specific inhibitors. *J Biol Chem* **264**, 749-756 (1989).
156 Adas, F. *et al.* Involvement of cytochrome P450 2E1 in the (omega-1)-hydroxylation of oleic acid in human and rat liver microsomes. *J Lipid Res* **39**, 1210-1219 (1998).
157 Nguyen, X., Wang, M. H., Reddy, K. M., Falck, J. R. & Schwartzman, M. L. Kinetic profile of the rat CYP4A isoforms: arachidonic acid metabolism and isoform-specific inhibitors. *Am J Physiol* **276**, R1691-1700 (1999).
158 Lands, W. E. *et al.* Quantitative effects of unsaturated fatty acids in microbial mutants. VII. Influence of the acetylenic bond location on the effectiveness of acyl chains. *Biochim Biophys Acta* **486**, 451-461, doi:0005-2760(77)90095-9 [pii] (1977).
159 Kishore, N. S. *et al.* in *J Biol Chem* Vol. 266 8835-8855 (1991).

160 Cox, A. P., Ewart, I. C. & Stigliani, W. M. Microwave-Spectrum, Structure and Dipole-Moment of Phenylacetylene. *Journal of the Chemical Society-Faraday Transactions Ii* **71**, 504-514 (1975).
161 Bayley, H. & Knowles, J. R. Photogenerated reagents for membrane labeling. 2. Phenylcarbene and adamantylidene formed within the lipid bilayer. *Biochemistry* **17**, 2420-2423 (1978).
162 Valvani, S. C., Yalkowsky, S. H. & Roseman, T. J. Solubility and partitioning IV: Aqueous solubility and octanol-water partition coefficients of liquid nonelectrolytes. *J Pharm Sci* **70**, 502-507 (1981).
163 Arnold, D. S., Plank, C. A., Erickson, E. E. & Pike, F. P. Solubility of benzene in water. *Ind. Eng. Chem. Chem. Eng. Data Series* **3**, 253-256 (1958).
164 Sulzle, D., Gatial, A., Karlsson, A., Klaeboe, P. & Nielsen, C. J. The Ir and Raman-Spectra and Conformations of Cyclohexyl Azide. *Journal of Molecular Structure* **174**, 207-214 (1988).
165 Jensen, F. R., Bushwell.Ch & Beck, B. H. Conformational Preferences in Monosubstituted Cyclohexanes Determined by Nuclear Magnetic Resonance Spectroscopy. *Journal of the American Chemical Society* **91**, 344-& (1969).
166 Duckworth, B. P., Zhang, Z., Hosokawa, A. & Distefano, M. D. Selective labeling of proteins by using protein farnesyltransferase. *Chembiochem* **8**, 98-105, doi:10.1002/cbic.200600340 (2007).
167 Gauchet, C., Labadie, G. R. & Poulter, C. D. Regio- and chemoselective covalent immobilization of proteins through unnatural amino acids. *J Am Chem Soc* **128**, 9274-9275, doi:10.1021/ja061131o (2006).
168 Davies, B. S. J. *et al.* Increasing the length of progerin's isoprenyl anchor does not worsen bone disease or survival in mice with Hutchinson-Gilford progeria syndrome. *Journal of Lipid Research* **50**, 126-134, doi:DOI 10.1194/jlr.M800424-JLR200 (2009).
169 Rangan, K. J., Yang, Y. Y., Charron, G. & Hang, H. C. Rapid Visualization and Large-Scale Profiling of Bacterial Lipoproteins with Chemical Reporters. *Journal of the American Chemical Society* **132**, 10628-10629, doi:Doi 10.1021/Ja101387b (2010).
170 Zornetzer, G. A., Fox, B. G. & Markley, J. L. Solution structures of spinach acyl carrier protein with decanoate and stearate. *Biochemistry* **45**, 5217-5227, doi:10.1021/bi052062d (2006).
171 Zambito, A. M. & Wolff, J. Palmitoylation of tubulin. *Biochemical and Biophysical Research Communications* **239**, 650-654 (1997).
172 Kim, H.-Y. H., Tallman, K. A., Liebler, D. C. & Porter, N. A. in *Mol Cell Proteomics* Vol. 8 2080-2089 (2009).
173 Martin, D. D. O. *et al.* in *Faseb J* Vol. 22 797-806 (2008).
174 Kumar, A., Erasquin, U. J., Qin, G., Li, K. & Cai, C. in *Chem Commun (Camb)* Vol. 46 5746-5748 (2010).
175 Musiol, H.-J. *et al.* in *Chembiochem* Vol. 6 625-628 (2005).
176 Godeau, G., Staedel, C. & Barthélémy, P. in *J Med Chem* Vol. 51 4374-4376 (2008).
177 Yang, Y. Y., Ascano, J. M. & Hang, H. C. Bioorthogonal chemical reporters for monitoring protein acetylation. *J Am Chem Soc* **132**, 3640-3641 (2010).

178 Goldberg, A. D. *et al.* Distinct factors control histone variant H3.3 localization at specific genomic regions. *Cell* **140**, 678-691, doi:S0092-8674(10)00004-8 [pii] 0.1016/j.cell.2010.01.003 (2010).
179 Hellman, U., Wernstedt, C., Gonez, J. & Heldin, C. H. Improvement of an "In-Gel" digestion procedure for the micropreparation of internal protein fragments for amino acid sequencing. *Anal Biochem* **224**, 451-455 (1995).
180 Kearney, R. E. *et al.* Elimination of redundant protein identifications in high throughput proteomics. *2005 27th Annual International Conference of the IEEE Engineering in Medicine and Biology Society, Vols 1-7*, 4803-4806 7776 (2005).
181 Stoffel, W. & Klotzbucher, R. Inhibition of Cholesterol-Synthesis in Cultured-Cells by 25-Azidonorcholesterol. *Hoppe-Seylers Zeitschrift Fur Physiologische Chemie* **359**, 199-209 (1978).
182 Ericson, J., Morton, S., Kawakami, A., Roelink, H. & Jessell, T. M. Two critical periods of Sonic Hedgehog signaling required for the specification of motor neuron identity. *Cell* **87**, 661-673, doi:S0092-8674(00)81386-0 [pii] (1996).
183 Maurer-Stroh, S. *et al.* MYRbase: analysis of genome-wide glycine myristoylation enlarges the functional spectrum of eukaryotic myristoylated proteins. *Genome Biol* **5**, R21 (2004).
184 Charron, G., Wilson, J. & Hang, H. C. Chemical tools for understanding protein lipidation in eukaryotes. *Curr Opin Chem Biol* **13**, 382-391 (2009).
185 Drisdel, R. C. & Green, W. N. Labeling and quantifying sites of protein palmitoylation. *Biotechniques* **36**, 276-285 (2004).
186 Roth, A. F. *et al.* Global analysis of protein palmitoylation in yeast. *Cell* **125**, 1003-1013 (2006).
187 Roth, A. F., Wan, J., Green, W. N., Yates, J. R. & Davis, N. G. Proteomic identification of palmitoylated proteins. *Methods* **40**, 135-142 (2006).
188 Kang, R. *et al.* Neural palmitoyl-proteomics reveals dynamic synaptic palmitoylation. *Nature* **456**, 904-909 (2008).
189 Zhang, J. *et al.* Identification of CKAP4/p63 as a major substrate of the palmitoyl acyltransferase DHHC2, a putative tumor suppressor, using a novel proteomics method. *Mol Cell Proteomics* **7**, 1378-1388 (2008).
190 Yang, W., Di Vizio, D., Kirchner, M., Steen, H. & Freeman, M. R. Proteome-scale characterization of human s-acylated proteins in lipid raft-enriched and non-raft membranes. *Mol Cell Proteomics* (2009).
191 Charron, G. *et al.* Robust fluorescent detection of protein fatty-acylation with chemical reporters. *J Am Chem Soc* **131**, 4967-4975 (2009).
192 Yap, M. C. *et al.* Rapid and selective detection of fatty acylated proteins using {omega}-alkynyl-fatty acids and click chemistry. *J Lipid Res*.
193 Meldal, M. & Tornøe, C. W. Cu-catalyzed azide-alkyne cycloaddition. *Chem Rev* **108**, 2952-3015, doi:10.1021/cr0783479 (2008).
194 Tsou, L. K., Zhang, M. M. & Hang, H. C. Clickable fluorescent dyes for multimodal bioorthogonal imaging. *Org Biomol Chem* **7**, 5055-5058 (2009).
195 Weerapana, E., Speers, A. E. & Cravatt, B. F. Tandem orthogonal proteolysis-activity-based protein profiling (TOP-ABPP)--a general method for mapping sites of probe modification in proteomes. *Nat Protoc* **2**, 1414-1425 (2007).

196 Dieterich, D. C., Link, A. J., Graumann, J., Tirrell, D. A. & Schuman, E. M. Selective identification of newly synthesized proteins in mammalian cells using bioorthogonal noncanonical amino acid tagging (BONCAT). *Proc Natl Acad Sci U S A* **103**, 9482-9487 (2006).
197 Fauq, A. H., Kache, R., Khan, M. A. & Vega, I. E. Synthesis of acid-cleavable light isotope-coded affinity tags (ICAT-L) for potential use in proteomic expression profiling analysis. *Bioconjug Chem* **17**, 248-254 (2006).
198 Park, K. D., Liu, R. & Kohn, H. Useful tools for biomolecule isolation, detection, and identification: acylhydrazone-based cleavable linkers. *Chem Biol* **16**, 763-772 (2009).
199 Dirksen, A., Yegneswaran, S. & Dawson, P. E. Bisaryl hydrazones as exchangeable biocompatible linkers. *Angew Chem Int Ed Engl* **49**, 2023-2027, doi:10.1002/anie.200906756 (2010).
200 Jaffe, C. L., Lis, H. & Sharon, N. New clevable photoreactive heterobifunctional crosslinking reagents for studying membrane organization. *Biochemistry* **19**, 4423-4429 (1980).
201 Fonovic, M., Verhelst, S. H., Sorum, M. T. & Bogyo, M. Proteomic evaluation of chemically cleavable activity based probes. *Mol Cell Proteomics* (2007).
202 Verhelst, S. H., Fonovic, M. & Bogyo, M. A mild chemically cleavable linker system for functional proteomic applications. *Angew Chem Int Ed Engl* **46**, 1284-1286 (2007).
203 Zhou, H., Ranish, J. A., Watts, J. D. & Aebersold, R. Quantitative proteome analysis by solid-phase isotope tagging and mass spectrometry. *Nat Biotechnol* **20**, 512-515 (2002).
204 Kim, H. Y., Tallman, K. A., Liebler, D. C. & Porter, N. A. An azido-biotin reagent for use in the isolation of protein adducts of lipid-derived electrophiles by streptavidin catch and photo-release. *Mol Cell Proteomics* (2009).
205 Orth, R. & Sieber, S. A. A photolabile linker for the mild and selective cleavage of enriched biomolecules from solid support. *J Org Chem* **74**, 8476-8479 (2009).
206 Landi, F., Johansson, C. M., Campopiano, D. J. & Hulme, A. N. Synthesis and application of a new cleavable linker for "click"-based affinity chromatography. *Org Biomol Chem* **8**, 56-59.
207 Rangan, K. J., Yang, Y.-Y., Charron, G. & Hang, H. C. Rapid visualization and large-scale profiling of bacterial lipoproteins with chemical reporters. *J Am Chem Soc* **in press** (2010).
208 Alvarez, E., Girones, N. & Davis, R. J. Inhibition of the receptor-mediated endocytosis of diferric transferrin is associated with the covalent modification of the transferrin receptor with palmitic acid. *J Biol Chem* **265**, 16644-16655 (1990).
209 Omary, M. B. & Trowbridge, I. S. Covalent binding of fatty acid to the transferrin receptor in cultured human cells. *J Biol Chem* **256**, 4715-4718 (1981).
210 Wu, L. *et al.* Global survey of human T leukemic cells by integrating proteomics and transcriptomics profiling. *Mol Cell Proteomics* **6**, 1343-1353 (2007).
211 Kang, R. *et al.* Neural palmitoyl-proteomics reveals dynamic synaptic palmitoylation. *Nature* **456**, 904-909, doi:nature07605 [pii] 10.1038/nature07605 (2008).
212 Gordon, J. I., Duronio, R. J., Rudnick, D. A., Adams, S. P. & Gokel, G. W. Protein N-myristoylation. *J Biol Chem* **266**, 8647-8650 (1991).

213 Liang, X., Lu, Y., Neubert, T. A. & Resh, M. D. Mass spectrometric analysis of GAP-43/neuromodulin reveals the presence of a variety of fatty acylated species. *J Biol Chem* **277**, 33032-33040 (2002).
214 Liang, X., Lu, Y., Wilkes, M., Neubert, T. A. & Resh, M. D. The N-terminal SH4 region of the Src family kinase Fyn is modified by methylation and heterogeneous fatty acylation: role in membrane targeting, cell adhesion, and spreading. *J Biol Chem* **279**, 8133-8139 (2004).
215 Horton, P. *et al.* WoLF PSORT: protein localization predictor. *Nucleic Acids Res* **35**, W585-587 (2007).
216 Jensen, L. J. *et al.* STRING 8--a global view on proteins and their functional interactions in 630 organisms. *Nucleic Acids Res* **37**, D412-416, doi:gkn760 [pii] 10.1093/nar/gkn760 (2009).
217 Yang, J. Y. *et al.* Submicromolar concentrations of palmitoyl-CoA specifically thioesterify cysteine 244 in glyceraldehyde-3-phosphate dehydrogenase inhibiting enzyme activity: A novel mechanism potentially underlying fatty acid induced insulin resistance. *Biochemistry* **44**, 11903-11912, doi:Doi 10.1021/Bi0508082 (2005).
218 Veit, M. Palmitoylation of the 25-kDa synaptosomal protein (SNAP-25) in vitro occurs in the absence of an enzyme, but is stimulated by binding to syntaxin. *Biochem J* **345 Pt 1**, 145-151 (2000).
219 Wolff, J., Zambito, A. M., Britto, P. J. & Knipling, L. Autopalmitoylation of tubulin. *Protein Sci* **9**, 1357-1364 (2000).
220 Hiol, A., Caron, J. M., Smith, C. D. & Jones, T. L. Characterization and partial purification of protein fatty acyltransferase activity from rat liver. *Biochim Biophys Acta* **1635**, 10-19 (2003).
221 Veit, M. *et al.* Palmitoylation of rhodopsin with S-protein acyltransferase: enzyme catalyzed reaction versus autocatalytic acylation. *Biochim Biophys Acta* **1394**, 90-98 (1998).
222 Duncan, J. A. & Gilman, A. G. Autoacylation of G protein alpha subunits. *J Biol Chem* **271**, 23594-23600 (1996).
223 Bizzozero, O. A., Mcgarry, J. F. & Lees, M. B. Autoacylation of Myelin Proteolipid Protein with Acyl Coenzyme-A. *Journal of Biological Chemistry* **262**, 13550-13557 (1987).
224 Bano, M. C., Jackson, C. S. & Magee, A. I. Pseudo-enzymatic S-acylation of a myristoylated yes protein tyrosine kinase peptide in vitro may reflect non-enzymatic S-acylation in vivo. *Biochem J* **330 (Pt 2)**, 723-731 (1998).
225 Kummel, D., Heinemann, U. & Veit, M. Unique self-palmitoylation activity of the transport protein particle component Bet3: a mechanism required for protein stability. *Proc Natl Acad Sci U S A* **103**, 12701-12706 (2006).
226 Quesnel, S. & Silvius, J. R. Cysteine-Containing Peptide Sequences Exhibit Facile Uncatalyzed Transacylation and Acyl-Coa-Dependent Acylation at the Lipid Bilayer Interface. *Biochemistry* **33**, 13340-13348 (1994).
227 Washbourne, P. Greasing transmission: palmitoylation at the synapse. *Neuron* **44**, 901-902 (2004).
228 Yang, J. *et al.* Submicromolar concentrations of palmitoyl-CoA specifically thioesterify cysteine 244 in glyceraldehyde-3-phosphate dehydrogenase inhibiting enzyme activity: a novel mechanism potentially underlying fatty acid induced insulin resistance. *Biochemistry* **44**, 11903-11912 (2005).

229 Mitchell, D. A., Mitchell, G., Ling, Y., Budde, C. & Deschenes, R. J. Mutational analysis of Saccharomyces cerevisiae Erf2 reveals a two-step reaction mechanism for protein palmitoylation by DHHC enzymes. *J Biol Chem*, doi:M110.169102 [pii] 10.1074/jbc.M110.169102.

230 Belanger, C., Ansanay, H., Qanbar, R. & Bouvier, M. Primary sequence requirements for S-acylation of beta(2)-adrenergic receptor peptides. *FEBS Lett* **499**, 59-64 (2001).

231 Bizzozero, O. A., Bixler, H., Parkhani, J. & Pastuszyn, A. Nitric oxide reduces the palmitoylation of rat myelin proteolipid protein by an indirect mechanism. *Neurochem Res* **26**, 1127-1137 (2001).

232 Britto, P. J., Knipling, L. & Wolff, J. The local electrostatic environment determines cysteine reactivity of tubulin. *Journal of Biological Chemistry* **277**, 29018-29027, doi:DOI 10.1074/jbc.M204263200 (2002).

233 Mitchell, D. A., Vasudevan, A., Linder, M. E. & Deschenes, R. J. Protein palmitoylation by a family of DHHC protein S-acyltransferases. *J Lipid Res* **47**, 1118-1127 (2006).

234 Bizzozero, O. A., Bixler, H. A. & Pastuszyn, A. Structural determinants influencing the reaction of cysteine-containing peptides with palmitoyl-coenzyme A and other thioesters. *Biochim Biophys Acta* **1545**, 278-288 (2001).

235 Leventis, R., Juel, G., Knudsen, J. K. & Silvius, J. R. Acyl-CoA binding proteins inhibit the nonenzymic S-acylation cysteinyl-containing peptide sequences by long-chain acyl-CoAs. *Biochemistry* **36**, 5546-5553 (1997).

236 Faergeman, N. J. & Knudsen, J. Role of long-chain fatty acyl-CoA esters in the regulation of metabolism and in cell signalling. *Biochemical Journal* **323**, 1-12 (1997).

237 Dunphy, J. T. *et al.* Differential effects of acyl-CoA binding protein on enzymatic and non-enzymatic thioacylation of protein and peptide substrates. *Biochim Biophys Acta* **1485**, 185-198 (2000).

238 Fetrow, J. S., Siew, N. & Skolnick, J. Structure-based functional motif identifies a potential disulfide oxidoreductase active site in the serine/threonine protein phosphatase-1 subfamily. *FASEB J* **13**, 1866-1874 (1999).

239 Magee, A. I. & Courtneidge, S. A. Two classes of fatty acid acylated proteins exist in eukaryotic cells. *EMBO J* **4**, 1137-1144 (1985).

240 Olson, E. N., Towler, D. A. & Glaser, L. Specificity of fatty acid acylation of cellular proteins. *J Biol Chem* **260**, 3784-3790 (1985).

241 Prescott, G. R., Gorleku, O. A., Greaves, J. & Chamberlain, L. H. Palmitoylation of the synaptic vesicle fusion machinery. *J Neurochem* **110**, 1135-1149, doi:JNC6205 [pii] 10.1111/j.1471-4159.2009.06205.x (2009).

242 Yang, X. *et al.* Palmitoylation supports assembly and function of integrin-tetraspanin complexes. *J Cell Biol* **167**, 1231-1240, doi:jcb.200404100 [pii] 10.1083/jcb.200404100 (2004).

243 Yang, X. *et al.* Palmitoylation of tetraspanin proteins: modulation of CD151 lateral interactions, subcellular distribution, and integrin-dependent cell morphology. *Mol Biol Cell* **13**, 767-781, doi:10.1091/mbc.01-05-0275 (2002).

244 Delandre, C., Penabaz, T. R., Passarelli, A. L., Chapes, S. K. & Clem, R. J. Mutation of juxtamembrane cysteines in the tetraspanin CD81 affects palmitoylation and alters interaction with other proteins at the cell surface. *Exp Cell Res* **315**, 1953-1963, doi:S0014-4827(09)00131-1 [pii] 10.1016/j.yexcr.2009.03.013 (2009).

245 Yang, X. H. *et al.* Contrasting effects of EWI proteins, integrins, and protein palmitoylation on cell surface CD9 organization. *J Biol Chem* **281**, 12976-12985, doi:M510617200 [pii] 10.1074/jbc.M510617200 (2006).
246 Heneghan, J. F. *et al.* The Ca2+ channel beta subunit determines whether stimulation of Gq-coupled receptors enhances or inhibits N current. *J Gen Physiol* **134**, 369-384, doi:jgp.200910203 [pii] 10.1085/jgp.200910203 (2009).
247 Wood, C. M. *et al.* The oxidised histone octamer does not form a H3 disulphide bond. *Biochimica Et Biophysica Acta-Proteins and Proteomics* **1764**, 1356-1362, doi:DOI 10.1016/j.bbapap.2006.06.014 (2006).
248 Luger, K., Mader, A. W., Richmond, R. K., Sargent, D. F. & Richmond, T. J. Crystal structure of the nucleosome core particle at 2.8 angstrom resolution. *Nature* **389**, 251-260 (1997).
249 Chantalat, L. *et al.* Structure of the histone-core octamer in KCl/phosphate crystals at 2.15 angstrom resolution. *Acta Crystallographica Section D-Biological Crystallography* **59**, 1395-1407 (2003).
250 Lambert, S. J. *et al.* Purification of histone core octamers and 2.15 angstrom X-ray analysis of crystals in KCl phosphate. *Acta Crystallographica Section D-Biological Crystallography* **55**, 1048-1051 (1999).
251 Banks, D. D. & Gloss, L. M. Folding mechanism of the (H3-H4)(2) histone tetramer of the core nucleosome. *Protein Science* **13**, 1304-1316, doi:Doi 10.1110/Ps.03535504 (2004).
252 Bode, J. & Standt, U. D. Structural Aspects of Histone Complexes and Nucleosomes Revealed by the Accessibility of Cysteine Side-Chains. *Zeitschrift Fur Naturforschung C-a Journal of Biosciences* **33**, 884-890 (1978).
253 Wong, N. T. N. & Candido, E. P. M. Histone H-3 Thiol Reactivity as a Probe of Nucleosome Structure. *Journal of Biological Chemistry* **253**, 8263-8268 (1978).
254 Lewis, P. N. & Chiu, S. S. Effect of Histone H-3 Sulfhydryl Modifications on Histone-Histone Interactions and Nucleosome Formation and Structure. *European Journal of Biochemistry* **109**, 369-376 (1980).
255 Ferrari, N., Pfeffer, U. & Vidali, G. Nucleosomal structure as probed by H3 histone thiol reactivity. Conformation of H3 histone variants is differently affected by thiol group reagents. *Cell Biophys* **10**, 1-13, doi:10.1007/BF02797069 (1987).
256 Garrard, W. T., Nobis, P. & Hancock, R. Histone H-3 Disulfide Reactions in Interphase, Mitotic, and Native Chromatin. *Journal of Biological Chemistry* **252**, 4962-4967 (1977).
257 Hake, S. B. & Allis, C. D. Histone H3 variants and their potential role in indexing mammalian genomes: The "H3 barcode hypothesis". *Proceedings of the National Academy of Sciences of the United States of America* **103**, 6428-6435, doi:DOI 10.1073/pnas.0600803103 (2006).
258 Chen, T. A. & Allfrey, V. G. Rapid and Reversible Changes in Nucleosome Structure Accompany the Activation, Repression, and Superinduction of Murine Fibroblast Protooncogenes C-Fos and C-Myc. *Proceedings of the National Academy of Sciences of the United States of America* **84**, 5252-5256 (1987).
259 Chen, T. A., Smith, M. M., Le, S., Sternglanz, R. & Allfrey, V. G. Nucleosome Fractionation by Mercury Affinity-Chromatography - Contrasting Distribution of Transcriptionally Active DNA-Sequences and Acetylated Histones in Nucleosome Fractions of Wild-

Type Yeast-Cells and Cells Expressing a Histone-H3 Gene Altered to Encode a Cysteine-110 Residue. *Journal of Biological Chemistry* **266**, 6489-6498 (1991).

260 Bazett-Jones, D. P., Mendez, E., Czarnota, G. J., Ottensmeyer, F. P. & Allfrey, V. G. Visualization and analysis of unfolded nucleosomes associated with transcribing chromatin. *Nucleic Acids Research* **24**, 321-329 (1996).

261 Shechter, D., Dormann, H. L., Allis, C. D. & Hake, S. B. Extraction, purification and analysis of histones. *Nature Protocols* **2**, 1445-1457, doi:DOI 10.1038/nprot.2007.202 (2007).

262 Loyola, A. & Almouzni, G. Marking histone H3 variants: How, when and why? *Trends in Biochemical Sciences* **32**, 425-433, doi:DOI 10.1016/j.tibs.2007.08.004 (2007).

263 Loyola, A., Bonaldi, T., Roche, D., Imhof, A. & Almouzni, G. PTMs on H3 variants before chromatin assembly potentiate their final epigenetic state. *Molecular Cell* **24**, 309-316, doi:DOI 10.1016/j.molcel.2006.08.019 (2006).

264 Ohno, Y., Kihara, A., Sano, T. & Igarashi, Y. Intracellular localization and tissue-specific distribution of human and yeast DHHC cysteine-rich domain-containing proteins. *Biochimica Et Biophysica Acta-Molecular and Cell Biology of Lipids* **1761**, 474-483, doi:DOI 10.1016/j.bbalip.2006.03.010 (2006).

265 Garske, A. L. *et al.* Combinatorial profiling of chromatin binding modules reveals multisite discrimination. *Nature Chemical Biology* **6**, 283-290, doi:Doi 10.1038/Nchembio.319 (2010).

266 Towbin, B. D., Meister, P. & Gasser, S. M. The nuclear envelope - a scaffold for silencing? *Current Opinion in Genetics & Development* **19**, 180-186, doi:DOI 10.1016/j.gde.2009.01.006 (2009).

267 Misteli, T. Concepts in nuclear architecture. *Bioessays* **27**, 477-487, doi:Doi 10.1002/Bies.20226 (2005).

268 Bartova, E., Krejci, J., Harnicarova, A., Galiova, G. & Kozubek, S. Histone modifications and nuclear architecture: A review. *Journal of Histochemistry & Cytochemistry* **56**, 711-721, doi:DOI 10.1369/jhc.2008.951251 (2008).

269 Chambeyron, S. & Bickmore, W. A. Chromatin decondensation and nuclear reorganization of the HoxB locus upon induction of transcription. *Genes & Development* **18**, 1119-1130, doi:Doi 10.1101/Gad.292104 (2004).

270 Bouvier, D., Hubert, J., Seve, A. P. & Bouteille, M. Characterization of Lamina-Bound Chromatin in the Nuclear Shell Isolated from Hela-Cells. *Experimental Cell Research* **156**, 500-512 (1985).

271 Polioudaki, H. *et al.* Histones H3/H4 form a tight complex with the inner nuclear membrane protein LBR and heterochromatin protein 1. *Embo Reports* **2**, 920-925, doi:DOI 10.1093/embo-reports/kve199 (2001).

272 de Oca, R. O. M., Lee, K. K. & Wilson, K. L. Binding of barrier to autointegration factor (BAF) to histone H3 and selected linker histones including H1.1. *Journal of Biological Chemistry* **280**, 42252-42262, doi:DOI 10.1074/jbc.M509917200 (2005).

273 Furukawa, K. LAP2 binding protein 1 (L2BP1/BAF) is a candidate mediator of LAP2-chromatin interaction. *Journal of Cell Science* **112**, 2485-2492 (1999).

274 Lee, K. K. *et al.* Distinct functional domains in emerin bind lamin A and DNA-bridging protein BAF. *Journal of Cell Science* **114**, 4567-4573 (2001).

275 Taniura, H., Glass, C. & Gerace, L. A Chromatin Binding-Site in the Tail Domain of Nuclear Lamins That Interacts with Core Histones. *Journal of Cell Biology* **131**, 33-44 (1995).
276 Maxfield, F. R. & Tabas, I. Role of cholesterol and lipid organization in disease. *Nature* **438**, 612-621, doi:nature04399 [pii] 10.1038/nature04399 (2005).
277 Ikonen, E. Cellular cholesterol trafficking and compartmentalization. *Nat Rev Mol Cell Biol* **9**, 125-138, doi:nrm2336 [pii] 10.1038/nrm2336 (2008).
278 Brown, M. S. & Goldstein, J. L. A receptor-mediated pathway for cholesterol homeostasis. *Science* **232**, 34-47 (1986).
279 Aneja, A. & Tierney, E. Autism: the role of cholesterol in treatment. *Int Rev Psychiatry* **20**, 165-170, doi:791893360 [pii] 10.1080/09540260801889062 (2008).
280 Lundbaek, J. A., Andersen, O. S., Werge, T. & Nielsen, C. Cholesterol-induced protein sorting: An analysis of energetic feasibility. *Biophysical Journal* **84**, 2080-2089 (2003).
281 Burger, K., Gimpl, G. & Fahrenholz, F. Regulation of receptor function by cholesterol. *Cellular and Molecular Life Sciences* **57**, 1577-1592 (2000).
282 Dietschy & Turley. Cholesterol metabolism in the central nervous system during early development and in the mature animal (vol 45, pg 1375, 2004). *Journal of Lipid Research* **46**, 1350-1350 (2005).
283 Infante, R. E. *et al.* Purified NPC1 protein. I. Binding of cholesterol and oxysterols to a 1278-amino acid membrane protein. *J Biol Chem* **283**, 1052-1063, doi:M707943200 [pii] 10.1074/jbc.M707943200 (2008).
284 Heller, R. A., Klotzbucher, R. & Stoffel, W. Interactions of a Photosensitive Analog of Cholesterol with Hydroxymethylglutaryl-Coa Reductase (Nadph) and Acyl-Coa - Cholesterol Acyltransferase. *Proceedings of the National Academy of Sciences of the United States of America* **76**, 1721-1725 (1979).
285 Yount, J. S. *et al.* Palmitoylome profiling reveals S-palmitoylation-dependent antiviral activity of IFITM3. *Nat Chem Biol*, doi:nchembio.405 [pii] 10.1038/nchembio.405.
286 Zhang, M. M., Tsou, L. K., Charron, G., Raghavan, A. S. & Hang, H. C. Tandem fluorescence imaging of dynamic S-acylation and protein turnover. *Proc Natl Acad Sci U S A* **107**, 8627-8632, doi:0912306107 [pii] 10.1073/pnas.0912306107.
287 Jao, C. Y., Roth, M., Welti, R. & Salic, A. Metabolic labeling and direct imaging of choline phospholipids in vivo. *Proc Natl Acad Sci U S A* **106**, 15332-15337, doi:0907864106 [pii] 10.1073/pnas.0907864106 (2009).
288 Cooper, M. K., Porter, J. A., Young, K. E. & Beachy, P. A. Teratogen-mediated inhibition of target tissue response to Shh signaling. *Science* **280**, 1603-1607 (1998).
289 Millard, E. E., Srivastava, K., Traub, L. M., Schaffer, J. E. & Ory, D. S. Niemann-Pick type C1 (NPC1) overexpression alters cellular cholesterol homeostasis. *Journal of Biological Chemistry* **275**, 38445-38451 (2000).
290 Vanier, M. T. & Millat, G. Niemann-Pick disease type C. *Clinical Genetics* **64**, 269-281 (2003).
291 Peake, K. B. & Vance, J. E. Defective cholesterol trafficking in Niemann-Pick C-deficient cells. *FEBS Lett* **584**, 2731-2739, doi:S0014-5793(10)00332-7 [pii] 10.1016/j.febslet.2010.04.047.

292 Butler, J. D. *et al.* Niemann-Pick Variant Disorders - Comparison of Errors of Cellular Cholesterol Homeostasis in Group-D and Group-C Fibroblasts. *Proceedings of the National Academy of Sciences of the United States of America* **84**, 556-560 (1987).
293 Frolov, A. *et al.* Cholesterol overload promotes morphogenesis of a Niemann-Pick C (NPC)-like compartment independent of inhibition of NPC1 or HE1/NPC2 function. *Journal of Biological Chemistry* **276**, 46414-46421 (2001).
294 Sugimoto, Y. *et al.* Accumulation of cholera toxin and GM1 ganglioside in the early endosome of Niemann-Pick C1-deficient cells. *Proceedings of the National Academy of Sciences of the United States of America* **98**, 12391-12396 (2001).
295 Kelley, R. I. & Herman, G. E. Inborn errors of sterol biosynthesis. *Annu Rev Genomics Hum Genet* **2**, 299-341, doi:2/1/299 [pii] 10.1146/annurev.genom.2.1.299 (2001).
296 Tsutsui, K. Neurosteroids in the Purkinje cell: biosynthesis, mode of action and functional significance. *Mol Neurobiol* **37**, 116-125, doi:10.1007/s12035-008-8024-1 (2008).
297 Pelletier, R. M. & Vitale, M. L. Filipin vs enzymatic localization of cholesterol in guinea pig, mink, and mallard duck testicular cells. *J Histochem Cytochem* **42**, 1539-1554 (1994).
298 Steer, C. J., Bisher, M., Blumenthal, R. & Steven, A. C. Detection of Membrane Cholesterol by Filipin in Isolated Rat-Liver Coated Vesicles Is Dependent Upon Removal of the Clathrin Coat. *Journal of Cell Biology* **99**, 315-319 (1984).
299 Severs, N. J. & Simons, H. L. Failure of filipin to detect cholesterol-rich domains in smooth muscle plasma membrane. *Nature* **303**, 637-638 (1983).
300 Knudsen, J., Neergaard, T. B., Gaigg, B., Jensen, M. V. & Hansen, J. K. in *J Nutr* Vol. 130 294S-298S (2000).
301 Yang, Y.-Y., Ascano, J. M. & Hang, H. C. Bioorthogonal Chemical Reporters for Monitoring Protein Acetylation. *J Am Chem Soc* **132**, 3640-+ (2010).
302 Hariton-Gazal, E., Rosenbluh, J., Graessmann, A., Gilon, C. & Loyter, A. Direct translocation of histone molecules across cell membranes. *J Cell Sci* **116**, 4577-4586, doi:10.1242/jcs.00757 116/22/4577 [pii] (2003).
303 Kummel, D., Heinemann, U. & Veit, M. Unique self-palmitoylation activity of the transport protein particle component Bet3: A mechanism required for protein stability. *Proceedings of the National Academy of Sciences of the United States of America* **103**, 12701-12706, doi:DOI 10.1073/pnas.0603513103 (2006).
304 Kümmel, D., Walter, J., Heck, M., Heinemann, U. & Veit, M. in *Cellular and molecular life sciences : CMLS* 10.1007/s00018-00010-00358-y (2010).
305 Greyling, H. J., Sewell, B. T. & Von Holt, C. in *Eur J Biochem* Vol. 171 721-726 (1988).
306 Perlstein, M. T., Atassi, M. Z. & Cheng, S. H. Desulfurization of sulfur amino acids and proteins with Raney nickel. *Biochim Biophys Acta* **236**, 174-182 (1971).
307 Greyling, H. J., Schwager, S., Sewell, B. T. & von Holt, C. The identity of conformational states of reconstituted and native histone octamers. *Eur J Biochem* **137**, 221-226 (1983).
308 Dyer, P. N. *et al.* Reconstitution of nucleosome core particles from recombinant histones and DNA. *Methods Enzymol* **375**, 23-44 (2004).

309 Xu, Y. *et al.* The p400 ATPase regulates nucleosome stability and chromatin ubiquitination during DNA repair. *J Cell Biol* **191**, 31-43, doi:jcb.201001160 [pii] 10.1083/jcb.201001160.
310 Lusser, A. & Kadonaga, J. T. Strategies for the reconstitution of chromatin. *Nat Methods* **1**, 19-26, doi:nmeth709 [pii] 10.1038/nmeth709 (2004).
311 Albert, I. *et al.* Translational and rotational settings of H2A.Z nucleosomes across the Saccharomyces cerevisiae genome. *Nature* **446**, 572-576, doi:nature05632 [pii] 10.1038/nature05632 (2007).